MACRO-MICRO ROBOTIC MANIPULATION: A LASER CUTTING CASE STUDY

A Thesis Submitted to the
Graduate School of Engineering and Sciences of
İzmir Institute of Technology
in Partial Fulfillment of the Requirements for the Degree of

DOCTOR OF PHILOSOPHY

in Mechanical Engineering

by

Emre UZUNOĞLU

July 2019

İZMİR

We approve the thesis of **Emre UZUNOĞLU**

Examining Committee Members:

Prof. Dr. Enver TATLICIOĞLU
Department of Electrical & Electronics Engineering, İzmir Institute of Technology

Prof. Dr. Serhan ÖZDEMİR
Department of Mechanical Engineering, İzmir Institute of Technology

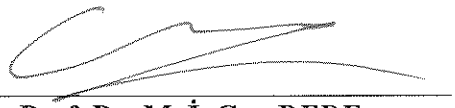

Assoc. Prof. Dr. M. İ. Can DEDE
Department of Mechanical Engineering, İzmir Institute of Technology

Assoc. Prof. Dr. Levent ÇETİN
Department of Mechatronics Engineering, İzmir Katip Çelebi University

Asst. Prof. Dr. Erkin GEZGİN
Department of Mechatronics Engineering, İzmir Katip Çelebi University

19 July 2019

Assoc. Prof. Dr. M. İ. Can DEDE
Supervisor, Department of Mechanical Engineering, Izmir Institute of Technology

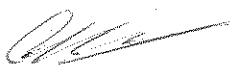

Assoc. Prof. Dr. Gökhan KİPER
Co-Supervisor, Department of Mechanical, Izmir Institute of Technology

Prof. Dr. Sedat AKKURT
Head of the Department of Mechanical Engineering

Prof. Dr. Aysun SOFUOĞLU
Dean of the Graduate School of Engineering and Sciences

ACKNOWLEDGMENTS

In the beginning, I would like to express my sincere gratitude to my supervisor and mentor Dr. Can DEDE not only for his tremendous academic support, patience, and motivation but also for giving me so many significant opportunities. Similar, my profound gratitude goes to my co-supervisor Dr. Gökhan KİPER for sharing his insightful academic knowledge and for his contributions to the dissertation studies. I gratefully acknowledge the guidance Prof. Enver TATLICIOĞLU provided for the studies mentioned in Chapter 6. I thank him for sharing his immense knowledge and his support.

Besides my supervisors, I would like to thank the rest of my thesis committee: Prof. Serhan ÖZDEMİR, Dr. Levent ÇETİN, and Dr. Erkin GEZGİN for their insightful comments and encouragement.

I also want to express my thanks to acquaintances from Coşkunöz Company who made it possible to carry out my research on an Industrial setup. I owe a sincere thank you to Ercan MASTAR for his contributions to the industrial project.

I would always remember and want to express my gratitude to my fellow labmates and too, Osman Nuri ŞAHİN, Omar MAAROOF, Barış TANER, Halil TETİK, Orhan AYİT, Murat DEMİREL, Cevahir KARAGÖZ, İbrahimcan GÖRGÜLÜ, Furkan KÜÇÜKOĞLU, Mert YILMAZ, Merve ÖZKAHYA, Çağhan KİRİŞCİ, Mert KANIK, Gizem ATEŞ, Emir MOBEDİ, Görkem KARABULUT, Oğulcan and Gizem IŞITMAN, Mert KANIK, Elvan DOĞAN KUMTEPE, Erkan PAKSOY, and Hazal EMET for it wouldn’t have been possible to conduct this research without their precious support.

In the end, I am grateful to my parents, Ahmet and Nuriye UZUNOĞLU, and my sister Hande who have provided me unbelievable support in my life and throughout this challenging work.

This dissertation is financially supported by the Republic of Turkey, Ministry of Science, Industry, and Technology and Coşkunöz Company via grant number 01668.STZ.2012-2. In addition, late studies of this dissertation were supported by TÜBİTAK via project number 116M272.

ABSTRACT

MACRO-MICRO ROBOTIC MANIPULATION: A LASER CUTTING CASE STUDY

This dissertation focuses on investigation and devising of proper methodology to utilize a special type of kinematic redundancy, namely macro–micro manipulation, in the scope of robotic science. Briefly, macro-micro manipulation is comprised of two kinematically different mechanisms that have distinct characteristics, which work on macro and micro-scale. Aim of this dissertation is to present the most convenient motion planning and control algorithm to resolve kinematic redundancy for macro-micro manipulation concept. Controller designs, including the motion planning algorithms are devised taking into account the selected industrial case study. Additionally, a general framework controller is developed for macro-micro manipulation. Experiments with industrial setup and simulation verifications are done for the proposed methodologies. It is proven with simulation test results and experiments that the task completion duration for a laser cutting machine is reduced by enhancing the acceleration capability with the macro-micro manipulation. Although the proposed methodologies are implemented for a specific case, it can also be used for other systems considering the versatility of the proposed methodology.

The core novelty of this research is the introduction of methodologies in order to achieve the maximum efficiency for the combined use of macro and micro-scaled manipulators. As an outcome of this study, a redundant laser cutting machine that can move with higher accelerations by making use of macro-micro manipulation is developed as a first of its kind in the Turkish machine industry and third of its kind in the world.

ÖZET

MAKRO-MİKRO ROBOTİK MANİPÜLASYON: BİR LAZER KESİM ÇALIŞMASI

Bu tez, robotik bilimi kapsamında, özel bir kinematik fazlalık türü olan makro-mikro manipülasyon için uygun metodolojinin araştırılması ve tasarlanmasına odaklanmaktadır. Kısaca, makro-mikro manipülasyon, makro ve mikro ölçekte çalışan ve belirgin avantajlara sahip kinematik olarak farklı iki mekanizmadan oluşur. Bu tezin amacı, makro-mikro manipülasyon konsepti için kinematik fazlalığı kullanarak en uygun hareket planlama ve kontrol algoritmasını sunmaktır. Endüstriyel uygulama çalışması göz önüne alınarak, hareket planlama algoritmaları dahil olmak üzere denetleyici tasarımları geliştirilmiştir. Ek olarak, makro-mikro manipülasyon için genel bir çerçeve denetleyicisi geliştirilmiştir. Önerilen yöntemler için endüstriyel kurulum ve simülasyon doğrulamaları ile deneyler yapılmıştır. Sayısal sonuç ve deneylerle, bir lazer kesme makinesinin görev tamamlama süresinin, makro-mikro manipülasyon ile hızlanma yeteneğini artırarak, azaltıldığı kanıtlanmıştır. Önerilen metodolojiler belirli bir durum için uygulanmakla birlikte, metodolojinin çok yönlülüğü dikkate alınarak, diğer sistemler için de kullanılabilir.

Bu araştırmanın temel yeniliği makro ve mikro ölçekli iki tip manipülasyonun birleşik kullanımı ile maksimum verimliliği sağlayacak metodolojilerin sunumudur. Yapılan çalışmaların bir sonucu olarak, makro-mikro manipülasyon konseptini kullanarak daha yüksek ivmelere ulaşabilen Türkiye makina endüstrisinde ilk, dünyada ise üçüncü lazer kesim makinası uygulaması geliştirilmiştir.

I dedicate this thesis to my parents and my sister, Ahmet, Nuriye, and Hande UZUNOĞLU. They are the most important people in my world.

TABLE OF CONTENTS

LIST OF FIGURES

Figure **Page**

Figure **Page**

LIST OF TABLES

CHAPTER 1

INTRODUCTION

This dissertation presents a mechatronic framework for an application of Macro-Micro Manipulation (MMM) into an industrial planar laser cutting machine. Most of the studies carried out in this dissertation is the outcome of the "Kinematically Redundant Laser Cutting Machine Design" by SANTEZ (Industrial Theses Support Program) which is funded by the Republic of Turkey, Ministry of Science, Industry, and Technology.

Although the concept introduced for the dissertation statement is on this framework, the research done is extended to devise proper novel methods for modeling and control of MMM. The findings achieved in this thesis can be extended to the development of new design, control and motion planning strategies for MMM. Theoretical and applied research aspects of MMM and planar laser cutting machines along with novel concepts are introduced in the forthcoming sections.

1.1. Background and Problem Definition

Kinematically redundant manipulators can provide the task designer with an infinite number of solutions that can achieve the same primary task since they possess more degrees of freedom (DoF) than required to execute a given task. Self-motions of a redundant manipulator, which have no effect on the primary task (Nakamura, 1987), have been used to achieve a variety of subtasks, e.g. singularity avoidance and minimizing total joint motion. Several redundancy resolution algorithms have been proposed in the literature that allow the ability to optimize for various criteria using subtasks without interfering with the primary task. Redundancy resolution in velocity level by making use of the pseudo-inverse approach has been widely used in various subtask controls such as singularity avoidance (Liu et al., 2001), joint velocity minimization (Seraji, 1992), obstacle avoidance (Chen et al., 2002), mechanical joint limit avoidance (Tatlıcıoğlu et al., 2009), and manipulability (Maaroof et al., 2012) These controllers have based their redundancy resolution algorithms on only kinematic parameters. Additionally, multi-

priority controllers which base their redundancy resolution algorithms on dynamic parameters with torque controllers were developed (Dietrich et al., 2015).

A special set of kinematic redundancy is formed by the use of different mechanisms that inherently have distinct capabilities. Such systems can be distinctly categorized under MMM because of their unique configurations. Macro–micro Manipulation, as its name suggests, is comprised of a macro mechanism with a relatively larger workspace and a lightweight micro mechanism dealing with confined motions with relatively higher dynamic capabilities. Concisely, mounting a micro manipulator to the end of a macro manipulator can provide fine adjustment of errors in position or force and thereby enhance accuracy and/or inertial characteristics of the overall manipulator while maintaining a large workspace. In this regard, the human upper limb can be observed and imitated as a macro-micro system, especially for tasks such as writing (Huang et al., 2009), where the arm acts as a macro manipulator for coarse positioning, and wrist and the hand deal with finer motions.

Machining from Industry 3.0 onwards has proved to provide precise and faster manufacturing methods in the industry. Among these developments, laser technology found application in planar and three-dimensional (3D) cutting, punching, welding etc. operations. Introduction of novel technologies in laser sources pushed the limits of such manufacturing systems further. Since it can deploy a large amount of focused energy with relatively better efficiencies, fiber laser technology has been used for high precision and time-efficient manufacturing systems, especially for cutting thin materials. Although fiber laser cutting provides fast machining for especially planar cutting operation of sheet metals, plastics, and ceramics, there still exists a demand from the manufacturing industry to decrease the manufacturing task completion durations. At the current state of fiber laser-cutting operation, cutting speed is mostly determined by the laser power source, material type and the width of the material. Therefore, to exceed the conventional laser cutting machine's task completion duration, the only option without changing the composition of the tool is to reach the maximum cutting speed as fast as possible. This provoked researches in the industry that lead to the development of machines with better dynamic capabilities, so to be called with better acceleration capabilities.

Conventional planar laser cutting machines are usually built to cover the whole sheet metal area and therefore, their workspace is relatively large which is usually in the range of 1~2 m by 2~3 m. During the cutting process of a workpiece with many small contours, mostly the maximum allowable tool speed is never reached by the conventional

machines since it has limited acceleration due to large inertial properties of the construction that is moving the tool in x-y axes. In the case of employing larger actuators with greater torque capabilities, it can be foreseen that the system will lose precision while increasing the acceleration capability. As a consequence of these facts, generally, acceleration limits of the conventional planar laser cutting machines are set at 1~1.5 g (gravitational acceleration).

One solution to go beyond the acceleration limits set by the conventional machines is by introducing kinematic redundancy to the conventional machine to take advantage of optimization of redundant manipulation. This strategy can shorten completion time especially for the cases in which there are relatively large number of small contours and sharp edges defined for the cutting path of the tool. Usually, conventional planar laser-cutting machines are built to cover the whole sheet metal area, and therefore, their workspace is relatively larger. During the cutting process of workpiece with complex contours, mostly the maximum allowable tool speed is never reached by the conventional machines, as it has limited acceleration due to large inertial properties of the construction that is moving the tool in x- and y-axes. In the case of using larger actuators with greater torque capabilities, it can be foreseen that the system will lose precision while increasing the acceleration capability. In this manner, it is deduced that a MMM, a special subset of redundant manipulators, can be utilized to shorten process duration for conventional laser cutting machines. Consequently, a mechatronic system solution with integration of MMM concept is the starting point of this thesis.

1.2. Aim of the Dissertation

In this dissertation, MMM concept is intended to be used for planar laser cutting process. This manipulator is comprised of two mechanisms, macro and micro mechanisms, with distinct acceleration and workspace characteristics. The macro mechanism, which is the primary mechanism, is the X-Y translational mechanism as used in the conventional laser-cutting machines. The micro mechanism, which is the secondary mechanism, is a modified five-bar (over-constrained six-bar) mechanism with two DoF. While the macro mechanism has a relatively large workspace (3000 mm x 1500mm), the micro mechanism has a better acceleration limit up and a workspace limit of 150 mm x 100 mm. Combined acceleration limit of the MMM is designated as 3.5 g. The

acceleration limit is set considering the capabilities of the hardware used, i.e. the laser cutting tool and the drive systems.

The main aim of the SANTEZ project is to shorten the duration of the process with a conventional size planar laser-cutting machine by utilizing the MMM concept. Regarding the control of the produced machine, the main aim of this thesis is to devise a method to utilize the MMM concept for shortening the task completion duration. For this purpose, it is foreseen that a novel method should be developed for trajectory generation for this unique redundant system. In addition, the precise control of the mechanisms has to be ensured so that the generated path is tracked and the material is cut. Moreover, the hardship has to be overcome in the integration of the devised algorithms while sustaining the quality of the laser cutting process with industrial setup. Regarding this, the validation of the positioning accuracy is aimed to be presented in this dissertation. Subsequently, the proposed algorithms for the case study aims to present a method to distribute a planar motion path to the macro and micro mechanisms to complete the task in minimum duration.

In addition, it is aimed to present an attentive and contemporary literature survey on MMM. Also, an investigation on the current laser cutting technology is aimed to be presented, especially for dynamic cutting machines. Another aim is to resolve redundancy for the MMM by making use of redundancy resolution of the manipulator. This controller is designated to be used in fully online control strategies without the integration of any additional pre-processing algorithms. Designing a null-space based controller utilizing a simplified dynamic model of the proposed MMM.

Furthermore, for future studies, the modeling and control of micro mechanism is investigated. Micro manipulator in this study is chosen as a modified six-bar mechanism with parallelogram loops. Due to the modeling problems of the over-constrained parallel (micro) mechanism, the dynamic model derivation and its integration to the nonlinear controllers are investigated.

Consequently, the aim of this thesis is summarized as follows:

i. To present a detailed review of the literature on MMM.
ii. To devise algorithms to be utilized in MMM system, to shorten process duration time.
iii. To apply one of the devised methods for industrial laser cutting application.
iv. To develop a fully online multi-priority controller for MMM for future studies.
v. To propose feasible nonlinear controllers to be used in future studies.

1.3. Contributions

Several novel ideas, concepts, and algorithms are introduced in this dissertation. These form the contributions to the field of manufacturing technology, robotics, motion planning, and control theory, and they are summarized as follows:

i. The research done in this thesis helped the development of the first redundant laser cutting machine in the Turkish Machine Industry, and third of its kind in the world that can reach higher accelerations using MMM concept.
ii. Three different algorithms for motion planning are devised to make use of kinematic redundancy and the most suitable method is adapted to a semi-online control strategy.
iii. A novel multi-priority controller strategy is developed for online control of MMM and the controllers are validated with simulations.

1.4. Organization of the Dissertation

Chapter 2 and 3 cover the literature survey. Chapter 4 and 5 summarize algorithms developed and tests are done in the project: "Kinematically Redundant Laser Cutting Machine Design" funded by SANTEZ (Industrial Theses Support Program). The first section of Chapter 6 comprises of controllers devised for micro manipulator for future studies in the scope of another project called "Methodologies for Increasing the Positioning Accuracy of High-Acceleration Parallel Robots Used in Industrial Applications". The second section of Chapter 6 covers the novel multi-priority controller developed for macro-micro manipulation.

The overall organization of the dissertation is listed below, respectively.

i. In Chapter 2, a literature review on MMM is presented.
ii. In Chapter 3, a literature review on laser cutting technology is presented.
iii. In Chapter 4, three algorithms developed for MMM laser cutting machine is given. As a conclusion, the most suitable algorithm is presented.
iv. In Chapter 5, the work done during SANTEZ project is presented. Industrial laser cutting application setup and procedure is given in detail. The conclusions realized in the project are presented with experimental results.

v. In Chapter 6, a reduced-order model of micro manipulator, nonlinear controllers of the micro manipulator, and a multi-priority controller developed for MMM are presented. Conclusions on these methods are given with simulation results.

vi. In Chapter 7, overall conclusions and discussions are given.

CHAPTER 2

MACRO-MICRO MANIPULATION

Redundancy in robotics, namely kinematic redundancy, is mostly used when the number of joints of a robot manipulator is greater than the degrees of freedom in its task-space (Conkur et al., 1997). Kinematic redundancy resolution is utilized in manipulators to attain better capabilities and enhance performance as well as to execute side tasks (Sciliano 1990). Despite the numerous possible configurations of mechanisms and the extensive work in the literature about kinematic redundancy, a subcategory of redundant manipulators called "macro-micro manipulation (MMM)" single-handedly provided specific problems to be discussed and solved in the literature. This unique set of kinematic redundancy can be devised by combining consecutively two kinematically different mechanisms that have distinctive advantages. Mounting a micro manipulator to the distal end of a macro manipulator, can provide fine adjustment of possible errors during the task that may occur by means of position and force, and thereby can increase accuracy and inertial characteristic of complete mechanism while maintaining a large workspace. A member of this type is set to have, in almost all cases, a macro mechanism with a relatively larger workspace and a lightweight micro mechanism with relatively higher dynamic capabilities. While there is no generally-accepted term for redundant robots with abovementioned distinct capabilities, in literature "macro-micro manipulator" (Sharon and Hardt, 1988) term is often used to refer them, also "macro-mini manipulator" (Khatib, 1989).

2.1. Concepts of MMM

Researchers who mentioned about macro-micro manipulators categorized them under redundant, underactuated (Yoshida, 1997), or moving-base (Siciliano and Khatib, 2016) manipulators/robots. Similar to the categorization of Yoshida (1996) for moving-base robots, the MMM structures in literature can be represented with the following

categories as illustrated in Figure 2.1 These representations are made regarding the associated research in the literature that mentions about an MMM system.

In a general manner, MMM in the literature, mostly have a structure where a micro manipulator is mounted serially at the distal end of a macro manipulator, shown in Figure 2.1 a. However type of the macro manipulator led various subcategories such as free-floating-base, flexible-base, and ground-base systems which are respectively illustrated in Figure 2.1. c Figure 2.1 d., and Figure 2.1 e. In this section, the literature is presented on how the researchers approach the MMM concept.

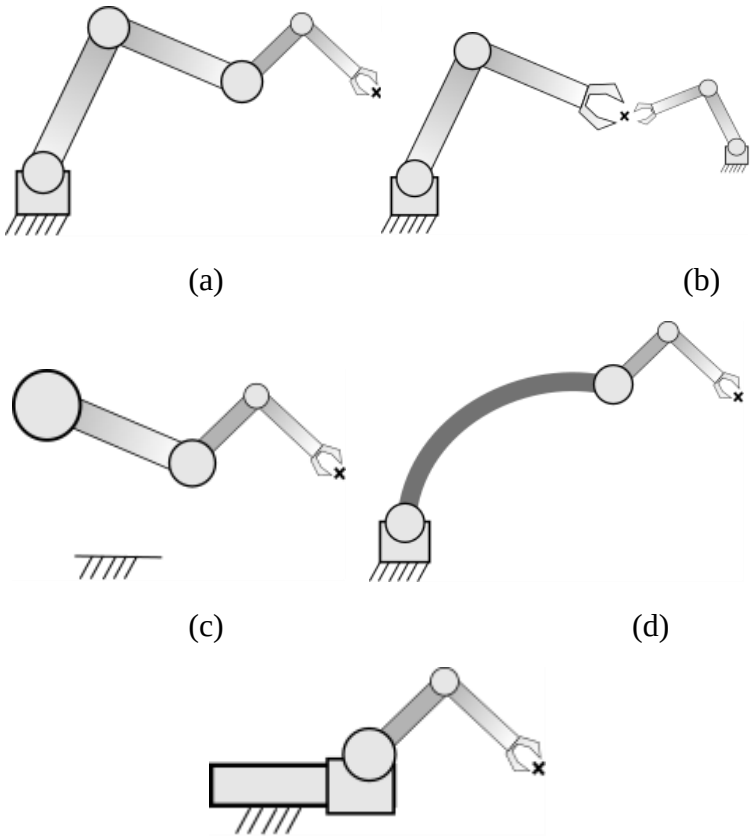

Figure 2.1. MMM structures in the literature (a) Rigid-rigid (b) Cooperative (c) Free-floating (d) Flexible-base (e) Ground base.

A free-flying space robot, an underwater robot, or a marine robot may be categorized as MMM, considering the applications when the moving body is considered as a virtual macro arm and modeled as a manipulator (Egeland, 1987, Russakow et.al,

1995). The control scheme for the coordination of motion in a spacecraft/manipulator system is presented where the augmented task-space approach is used to show how end-effector motion can be decoupled from satellite motion (Egeland and Sagli, 1990). A similar analogy is used for the underwater robotic system by Antonelli and Chiaverini (1998).

A rigid manipulator attached serially to the end of a flexible manipulator is often called as a flexible-base manipulator, and many researchers categorized this type as MMM. Hybrid, by means of structural flexibility, MMM systems contributed in the development of various methods in the scope of control theory, including nonlinear (Parsa et al., 2005), fuzzy (Xu et al 2000), neural network-based (Cheng et al(flex)) control. In addition to this, flexible base manipulators are seldom mentioned as underactuated systems where a manipulator is attached to a large and underactuated structure that the micro manipulator becomes susceptible vibrations and accuracy decrement (Yoshida 1998, Lin and Huang 2007, Lew and Moon 2001). An underactuated robotic system means that system comprises more DoF than its actuators which are namely called as floating base, moving base, flexible base.

In the earlier studies, (Yoshikawa, 1996) introduced dynamic trajectory tracking control for flexible-base MMMs. In addition to that Jiang and Geoldenberg (1999) discussed the stability of such controllers by using Lyapunov stability theorem. A learning algorithm for the neural network using Lyapunov stability theory is devised by (Cheng and Patel 2003). Yoshikawa et al. (1996) come up with hybrid position/force controllers to be used on mechanisms which are combinations of flexible macro and rigid micro mechanisms. Due to the flexibility of the macro mechanism, the macro mechanism has coarse positioning accuracy, which is why the micro mechanism is used to compensate both position and force errors. Being tested by both quasi-static hybrid control and dynamic hybrid control, it is deduced that dynamic hybrid control gives better results in means of accuracy and vibration rejection. Studies (Zhang et al., 2006; Xu et al., 2000) are used to establish control and motion generation methods for flexible macro and rigid micro mechanisms in which the preservation of the stability and positional accuracy are crucial in the case of the apparent effect of flexibility of the macro manipulator.

In rare cases (Olof et al. 2012, Ulrich et al. 2014), cooperatively working robotic systems (Figure 2.1 b) are called as MMM. In these studies, a smaller micro system

attached to the ground is placed in front of a macro manipulator, is used to process a workpiece simultaneously for industrial processes.

2.2. Research on MMM

In this section, the history and research carried out are presented with respect to the scheme in Figure 2.2. Briefly, the methodology developed for MMM in the literature can be categorized in terms of control, structure, optimization, and analysis. In the structure category, many various MMM types are investigated regarding the mechanisms used, i.e., series, parallel, and cable-driven mechanical systems. Moreover, systems are investigated regarding their flexibility. The control-wise research is categorized with their objective which is the enhancement of the motion capability, force capability, vibration suppression, or combination of these.

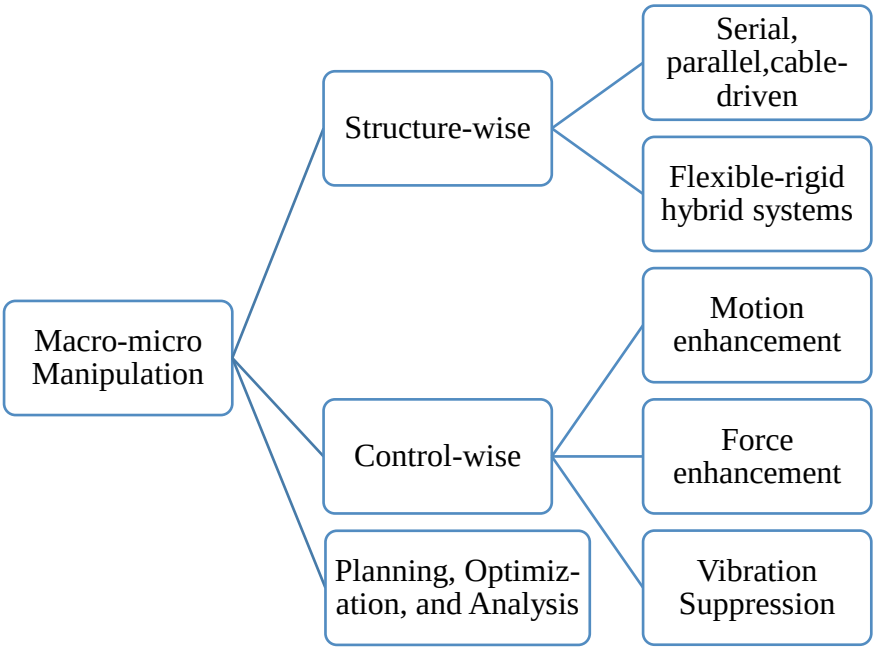

Figure 2.2. MMM research categorizations in the literature.

To the best knowledge of the author, the groundwork for macro–micro manipulation is explicitly the study of Sharon and Hardt, 1984. They propose a manipulator structure by mounting a micro manipulator to the end of a larger manipulator that alleviates the problem of positioning accuracy. The macro-micro manipulation is originated from the need for better accuracy and dynamic performance (Sharon et al.,

1993). Briefly, this feature is originated to distribute the end-effector motion to higher and lower frequency components, which refers to high inertia and low inertia components. They introduced a robust controller to macro-micro manipulator to reduce the endpoint inertia as well as regulating interface forces for a high bandwidth force control. In addition to this, they investigated the dynamic coupling between macro and micro part: subsequently, they concluded that there exists an instability band in the neighborhood of the structural frequency of the macro manipulator (Sharon et al., 1988).

A remarkable example of MMM is the robotics facilities mounted on the International Space Station (ISS). The ISS holds robotics facilities including the Space Station Remote Manipulator System (SSRMS) attached to the Special Purpose Dexterous Manipulator (SPDM/Dextre) and Japanese Experimental Module Remote Manipulator System (JEMRMS), which have been developed using the concept of MMM. The SSRMS attached to the SPDM and the 12 DoF JEMRMS are examples. These facilities are employed for dexterous and fine manipulation for construction and maintenance of ISS, the assistance of extravehicular activities, and operation of scientific experiments or observations (Abiko, 2005). JEMRMS has six DoF macro and six DoF micro manipulator and a total of 11.8 meter reach. Vibration suppression and precise end-point control issues, and adaptive control are studied (Abiko and Yoshida, 2003, Abiko, 2005). For advanced control, reactionless motion control including the vibration suppression capabilities is presented for the same system by (Fukazui 2009). The adaptive control in (Abiko, 2005) is used to adjust dynamic parameters, especially when an unknown payload is present, in the controller to overcome the vibration problem.

Khatib (1988) analyzed control and effective inertial characteristics systems involving macro-micro manipulators. He pointed out that, especially for serial structures, the dynamic characteristics of a combined manipulator are shown to be dominated by the inertial characteristics of the micro-manipulator and utilizing decoupled motion/force control of manipulators this may exceed the inertial characteristics of micro manipulator's alone. Henceforth, the macro-micro manipulators become a field of study for the sake of improving positional and force accuracy as well as dexterous manipulation.

Khatib (1989) also investigated a high bandwidth control to reduce the effective inertia with dynamic coordination of macro and micro manipulators. In his work, control of the macro-micro manipulator is treated as redundant control where null-space motions are reserved to diminish the dynamic effects of the internal motions to the end effector. An experimental study and its discussion on applicability to medical robotics are

proposed by Marzwell et al. (1994) where a force controllable 8 DoF macro-micro manipulator is utilized. Sharon et al. (1994) used a high-performance micro manipulator which has a 5 DoF that can accelerate a 22 kg mass at 45 m/s2, is used in MMM case. In this work, it is deduced that macro-micro manipulation is shown to be inherently stable and well suited for high performance for end-effector control. However, it is criticized that the dynamic coupling of macro and micro mechanism should be taken into consideration and investigated for instability issues.

Types of mechanisms used for MMM concepts vary with the operating conditions and needs. As studied by Tol et al. (2002), a planar 2 DoF micro manipulator is mounted on the Stewart-Gough platform, which is a 6 DoF parallel mechanism for robotic deburring and finishing processes. Micro manipulator is used to carry out the corrections at the path tracking of parallel manipulator throughout its workspace. In another work, a robot arm with macro-micro configuration for lightweight minimally invasive surgery is proposed with spherical mechanisms (Lum et al., 2000). It is proposed that spherical "C-arm" macro-manipulator is to be used to position the dexterous micro-manipulator to overcome collision issue. A mechanism inspired by dexterous motion capabilities of human hand-arm motion coordination is realized as a macro-micro system in (Quan et al., 2016). A 3 DoF robot finger is mounted to the end-effector of a 6 DoF robot arm to imitate a human upper limb. In this study, the macro mechanism is actuated when the demanded motions exceed the motion capabilities of finger-like micro mechanism. A kinematic structure improvement on the positioning of a next-generation giant radio telescope is done by using the macro-micro concept in (Taghirad et al, 2008). This structure is composed of two cable-driven, 3-DoF parallel redundant manipulators at the macro and micro level.

The control algorithms on MMM are heavily based on the dynamic and inertial characteristics of the system in which the manipulators are mostly treated as a coupled dynamic structure as mentioned in the aforementioned studies. Since then, various control objectives and methods are developed for macro-micro concept. In (Luo et al., 2000) a new method for global optimization motion planning of a macro-micro manipulator system based on an estimation of distribution algorithm is developed. Simulations are done for 4-DoF macro-micro manipulator system and the effectiveness of this proposed method is discussed in this study. In (Duan et al., 2011) combinations of cable-driven macro and Stewart platform micro mechanism, supervisory control is devised and tested at the field. To ease the control of macro-micro parallel manipulator system, an adaptive

interaction PID controller is devised as the supervisory controller in the joint space of the micro parallel manipulator. A macro-micro welding robot based on vision navigation is designed in Chen et al. (2010), which is used for seam tracking. The control is done with a task space division method in which motion is planned for the macro mechanism whilst micro manipulator is used to compensating errors in real-time. In the study (Arifin et al., 2013), a general control framework for macro/mini manipulator to improve the force and compliant motion control is introduced. The experimental system in this study comprises of 7-DoF Mitsubishi PA-IO as the macro manipulator and 1-DoF voice coil as the mini manipulator. A force/position controller is devised so that it could reduce the impact when the manipulator makes contact with the workpiece. In this case micro manipulator is used for maintaining the contact forces during the motions of macro manipulator. If micro manipulator reaches its workspace limit, it is proposed that macro manipulator can move along the same axis with the force control. Macro-micro manipulator control architecture is developed by Ma et al. (2016) to enhance the accuracy of robotic machining. An industrial robot KUKA model KR125 is used as a macro mechanism while an external piezo-actuated compensation mechanism is used as the micro system. The integrated system offers significantly higher bandwidth control of the relative position between the tool and the workpiece. In the results of the experiments, it is shown that the proposed approach to machining offers higher accuracy, up to eight times improvement for milling.

2.3. Conclusion on MMM Literature Survey

The foundation of MMM concept is built on motion and inertial capability enhancement of robotic manipulators. Later, MMM is utilized in the long-reach manipulation systems. Best examples of such systems are space robotic applications, e.g. SSRMS, SPDM/Dextre, JEMRMS deployed in ISS. The challenges realized in the controller development of flexible systems led researchers to investigate hybrid flexible/rigid MMM systems. MMM also has been utilized in the fields of manufacturing, medical robotics, and large cable-driven systems.

In Table 2.1 a summary of the literature that involves MMM is given by means of the structure of macro and micro parts; DoF, the objective of the work; validation method; control, optimization, or analysis methodology used. Abbreviations used in Table 2.1 are given below the Table.

Table 2.1. Summary of literature review.

Study	Structure		DoF	Objective	Validation	Methodology	Remarks
	Macro	Micro					
Sharon et al., 1984	S	S	6+5	M	Sim/E	Position Control	MIMO LQ analysis performed
Sharon et al., 1988	S	S	6+5	M/F	E	End-point position control /Force Control	Control achieved in the bandwidth higher than the structural frequency of macro manipulator
Egeland and Sagli, 1990	MB	S	6+6	M	Sim	Coordination of motion in spacecraft and manipulator systems	Recursive formulation of Jacobians and the dynamics Moving base is formulated as in the macro-micro concept
Lees and Lee, 1990	S	S	5+4	M	Sim	Task distribution algorithm	Macro manipulator facilitates a positioning /micro manipulator provides a high bandwidth
Jew and Book, 1993	S	S	2+2	F	E	Hybrid Controller	Control for Flexible manipulator with multiple contacts
Sharon et al., 1993	S	S	-	F	Sim	Robust controller design based on physical equivalence and impedance matching	Reduced the endpoint inertia.

(cont. on next page)

Table 2.1 (cont.)

Zheng and Lu, 1993	P	S	-	M/F	A	Parallel-series connections	Duality behaviors of the two connections of MMM in velocity, force, and inertia are investigated
Marzwell et al., 1994	S	P	5+3	F	E	Impedance Control	Minimally invasive surgery application
Osumi et al.,1995	Flex	S	2+2	F/M	E	Cooperative control algorithm	Two macro/micro manipulators collabrates.
Yoshikawa et al., 1996	Flex	S	2+2	M,F	E	Trajectory planning,quasi-static hybrid (position/force) control algorithm	The micro part is controlled to compensate for the position and force errors
Bowling and Khatib, 1997	S	S	3+3	O	Sim	Optimization techniques are used to determine the design parameters which improve manipulator performance	Design criteria with inertial and acceleration properties
Lew, 1997	Flex	S	1+3	F	E	Force control	Regulation of contact force
Nagai et al.,1997	S	S	3+3	M	E	Compliant control	Development of a micro manipulator is presented for a given macro manipulator
Woosoon and Singh, 1997	Flex	S	1+2	M	Sim	Nonlinear inversion and predictive control techniques	Stability analyzed for Point to point control
Antonelli and Chiaverini, 1998	MB	S	6+3	M	Sim	Task-priority with inverse kinematics	Underwater vehicle-manipulator system

(cont. on next page)

Table 2.1 (cont.)

Potkonjak et al.,1998	S	S	6+2 /3+2	M	Sim	Distributed positioning (DP)	Anthropomorphic robot arm for writing task
Jiang et al., 1999	Flex	S	2+2	M	Sim	End-effector trajectory tracking of flexible macro rigid micro robots	Performance of both end-effector trajectory tracking and link vibration damping/ Used Lyapunov stability theory
Lew et al.,1999	Flex	S	2+2	M	Sim	Acceleration feedback control	Manipulator with 2 DoF compliant base treated as macro manipulator
Nenchev et al.,1999	S	S	1+2			Acceleration based and torque based control laws with	End –effector path tracking base vibration suppression subtask
Shim and Cho, 1999	S	Voice coil	1+1	M/F	E	A conventional passive compliance method and a force feedback control	Robotic probing system for the in-circuit test of PCBs
Yoshida, 1999	MB	S	+2	M	E	Vibration suppression control subtask the reactionless motion control subtask for redundancy	For space robotic application /an experimental setup
Xu et al., 2000	Flex	S	2+2	M	Sim	PD controller with a fuzzy adaptive tuner	Dynamic model, feed-forward signals from flexible macro fed to the rigid micro
Tol et al., 2002	P	S	6+2	M,F	E	Hybrid position/force control	Automated deburring and finishing application
Cheng and Patel, 2003	Flex	S	1+3	M	Sim	Neural network-based control	Control under unmeasurable disturbances

(cont. on next page)

Table 2.1 (cont.)

Abiko and Yoshida, 2005	S	S	6+6	M	Sim	Adaptive control for vibration suppression	JEM-RMS /Space robotics
Cho et al., 2005	S	S	6+1	M	E	Macro-micro manipulation with visual tracking	Wheel assembly application
Parsa et al.,2005	Flex	S	2+2	M	Sim	Computed-torque control.	Control algorithm is developed for stable flexural dynamics
Lum et al., 2006	Spherical S	S (cable driven)	2+6	O		Optimization Algorithm	Aimed to define the smallest mechanism configuration that would satisfy the workspace requirements
Quan et al., 2006	S	S	6+3	M	E	PID controller	Motion generation algorithm according to the manipulability of micro part
Wang et al.,2006	S	P	+3	M	E	Tool trajectory planning	Design of a parallel robotic attachment for industrial machines.
Zhang et al.,2006	Flex	S	2+2	M,O	Sim	genetic algorithm and a neural network	Optimal joint motion generation
Mannani and Talebi, 2007	Flex	S	1+2	M	E	Model-free fuzzy controllers / nonlinear controller	Lyapunov-based stability theory is used
Taghirad et al., 2008	CD P	CD P	3+3	A	Sim	PD Controller	Kinematic, Dynamic analysis for cable driven systems
Fukazu et al., 2009	S	S	6+6	M	S	Reaction null-space based control law	Vibration suppression control via manipulator self-motion / Space robotics JEMRMS/SFA
Harmanpreet et al., 2009	S	CD	4+5	M/F	E	PID with gravity compensation	Design of a novel micro manipulator for brachytherapy

(cont. on next page)

Table 2.1 (cont.)

Huang et al., 2009	S	S	6+3	F	E	Impedance control	A dynamic external force is applied during the experiments
Chen et al., 2010	S	S	2+2	M	E	PD controller with gravity compensation	Welding process based on the vision navigation
Huang et al., 2010	S	S	6+3	M	E	Motion generation	The motion generation emulates the finger arm system of a human-based system
Luo et al., 2010	Flex	S	2+2	M	Sim	Trajectory planning with task space division method	The error compensation and energy consumption are optimized
Bourges et al.,2011	S	P	7+	M	E	Robotic system development for eye surgery	Hexapod Surgical System (HSS) for micro robot and Da Vinci macro robot
Duan et al.,2011	CD	P	6+6	M	E	Spervisory controller, PID controller	Aperture for spherical radio telescope
Pål et al.,2011	S	S	5+4	M	Sim/E	Computed torque control/ motion planning with motion estimation	Experiments cariied out with gantry mech and manipulator to simulate dynamic coupling between a ship and a manipulator.
Olof et al., 2012	S	PZT	6+1	M	E	LQG control	Milling application with an industrial setup
Yun et al.,2012	P	P	3+3	M	Sim, A	Active vibration control strategy	3-PUPU manipulator, dual parallel mechanism combining a 3-PUU with another spatial 3-UPU
Arifin et al., 2013	S	S	7+1	F/M	E	Compliant control	Micro part is used to avoid the loss of contact with the workpiece

(cont. on next page)

Table 2.1 (cont.)

Ulrich, 2014	S	S	6+1	F	E	Composite nonlinear system	Polishing application
Deng et al.,2015	S	PZT	1+2	M	E	Error analysis and compensation	Positioning error compensation for machining application
Lai et al., 2015	S	S	6+4	M	E	Time optimal trajectory planning	Flexible in-vessel inspection robot
Preda et al.,2015	P	S	4+2x5	M/F	Sim	Online collision-free path planner/ admitance control	Novel surgical robot
Stefano et al.,2015	S	S	6+7	M	E	Torque controller based on inverse dynamics linearization	Flexible joint dynamics
Ma et al.2015	S	S	-	M	Sim	Mid-ranging control	Industrial case study
Huang et al.,2016	P	S	3+1	M	E	Position compensator for an industrial robot	High-speed vision sensing
Labrecque et al.,2016	S	S	3+1	M	E	PD combined with a nonlinear function for a macro-mini robot and an optimal admittance control	Impedance mini mechanism specifically designed for physical human-robot cooperation
Barbazza et al.,2017	CD	S	2+2	M	Sim	a multiobjective optimization framework	Minimization of movement time and control effort
Kim et al., 2017	S	P	6+5	M	Sim,E,A	Design and kinematic calibration model	Robot for neurosurgery, deep brain surgery (DBS)
Schindlbeck et al., 2017	S	PZT	6+3	M/F	E	A model-free and decoupled disturbance rejection controller via visual feedback	Industrial robotic manipulator for milling application
Amokrane et al., 2018	S	S	6+1	M	Sim,E	Macro-micro manipulation design	Medical application: ineerdrug drug delivery

(cont. on next page)

Table 2.1 (cont.)

Mohammad et al., 2018	S	S	6+1	F	E	Force control in task space	Robotic polishing cell
Suarez et al., 2018	MB	Flex	6+5x2	M	Sim/E	Vibrations suppression, contact force control, and obstacle localization	A lightweight dual-arm system installed at the base of the aerial platform investigated as macro-micro configuration
Yang et al., 2018	S	Flex	1+1	M, O	Sim	Optimal trajectories using a genetic algorithm and a fuzzy variable structure control with a nonlinear adaptive control law	Optimization indices include the torques and vibrations
Yao et al., 2018	P		3+	M	E	Fuzzy controller and a PI controller	Control and calibration of macro manipulator of macro-micro system

List of abbreviations used in the table:
Flex: Flexible structure
S: Serial structure
P: Parallel structure
M: Motion capability enhancement
F: Force capability enhancement
A: Analysis
O: Optimization
MB: Moving base
CD: Cable-driven
Sim: Simulation
E: Experiment

CHAPTER 3

LASER CUTTING TECHNOLOGY

The breakthrough that led to the invention of laser technology was introduced by Albert Einstein with stimulated emission concept in his publication, “The Quantum Theory of Radiation” (1917). Einstein stated that addition of thermal, electric or optical energy to atoms in the ground state (the lowest energy state of an atom or another particle) converts the ground state atoms to higher energy levels which results in the creation of energy in the form of photon or electromagnetic waves. Einstein also discovered that an incoming photon of a specific frequency (optical frequency) of light energy can interact with an excited atom (laser-state atom), causing a drop to a lower energy level. In effect, the power of the incoming radiation is amplified which is the basis of light amplification in laser amplifiers and oscillators. The acronym for the laser was later introduced by an American physicist, Gordon Gould, in 1957, which stands for ‘‘light amplification by stimulated emission of radiation’’ (Gross and Hermann, 2007)

Since then, the technology for lasers kept growing. First, commercially available laser-based on Einstein’s theory was developed by Dr. Theodore Harold Maiman. It was an optically pumped laser using a ruby crystal as a gain medium (Gross and Hermann, 2007). The active laser medium (gain medium) refers to the source of optical gain within a laser which is caused when high energy photons strike the medium (Steen and Mazumder, 2010). In short, laser mediums can be given as:

i. Solid-state mediums (Ruby, ND YAG, etc.)
ii. Gas mediums (argon-ion lasers, carbon dioxide lasers, etc.)
iii. Liquid mediums (dye laser)
iv. Semiconductor mediums (direct diode)

which are also used to classify the laser types and utilized in various developed applications considering their efficiencies, power rates, costs.

The first experiment, shown in Figure 3.1, led to the industrial usage of lasers was conducted by Peter Houldcroft using oxygen assisted gas to cut 1mm thick steel sheet with CO2 gas mediums. In 1975 the first 2-axis laser cutting machine (Figure 3.1 b) was introduced for commercial usage by Laser Work AG in Switzerland (Hilton, 2007).

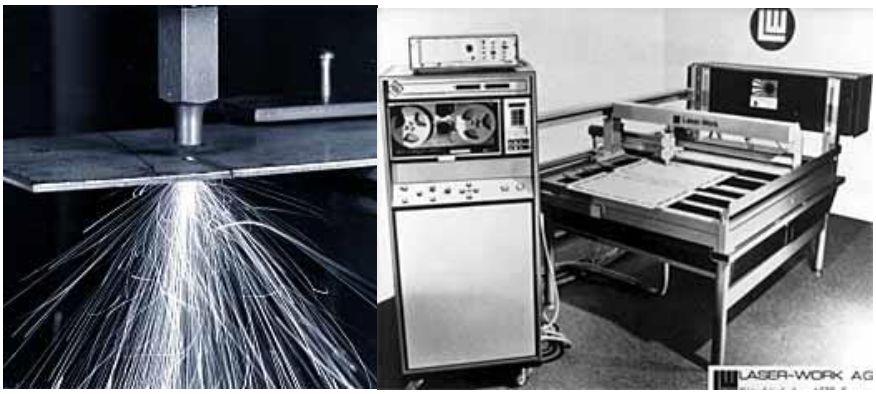

(a) (b)

Figure 3.1. (a) The first laser cutting, 1967. (b) First 2-axis flying optics laser cutting machine, 1975. (Source: Steen and Mazumder, 2010)

3.1. Laser Beam Cutting

Laser beam technology has been successfully used in several machining processes which are cutting, marking, grooving, punching, welding, drilling, cleaning, 3D printing and surface treatment of materials. Unlike conventional machining, laser beam machining is based on the processing without physical contact between the tool and the workpiece. Since the tool is not in contact with the material, no reactive forces are induced on the machine which means there is no constraint such as tool force limits as well as built-up edge formation and tool chatter (Bellows and Kohls, 1982). In addition, laser beam machining has the ability to process most of the materials unbound to the material's hardness. It is possible to process fragile materials with a variety of other materials including metals, ceramics, and plastics, some of which are difficult to process with conventional methods. A wide variety of contours including tiny holes or holes with arbitrary entrance angles can be cut without having any limits on cutting path by the aid of a CNC (computer numerical control). Laser beam machining, additionally, produces quality finishes without additional finishing requirements (Chyrssolouriss 1991). When compared to the conventional cutting methods laser beam cutting is superior regarding material versatility, no wear or change of tool, high material utilization, production flexibility, high accuracy and finishing quality (Hassan et al., 2017). A single machine can be used for drilling, cutting, grooving, welding, and heat-treating processes. On the contrary, there are several disadvantages of using laser beam cutting such as; Laser beam

cutting involves high capital investments and high operating cost. Precautions must be taken since the reflected laser beam can lead to safety hazards. Moreover, cutting of materials is tapered, for especially cutting of thicker workpiece, related to penetration depth (Brown and Arnold, 2010). Assist or cover gases are required which adds to operating costs.

The quality of the cut depends on the assigning process parameters such as laser power, type, the pressure of assist gas due to sheet material thickness and its composition, cutting speed, and mode of operation (CW: continuous wave or PM: pulsed mode) (Meijer et al., 2004). The laser source in laser cutting is either operated on continuous wave (CW) or pulsed modulation (PM) depended on the laser power output (CW: constant output PM: pulsed peak laser output). Gas medium laser sources can mostly be operated in CW, on the other hand, a solid-state medium such as fibers are generally operated in PM. CW laser beams tolerate the smooth cutting of thicker material with higher speeds. On the other hand, PM mode offers better efficiency and better surface finish of thinner material and materials with high thermal conductivity (Meijer, 2004, Sun and Brandt, 2013)

Laser cutting is a thermal process in which a laser beam guided by focusing optics is used to melt the material. The illustration of the laser beam cutting process is shown in Figure 3.2. Focused high energy laser beam heats and transforms the material in the heat zone, which transforms the localized volume of the workpiece into a molten, vaporized, or chemically changed state (Sundar and Joshi, 2009). During cutting, material in the effected zone undergoes different stages:

i. melting
ii. vaporization
iii. chemical degradation (chemical bonds are broken)

The process with laser cutting does not need a lubricant instead does need a continuous flow of assistive gas which aids cutting and evacuates molten material that can easily be removed by the flow of high-pressure assistive gas through the nozzle.

The laser processing mainly differs regarding the laser source used on the machine. For material cutting, CO_2, and fiber lasers are the broadest systems used in the industry besides excimer and diode lasers which are also fast appearing on the market with the recent development (Steen and Mazumder, 2010). Considering the laser sources, each laser type has its own advantages and disadvantages and is suited for their use on

different materials. In Table 3.1, the laser sources used for cutting are listed with their properties (Kellens et al., 2014). The economy and quality of the cut for a laser machine depend strongly on the materials and thicknesses to be cut.

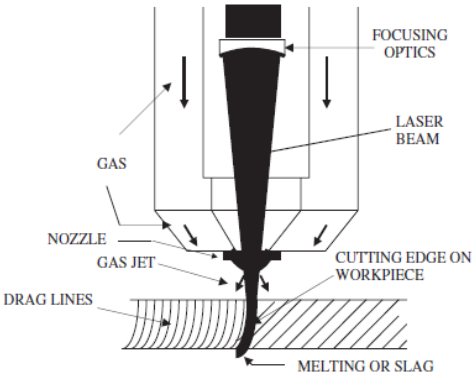

Figure 3.2. Material removal in laser cutting process
(Source: Brown and Arnold, 2010)

CO_2 lasers are one of the earliest used lasers that are based on stimulation of carbon dioxide gas mixture electrically. CO_2 laser cutters are also used in cutting wood, acrylic, glass, paper, textiles, plastics, leather, and stone CO_2 lasers operate on a wavelength of 10.6 μm and have a power range 1.5-6 kW, although some work at continuous power levels of 10 kW and beyond (Steen and Mazumder, 2010). The wavelength of a laser beam plays a vital role in the cutting quality of different workpiece materials and thickness. A wavelength of 10.6 μm, are most suited for working on thick metallic materials, non-metallic materials and on most plastics with better finishing quality. Higher wavelengths are for fine cutting of thicker sheet metal at high speed when operated in CW mode (Ghany and Newishy, 2005). In Table 3.1, in which the comparison of three laser sources is given, CO_2 lasers have drawbacks as lower efficiency, operating hours. CO_2 lasers have relatively lower initial costs but higher operating costs.

Disk and Fiber lasers belong to the solid-state laser group. They generate a laser beam with solid medium and amplify it in designed glass fibers or disks, which are supplied with energy via diode pumps. They are suited for cutting metals, coated metals, and plastics. Having a wavelength of 1.064 μm, fiber lasers produce an extremely small focal diameter which ends up in higher efficiencies during the process (Kellens et al., 2014). In disk laser systems instead of a crystal rod with a low surface to volume ratio, a very thin crystal disk is used as the medium which allows more efficient cooling

(Rodriguez, 2008). These laser types generally have lower maintenance cost but high initial costs with a long service life of at least between 50,000 to 100,000 working hours. They are most efficient in cutting thin metal sheets with better cutting speeds. When compared with CO_2 lasers, they have better wall-plug efficiency and better beam absorption behavior in highly reflective metal sheets due to the shorter wavelength of the generated laser beam. On the contrary, the surface quality is much worse than the CO_2 technology, especially for materials with higher thicknesses (> 4 mm) (Powell and Kaplan, 2012).

Table 3.1. Laser Sources Comparison

(Source: Hilton, 2007; Kellens et al., 2014)

	CO_2	**Fiber/Disk**	**Direct Diode**
Wavelength	10.6 μm	1.06 μm	808 nm- 1550 nm
Operation condition	CW	CW and PM	CW
Efficiency	5- 15 %	20- 35 %	30- 40 %
Lifetime	~20,000 Hours	50,000 To 100,000 Hours	50,000-100,000 Hours
Beam path	Optical path with mirrors Loss of beam quality and significant power drop-off	Fiber guided Flexible and supports up to 50 m	Fiber guided Flexible and supports up to 50 m
Benefits	Relatively Low Purchasing Cost Good Surface Quality	Efficient High Beam Quality Lower Maintenance High Speed For Fusion Cutting Of Thin Sheets	Highest Efficiency Lower Maintenance Compact Wavelength Flexibility Relatively Low Purchasing Cost
Drawbacks	Low Efficiency Mirror Guided	Lower Surface Quality For Thick Materials High Purchasing Cost	Lower Surface Quality For Thick Materials

Recent developments in the diode laser technology made it possible to develop high power and more efficient diode lasers, which eventually become a viable alternative

for material processing. The diode laser power output has already reached to 4 kW commercial applications. Although it has drawbacks, the advantages of diode lasers, creates an opportunity to expand the field of applications for this technology. As given in Table 3.1, the direct laser diodes have better wall-plug efficiency than fiber and CO_2 lasers (Bruns, 2012). Compared to other laser sources, laser diode's apparatus are more compact and lightweight, which makes it easier to adapt existing systems, especially to robotics and automation applications. They have wavelength versatility but in shorter lengths, which makes them disadvantageous for a specific process. Direct diode lasers also have lower cooling requirements, higher life, and lower running costs but have low beam quality especially in comparison with CO_2 lasers (Rodrigues et al., 2014; Huang et al., 2012).

3.2. Laser Cutting Machine

A representative illustration of a conventional planar laser cutting machine is presented in Figure 3.3, which shows the typical components of the machine. As indicated in Figure 3.3, laser cutting machine contains a laser source generator (resonator), a cooling unit (chiller), focusing head, and assistive gases, positioning mechanism, beam and gas delivery systems as well as control and operator unit. The laser source diverges as with the laser medium used, power and operation mode for the dedicated cutting material which is explained in the previous section. The cooler (chiller) is essential since the laser generation is an exothermic process and must be cooled efficiently to be operated at peak efficiency. The type of laser source, laser power, and chiller choices are main aspects in assessing the power consumption and energy efficiency of the machine. Laser cutting machines require extraction and ventilation module since laser cutting process produces a high amount of hazardous contaminants that need to be removed to protect the operator and ensure the quality of cut (Frevel et al., 1995).

In planar cutting, the motion along the X-axis generally refers to the motion on the gantry while the motion along the Y-axis refers to the motion of the gantry. The axes are actuated mostly by servo motors by direct or geared transmission with the aid of motion controllers in communication with the CNC system. There exists many ways to build linear systems for motion in the X-, Y-, and Z-directions, also known as Cartesian coordinates.

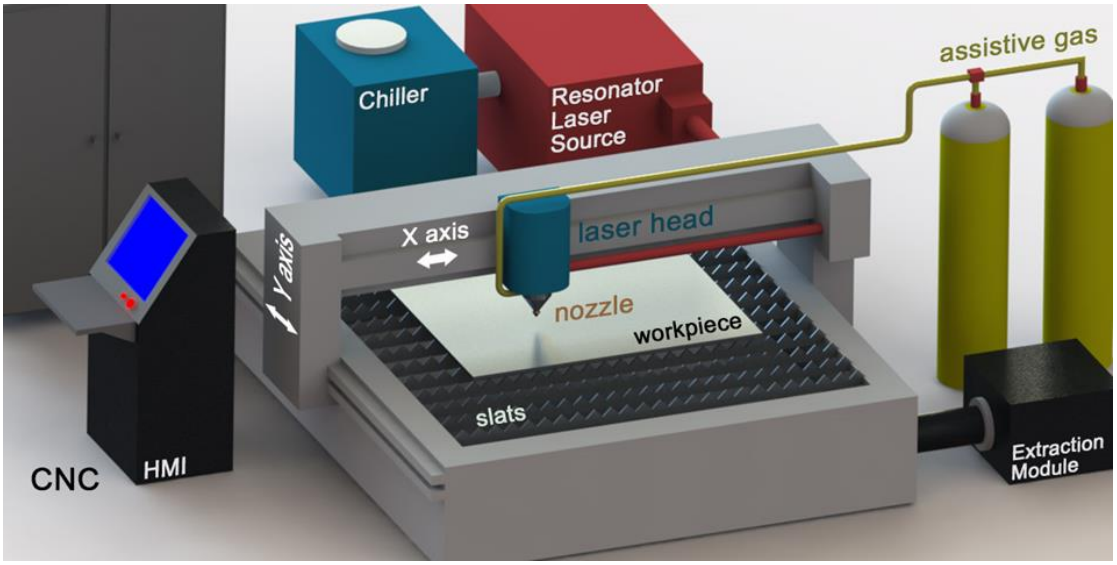

Figure 3.3. An illustration of a conventional planar laser cutting machine.

Additionally, alongside the axis of the cutting plane (z-axis) a small stroke motion is actuated, usually with a capacitive sensor, to keep the material and nozzle distance constant in case of surface defects. Assistive gases are used to aid cutting by directing the laser beam through the nozzle and evacuates processed material. O_2 and N_2 are the commonly used assistive gases depending on the workpiece material. The assist gas flow is controlled by electronic valves delivered to the laser (optic) head through a proper pipeline. For a specific cutting process, the gas flow rates are calibrated mainly by material type and cutting speed. In short, the assistive gases prolong cycle rate of the optical component, improves the cutting quality, and allows cutting at higher speeds (Chen et al., 2001).

Beam delivery is another crucial part of laser machines in means of laser beam efficiency. CO_2 laser cutters are guided with mirrors, which results in loss of beam quality and significant power drop-off (Kellens et al., 2014). On the other hand, solid-state and diode lasers utilize fiber guided delivery systems which are more efficient and flexible (Sun and Brandt, 2013).

A CNC controller automates the laser cutting process with embedded pre-processed and on-line real-time algorithms. The CNC unit calculates and adjusts travel position, speed, acceleration, jerk, laser power, air and gas flow, beam output, beam delivery factors, and other parameters of the laser cutting process. The contours to be cut are defined using computer-aided design (CAD) software and then translated into

machine's codes (mainly G-codes) by computer-aided manufacturing (CAM) software which is compatible with the CNC unit. Most of the machines are operated with preprogrammed algorithms require little intervention of the operator via the operator panel which uses a human-machine interface.

3.2.1. Laser Cutting Machine Configurations

A laser cutting machine has an optic head where a laser beam is condensed by lenses and collimated in order to be applied to a workpiece. In conventional planar laser cutting machines, the laser optics and the workpiece are moved relative to each other to cut a certain pattern. This optical axis movement controlled by CNC machine depends on machine configuration (Sun and Brandt, 2013). Regarding this, laser cutting machines can be categorized as in Figure 3.4. Briefly, there are five categories for their movements comprises of moving material, flying optics, hybrid type of moving material and flying optics, tube cutting, robotic cutting. Tube cutting and robotic cutting type machines are generally used for three-dimensional cutting approaches.

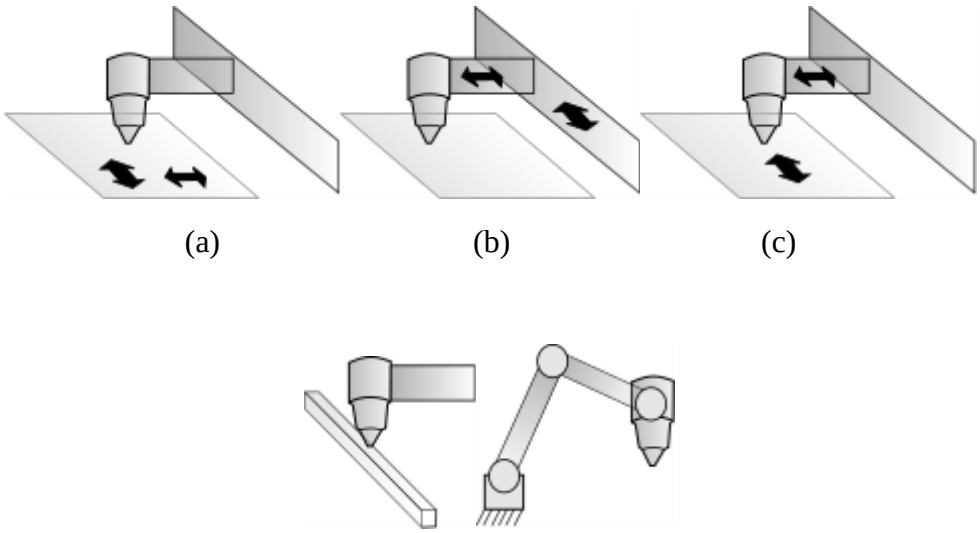

Figure 3.4. Laser cutting machine configurations (a) Moving material, (b) Flying optics (c) Hybrid, (d) Tube cutting, (e) Robotic cutting.

For planar and some 3D laser cutting machines mostly Y-axis represents the motion of the gantry on rails. Thus X-axis is reserved to the optic or moving material

motion on gantry motion. By actuating each axis and coordinating the motion of the two axes simultaneously, the planar cutting is realized. The motion in X-axis varies by the type of the structure: it could either have rails in double sides (gantry or bridge types), one side (cantilever type), or be fixed (column type) (Grote and Antonsson, 2009).

Laser cutting machines that feature the moving material configuration have a stationary laser optic head and a movable cutting table to which the material is affixed. One of the benefits of using moving material laser cutting machines is that they allow the workpiece to be kept at a constant distance from the laser nozzle. This type of laser cutting configuration requires fewer optics, and beam delivery is less complicated. In Figure 3.5, Preco SL series laser cutting machine that has moving XY table is shown. As can be seen in the figure, both X and Y axes are actuated from the base.

Figure 3.5. Preco SL series Laser cutting machine in moving workpiece configuration. (Source: Preco SL)

The most common machine configuration is flying optics cutters in which the laser moves while the material is stationary. In most applications, the material does not need to be clamped since no tool-workpiece contact exists. The cutting laser on flying optics systems can move over the material on both the X- and Y-axis as shown in Figure 3.6, and this flexibility fosters faster processing times. During cutting with flying optics the

changing beam length and beam transmission during has to be taken into consideration, in such cases laser sources that can be fiber guided are advantageous.

Figure 3.6. Prima Power Platino laser cutting machine with flying optic head.
(Source: Prima Platino)

Hybrid laser cutting machines feature a combination of the motion of both cutting table (moving material) and optic head. In this configuration, mostly, the material table moves on the X-axis, and optic head moves on Y-axis as it is in TLV series of Ntclaser, in Figure 3.7. Hybrid Laser cutters have a more straightforward laser cutting delivery system in specific applications and have a more continuous laser beam delivery when compared to flying optic laser systems.

Figure 3.7. Ntclaser TLV Series X-axis moving table and Y-axis moving optics.
(Source: Ntclaser TLV)

Another hybrid type laser cutting configurations is tube cutting systems which are utilized for precision cutting of tubes, profiles, and pipes. Generally, the workpiece is

rotated under the optic head which also has motion along the tube. With the capability of cutting a variety of shapes and materials, tube cutting is cost-effective, fast for tube oriented cutting. Trumpf Trulaser series Tube 7000 laser tube cutting machine in Figure 3.8 displays how a profile workpiece is cut.

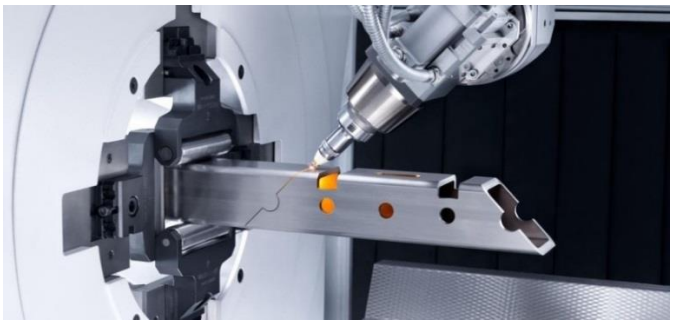

Figure 3.8. Trumpf Trulaser tube cutting machine.
(Source: Trumpf Trulaser 7000)

Although three-dimensional cutting can be realized by using 5-axis cutting machines which have extra two actuation besides, a robotic arm can be used to direct the laser beam. Ease of integration to the automation system with commercial robots is particularly adapted to the automotive industry for its versatility and redeployment. The robot-aided cutting allows cutting detailed contours on complex surfaces, in some cases, even kinematic redundancy is utilized to direct the laser beam onto hard to reach zones of the workpiece (Dolgui and Pashkevich, 2009). In Figure 3.9, Trumpf TruLaser Robot is shown where robot cutting is implemented into a hybrid cutting method.

Figure 3.9. Trumpf TruLaser Robot Series 5000.
(Source: Trumpf Trulaser 5000)

3.2.2. Dynamic Cutting with Planar Laser Cutting Machines

Regarding the machine configuration, parameters such as laser power, laser intensity, operation mode (CW or PM), focal length, focal position, nozzle diameter, and limits of the mechanism are used in assessing the performance of the process. However, these parameters are mainly already limited/bounded pre-purchasing a laser cutting machine and should be considered regarding efficiency, cost, technology, process, process material and quality of end product. Apart from machine configuration, cutting performance may be altered by the process parameters that are generally handled by the operator such as cutting speed, piercing time, assistive gas pressure, etc. These parameters are chosen, for a specific cutting machine mostly depended on the workpiece material and thickness. In short, in laser beam cutting, task completion duration, quality and cost of the process depends not only on the capabilities of the machine and laser source but also the workpiece material and thickness (Meijer, 2004; Chyrssolouris, 1991)

One of the emergent issues in the laser cutting process is shortening the process completion duration. Not only the laser source development but also machine configurations offer a remedy to this issue. Since the cutting speed is limited by laser power and workpiece properties, one way to shorten the process completion duration is dynamic cutting. Dynamic cutting can be realized with tool path optimization or development of trajectory generation algorithms such as on-the-fly cut tool path generation. Employing mechanical properties of the machine, dynamic cutting refers to machines with better acceleration capabilities. The dynamic cutting makes its case, for shortening task completion duration, especially where complex and small contours are frequently cut. Complex cutting contours with small detailed shapes add up to short strokes on machine axes which in some cases even make the axes impossible to reach the maximum allowable tool speed. Cutting in such cases with conventional planar laser-cutting machines, which are built to cover the whole sheet metal area, raise difficulties due to large inertial properties of the construction that is moving the tool in X- and Y-axes. As a result, machines with better acceleration capabilities with respect to conventional planar laser cutting machines are introduced in the commercial market by leading companies in the industry. The cutting machines developed for such systems mostly use fiber lasers and have an operating range of 2 to 4 kW. In Table 3.2, remarkable commercial planar laser cutting machines developed by international companies with the

highest dynamic capabilities are listed. These laser cutting machines are compared with respect to their axes properties, accuracy, repeatability, and maximum acceleration limits in Table 3.2.

Table 3.2. 2D Laser cutting machines in the market with high dynamics.

	Trumpf	Bystronic byspeed 3015	Amada FOL AJ	PrimaPower Syncrono	Salvagnini L5
Power	4 kW	4.4 kW	2-4 kW	2-4kW	2-4 kW
Axes	XY+x	XY	XY	XY+uv	X+ yθ
Workspace	XY: 2540x 1570 mm	XY: 3070x 1550 mm	XY: 3070x 1550 mm	XY: 3050x1540 mm UV:100x100m m	XY: 3048x152 4 mm
Maximum Speed	X axis: 100 m/min Y axis: 60 m/min Combined: 116 m/min	X&Y axes: 120 m/min Combined: 169 m/min	X&Y axes: 240 m/min Combine d: 340 m/min	X&Y axes: 100 m/min u&v axes: 100 m/min Combined: 200 m/min	X&Y axes: 120 m/min
Maximum Acceleration	-	30 m/s^2	5 g	XY: 0.8 g uv: 6 g	5 g
Positional Accuracy	±0.1 mm	±0.1 mm	±0.01 mm	XY: ±0.03 mm uv: ±0.02 mm	±0.08 mm
Repeatability	±0.03 mm	±0.05 mm	-	XY: ±0.03 mm uv: ±0.02 mm	±0.03 mm
Maximum Sheet Thickness (Mild Steel)	8 mm	20 mm	22 mm	10 mm	20 mm

To make the laser cutting machines more dynamic with higher acceleration capabilities, different companies utilize different approaches in their products drive systems. One of which is using line drive systems, synchronized components for optimum performance, and high processing accuracy of drive systems. Amada, from Japan, introduced FOL AJ Series planar laser cutting machine with the highest traveling speeds in the market with these configurations. Both the laser resonator and the machine designed by Amada, this series can reach 240 m/min of traveling speeds in *X*- and *Y*- axes

with 5 g acceleration capability. Another planar laser cutting machine is developed by Bystronic, from Switzerland, with 30 m/s^2 acceleration capability and 120 m/min maximum speed.

Another approach used to enhance the acceleration capability drastically is designing the machine kinematically redundant by adding extra degrees of freedoms, or in other words with macro-micro manipulation. Trumpf, from Germany, in their machine Trumatic 7000 come up with a solution to increase the acceleration of the machine by adding an additional axis alongside the X-axis, namely making the configuration of machine *XY+x*. Trumatic 7000 is introduced as a combination of laser punching and cutting machine. The movement of additional axis combined with other axes increasing the maximum combined axis speed to 116 m/min (Leibinger, 2004).

PrimaPower Company, from Italy, designed Syncrono Series machine with two additional axes (Figure 3.10). The conventional axes (*X* and *Y*) are used to position optic cutting tool in macro displacements, and the additional two axes (*u* and *v*) are used to move in the local range of mechanism, respectively in the smaller workspace.

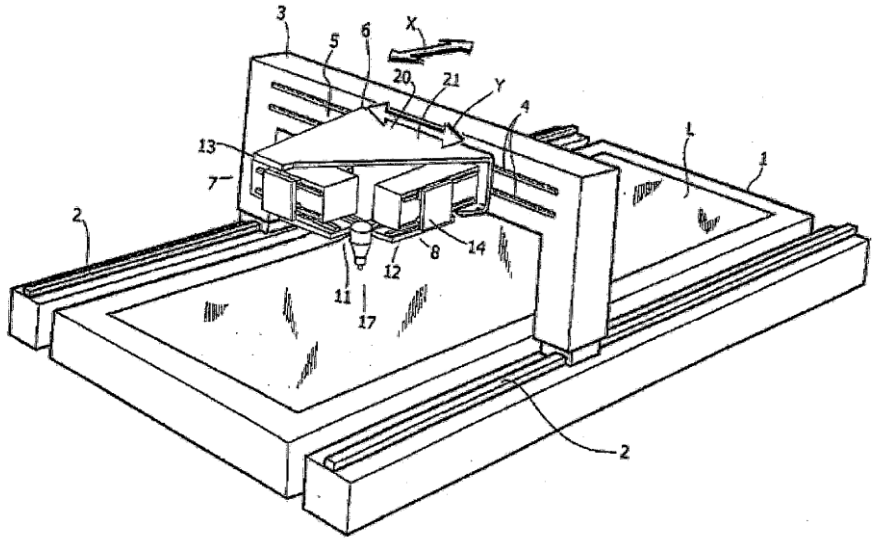

Figure 3.10. Syncrono redundant laser cutting machine.
(Source: Sartorio, 2004)

Syncrono has the capability of reaching 6 g acceleration with PPPP (P: Prismatic Joint) mechanism (Sartario, 2004; Gattiglio et al., 2008, Gattiglio and Chirico, 2011). The X and Y axes, which have larger inertias, realizes only the large movements; while local mechanism axes make the dynamic motion for smaller displacements with small inertia

and high acceleration. They also studied the dynamic balancing of the local axes (Sartario and Babli, 2006) and devised a redundant control algorithm (Cardinale et al., 2007) for driving the system. Salvagnini, from Italy, introduced L5 series cutting machine (Figure 3.11) with high dynamics by using local PRRRP (R: Revolute Joint) mechanism (Battheu, 2011; 2012) The additional revolute joints allow the optic head to be moved parallel to the XY plane over a distance of 170 mm, with dynamics of up to 5 g. In this mechanism, two actuated slides are positioned on the gantry which has motion along the *X*-axis, which is realized to create motion on machine's *Y*-axis alongside with gantry's motion. Hence the large displacements are performed with the gantry *X*-axis while the local, frequent displacements are performed with the combination of the three axes (*XY+y*).

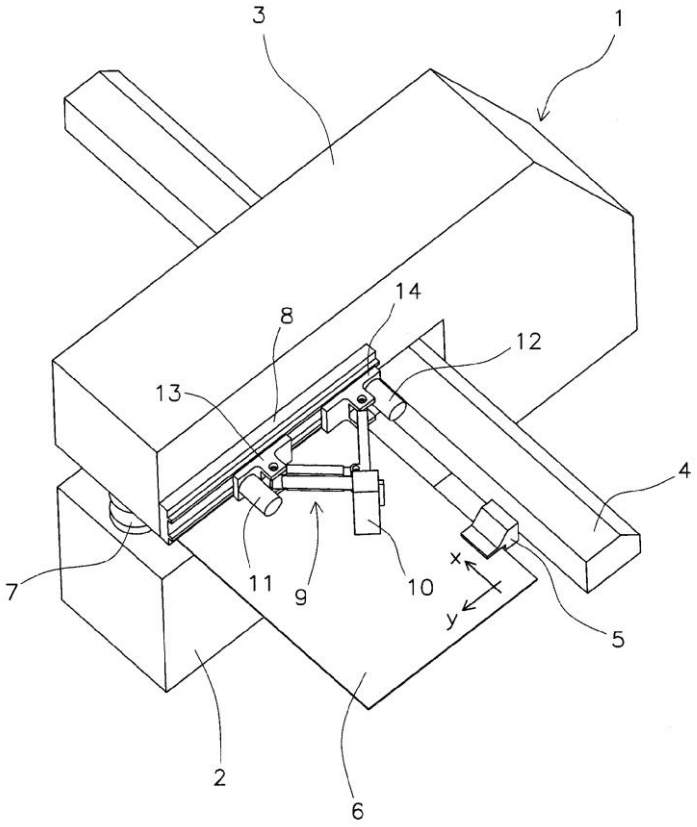

Figure 3.11. L5 series redundant laser cutting machine.
(Source: Battheu, 2011)

CHAPTER 4

ALGORITHMS FOR THE CASE STUDY

In this Chapter, a brief description of the case study (planar manipulation case) and the developed algorithms are presented. First, the motion planning problem is discussed emphasizing on the case study of this dissertation. Later, considering the problem definition and the system setup, three different trajectory planning solutions are devised for the MMM. The main difference of developed algorithms is that one of them works as an offline post-processor while for the other two, the trajectory for the micro mechanism is generated with the semi-online method which is presented for MMM structure. In both methods, generated G-codes for the tool path behavior are used. First, the description of the MMM is presented for a better understanding of devised algorithms. In the next sections, these three algorithms are explained. Following that, as a conclusion, a discussion is made on the feasibility of the methods.

4.1. Survey on Motion Planning Problem

The motion planning problem is defined as finding a motion law along a given geometric path by taking some predefined requirements into account, in other words, to be able to generate suitable reference inputs for the control of the system (Craig, 2005). The inputs of a motion planner can be a geometric path, kinematic, and dynamic constraints. The outputs are the trajectories of the joints or the end-effector, expressed as a time sequence of displacement, velocity, and/or acceleration values. Most of the proposed motion planning algorithms are based on a minimization of an objective function that depends on execution time, actuator effort, the absolute value of the jerk, or a combination of these variables.

The motion planning algorithms can be grouped into two categories: predefined path and point-to-point planners (Chebetti et al., 2004). If the end effectors have a predefined path that obliged to follow, such as in arc welding, laser cutting operations, the planner defines the optimal tracking modalities of the imposed path. In this cases, path

planning algorithms, constraints are path geometry, admissible velocities and accelerations, and joint torques or forces. For point-to-point motion as in pick-and-place operations, the end effectors motions between targets are designed to achieve optimal trajectory.

Depended on execution time, the trajectory can either be generated entirely pre-process, off-line or can be generated concurrently during the process, on-line. Off-line trajectory generation methods are convenient for machining, so for applications where all the process parameters can be calculated prior to the process. On the contrary, in online trajectory generation, the algorithm should be devised to complete planning action prior to the next step. The online trajectory generation algorithms are broadly used in systems in which the system confronts a change of state in the system or in the environment.

The first proposed trajectory planning techniques are minimum-time algorithms due to the need for increased productivity in the industry (Lin et al., 1983; Piazzi and Visioli, 1998). The main disadvantage of minimum-time algorithms is that the trajectories may have discontinuous values of acceleration and joint torque; hence, dynamic problems arise during the execution of the trajectory. In order to generate trajectories with continuous accelerations, a common strategy is to use smooth trajectories, such as the spline functions, that have been extensively employed in the literature on both kinematic and dynamic trajectory planning (Wang and Yang, 1993; Flesig and Spence, 2001). An alternative approach lies in minimizing energy consumption instead of the execution time (Field and Stepanenko, 1996). This approach leads to smooth trajectories, with smaller stresses on the manipulator structure and forces on the actuators.

The trajectory generated by the planner must not excite the mechanical resonances of the manipulator, which leads to the generation of smooth trajectories, i.e., the trajectory itself and its derivatives are continuous functions. In particular, it would be desirable to obtain trajectories with continuous joint accelerations, so that the absolute value of the jerk is bounded. Limiting the jerk is crucial, because high jerk values can wear out the mechanical structure, and can heavily excite its resonance frequencies. Vibrations induced by non-smooth trajectories can damage the robot actuators, and introduce significant errors while the robot is performing tasks such as trajectory tracking. Moreover, low-jerk trajectories can be executed more rapidly and accurately (Sonja and Croft, 2003).

As a result, trajectory planning by taking jerk objectives into consideration allows reducing the errors during trajectory tracking, the stresses to the actuators as well as to

the mechanical structure of the robot, and the excitation of resonance frequencies. Kyriakopoulos and Saridis (1988) exploit the Pontryagin Principle to obtain minimum-jerk point-to-point trajectories through a mini-max approach. Simon and Isik (1993) use trigonometric splines to interpolate the trajectory, ensuring the jerk continuity. Piazzi and Visioli (2000) use an interval analysis method to generate trajectories which globally minimize the maximum absolute value of the jerk along a trajectory whose execution time is set a priori: hence, an approach of the type minimax is used. The trajectories are expressed utilizing cubic splines, and the intervals between the via-points are computed so that the lowest possible jerk peak is produced.

Many researchers similar to Luh and Gu (1985), has been investigated the trajectory planning problem for redundant manipulators in industrial robots. Mostly, there are three main approaches for trajectory planning of redundant manipulators: pseudo-inverse of the Jacobian matrix, variational approach, and optimization techniques (Ata and Myo, 2005). A conventional way to realize the motions on redundant systems can be done with the calculation of inverse kinematics employing a pseudo-inverse of the Jacobian matrix. The commonality of these approaches is that a side task is utilized in the self-motions of the kinematically redundant systems.

Martin et al. (1989) presented a variational approach by taking positional constraint and joint variable functions into consideration and obtains an optimization of the integral cost function. A new scheme based on the variation approach is proposed by Sakamoto and Kawamure (1994), in which the trajectory in the joint space is modeled as a B-spline curve, and the performance index is integrated in a straightforward manner through the desired trajectory of the end-effector. A method by Hirakawa and Kawamura (1996) is introduced to solve the trajectory generation the variational approach, and the B-Spline curve are introduced for minimization of the consumed electrical energy.

Davidor (1991) applied genetic algorithms (GAs) to the trajectory generation by searching the inverse kinematics solutions to pre-defined end-effector robot paths. The trajectory planning is carried out in the joint space, and the path is represented by knots connected through cubic splines. Pires et al., (2001) propose an evolutionary method which optimizes the robot structure and the required manipulating trajectories.

In the industry, there are few examples of laser cutting machines which adapts kinematic redundancy. Three different approaches were found in the industry that makes use of this redundancy. A system (Figure 4.2) was designed by Sartorio (2004) to decrease

the process duration while preserving the positioning precision, as mentioned in Section 3.2.2.

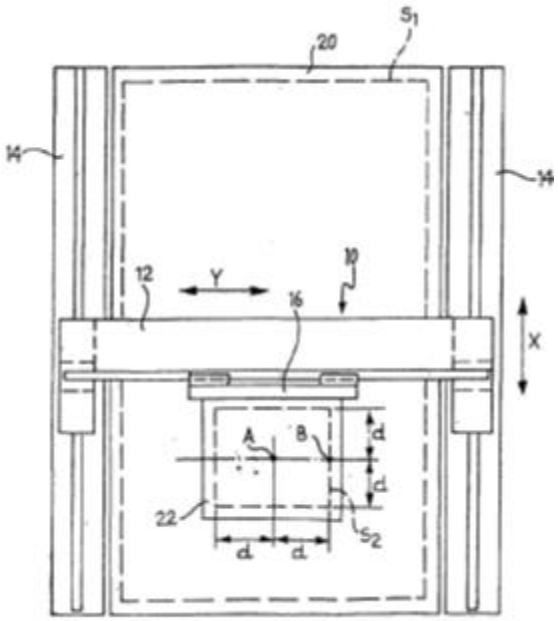

Figure 4.1. A system described for redundant laser cutting machine
(Source: Sartorio, 2004)

The system indicated with number 22, in Figure 4.2, is the micro and lightweight machine that generates kinematic redundancy to the machine. The conventional axes, presented by 10 in Figure 4.2, is aimed to work simultaneously with redundant axes. In this methodology, the lightweight system's motions are to be designed with the highest possible acceleration. Sartorio (2008) came up with a trajectory planning scheme where the velocities of distinctive parts are denoted with v_1 and v_2, as shown in Figure 4.2. The main aim of this method is to reach the highest cutting speed, v_t, as soon as possible (Figure 4.2).

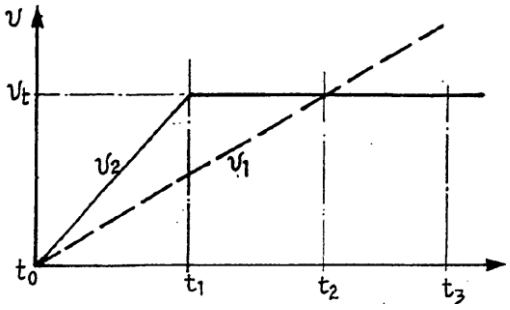

Figure 4.2. The trajectory generation scheme used by Sartorio.
(Source: Sartorio, 2008)

Meanwhile, the axis presented with 10, is required to achieve the same cutting speed t_2 in time and even exceed the highest cutting speed. Thus, the main axes can recover the lost time and stay within the boundaries of the lightweight system, s_2, as shown in Figure 4.2. Associated with the systematic methods mentioned in Sartorio (2008), the speed and acceleration of the local axes and the speed of the tool have to be limited to remain within the workspace boundaries. In this method no redundancy resolution is devised in control by making use of algebraic equations describing the self-motion, instead an offline preprocessing algorithm is used to generate the motion demands separately.

In another study (Leibinger et al., 2004), the two actuators were reserved for the main *X* and *Y* axes, while the third actuator was used for the rapid movements of the cutting tool. Figure 4.3 shows the flow diagram of the algorithm used in the study. In this case, a motion division is realized between the main and redundant axes considering the workspace, but it is understood that there is no supervision for the regulation of internal motion for optimization purposes.

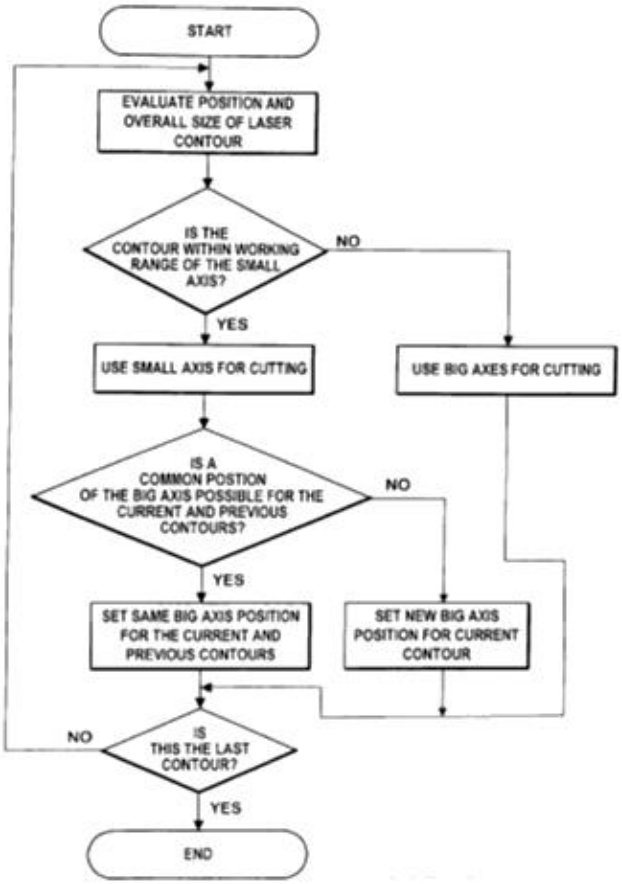

Figure 4.3. A control strategy used in redundant laser cutting machine.

(Source: Leibinger et al., 2004)

Figure 4.4 summarizes the supervisory system used in another study (Cardinale et al., 2007). In this system, the cutting trajectory parameters from the CAM program or similar system are specified by *Xs* and *Ys*, while the main axis variables are indicated by *X* and *Y* and the local axis variables are indicated by *U* and *V* as shown in Figure 4.4. They utilized a smoothening on the cutting trajectory to create the trajectory of the main axes. Moreover, the trajectory of the local axes is formed by taking the difference between the cutting trajectory and the main axis trajectory.

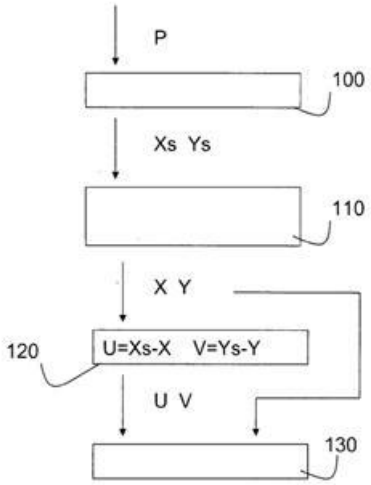

Figure 4.4. Main and redundant axes motion generation flow.
(Source: Cardinale et al., 2007)

4.2. Description of the Planar MMM

In the scope of this work, the major concern is to increase the acceleration limits of the conventional laser cutting process using the macro–micro manipulator concept. Hence, the process duration would decrease, especially cutting thin materials with complex contours. The tool/end-effector motion must be generated to track a definitive trajectory while keeping the acceleration of the macro mechanisms limited at 1~1.5 g. The limitation for the macro mechanism is set to avoid high amplitude vibrational behavior due to large inertia of the macro mechanism, which otherwise would have resulted in imprecise motion. The total acceleration limit aimed for the tool trajectory is set at 6 g at the beginning of the project. However, this limitation is lowered to 3.5 g due to the limitation of the chosen harmonic drivers and the maximum acceleration the laser cutting head can handle.

Another limitation of motion planning is the boundaries of both macro and micro mechanism's workspace. The workspaces of the macro and micro mechanisms are limited as 3 m x 1.5 m and 0.1 m x 0.15 m, respectively. An illustration of the macro–micro mechanism design is shown in Figure 4.5, where macro and micro mechanism's axes are denoted, respectively, by X-Y and u-v. In Figure 4.5, the micro manipulator is presented with red lines, the macro manipulator is presented with blue lines, and the workspace of both manipulators are presented with dashed lines.

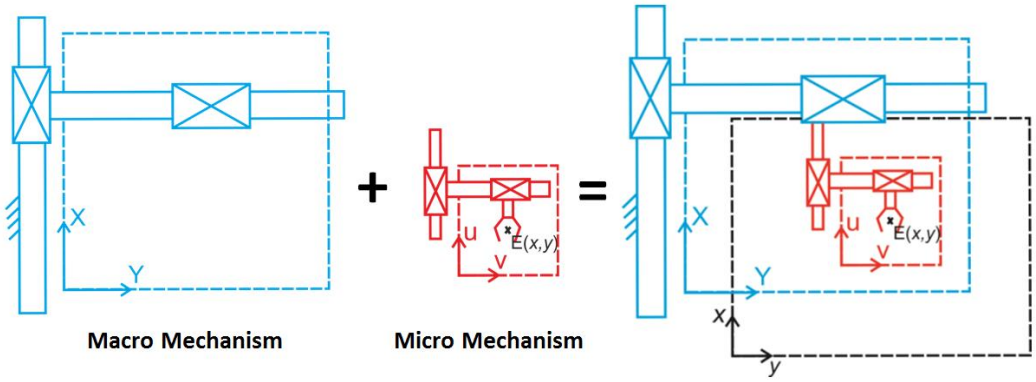

Figure 4.5. Macro-micro mechanism representation.

Planar redundant manipulator that is used in aimed trajectory generation algorithms is composed of two mechanisms that have independently controlled two DoF in planar space. As illustrated in Figure 4.5, the micro mechanism, with relatively smaller workspace, is mounted onto the macro mechanism, which has lower acceleration capabilities due to its higher inertial properties. End-effector is assembled on the micro mechanism, which gives the desired output *E(x,y)* of motion as a result of unified motions of the two mechanisms.

The motion of the macro mechanism is indicated with capital *X* and *Y*, while the micro mechanism's motion happens along *u*- and *v*- axes. The workspace location of *u* and *v* axes, which is shown in red in Figure 4.5 depends on the position of *X*- and *Y*- axes. End-effector path, in this case, is defined with respect to the global coordinates, which are *x*- and *y*-axes. It should be noted that, since the designated system is planned to be used in industrial applications, such as machining tools, the end effector velocity is limited for the application type. For example, during operation, a mounted tool will be

most likely required to have relatively lower speed limit below the maximum achievable speed of mechanism for proper operation.

4.3. Velocity Level Planning Algorithm (VLPA)

Trajectory planning algorithm is developed to achieve the main task, which is position tracking of end-effector provided in the global workspace. In general, the algorithm uses the advantage of higher acceleration capabilities of micro, low weight mechanism to reach the maximum allowed velocity of endpoint, *E*, as quickly as possible. Unlike defining a main task and subtasks for redundant mechanisms, this algorithm comprises trajectory planning and control of two different mechanisms simultaneously. A possible solution to achieve a high acceleration trajectory planning algorithm for redundant manipulator can be determined in the velocity profile generation level. In this algorithm, the end-effector velocity profile is designed to have a trapezoidal velocity profile with the highest possible acceleration for the end effector as earlier proposed by Sartorio (2004). The main aim is to shorten the task completion duration with respect to the task completion duration of the conventional machine with only two axes.

The generated algorithm is devised to distribute the global motion demand to the main axes (macro mechanism) and redundant axes (micro mechanism). Advantage of the algorithm is proved by numerical examples conducted for both machining and traveling segments. However, the algorithm has a practical disadvantage that in real-life conditions, jerks are not infinite as utilized in this algorithm. The effects of this disadvantage is investigated and compensation for these effects are devised with another algorithm.

The main function of the algorithm is to deploy end-effector position demands extracted from G-code segments on MMM to utilize formerly mentioned capabilities. Trajectory planning algorithm is designated to be used as a built-in function in between G-code extractions of MMM and machine controller, which is typically a CNC system. The input data for motion planning are extracted from G-codes as segments in two categories; machining segments or traveling segments.

In machining segments, the maximum speed of end-effector, or machining tool expressly, is limited by machining process type specifications. On the other hand, the traveling segments are created as the positioning of the tool before or in between machining segments with maximum motion capabilities of MMM. After the segments are

created, the algorithm creates motion profiles sequentially with respect to the presented flowchart in Figure 4.6. Segments data is fed as input to the motion planning scheme, which contains information about motion (distance traveled, start and endpoints of the segment) and segment type. At first, the algorithm checks if there are any motions on the macro and micro mechanisms from previous segments while the end-effector is kept at a fixed position, which is further discussed in the next sections. After, if necessary, when acceleration adjustment is completed, the algorithm generates the velocity profile according to motion limitations for either traveling or machining segments.

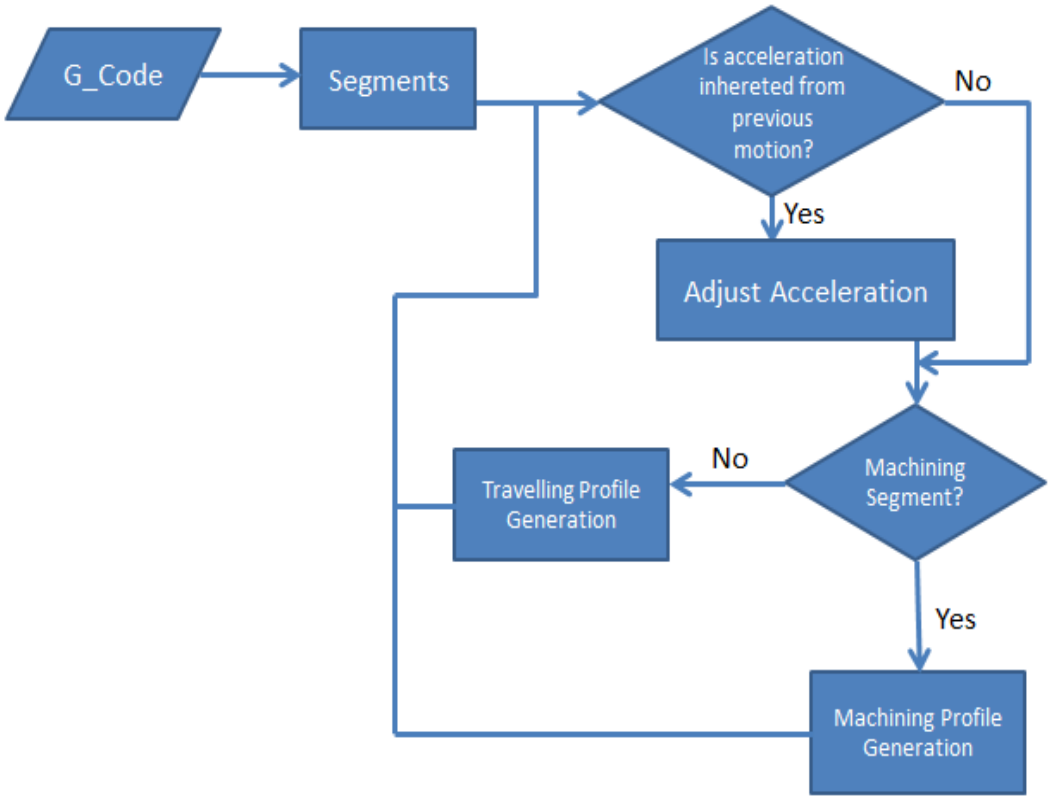

Figure 4.6. Flowchart of VLPA.

In this study, the acceleration of the macro axes are designed to be limited with 1 g for macro mechanism and 5 g for the micro mechanism, and end-effector velocity is limited with 40 m/min. The maximum velocities are set as 200 m/min for the macro mechanism, and 100 m/min for micro mechanism. The position demands delivered to the micro mechanism were held within workspace limitations as predesigned between ±50 mm along both *u* and *v* axes.

4.3.1. VLPA for Machining Segment

A machining segment represents the motions that the end-effector follows during working on a workpiece. With redundancy resolution, this is achieved by adding two independently created velocity profiles for the macro mechanism, v_a, along X-Y axes and micro mechanism, v_b, along u-v axes to obtain the end-effector velocity profile. In order to explain the algorithm, a continuous velocity profile, which is usually a small part G-code sequence, is illustrated in Figure 4.7. The velocity of the end-effector is limited with v_e (max), which is the velocity limit for the designated machining process. The profile generation is designed such that the micro mechanism is designated to start the motion in the middle of its workspace, which is marked in red in Figure 4.3.

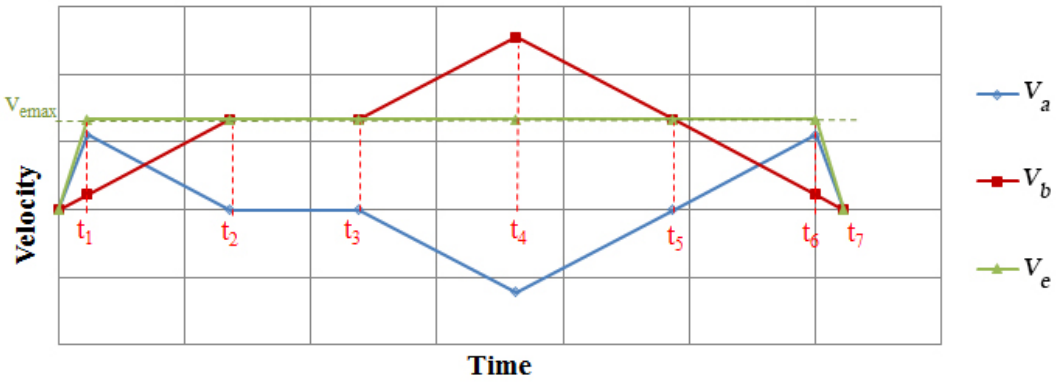

Figure 4.7. VLPA motion generation for machining segments.

After $v_e(max)$, maximum tool velocity, is reached with combined accelerations of two mechanisms, velocities of the two mechanisms are consistently regulated to preserve end-effector velocity at $v_e(max)$ until t_6. After the macro mechanism reaches the $v_e(max)$ at t_2, the velocity of both mechanisms are kept constant until t_3. The velocity of macro mechanism exceeds the end-effector velocity between t_3 and t_5 in order to retract the micro mechanism to the mid-position of its workspace. As a result of this, at the completion of the total motion, the relative position of the micro mechanism will be at the middle of its workspace to be ready for the next motion segment. Advantage of this algorithm is that the acceleration and deceleration are much higher at the beginning and termination of the motion, which shortens the total task completion duration.

As a numerical example, motion planning of a machining segment with a travel of 0.5 meters for the end-effector is presented. The motion is generated with respect to the described algorithm in this section for continuous motion of end-effector. According to calculations, the task is completed in 0.761 seconds with a maximum velocity of 40 m/min. When compared with task completion duration (0.818 seconds) of the conventional mechanism, there is a 6.97% time gain. Although the time reduction magnitudes for longer-distance machining are smaller, for a task with many smaller-distance contours, the algorithm will result in remarkably higher reductions in total.

4.3.2. VLPA for Traveling Segment

Traveling segments are reserved for motions generated for moving end-effector or machining tool to desired machining process' initiation coordinates. Traveling segments are planned between machining segments if there is an offset between termination and initiation coordinates of sequences of G-code. Similar to preparation of a machining segment, traveling velocity profile generation is carried out for macro mechanism velocity, v_a, along *X*-*Y* axes and micro mechanism, v_b, along *u*-*v* axes. In the traveling velocity profiles, the maximum acceleration duration and velocity generated by micro mechanism is limited with respect to its workspace.

In Figure 4.8, the velocity profiles generated for traveling segment are drawn according to macro and micro mechanisms' velocity limits, v_a *(max)* and v_b *(max)*. In this Figure, v_a *(max)* is set by macro mechanism's maximum velocity while v_b *(max)* is chosen to preserve the micro mechanism's motions inside its workspace. During t_0-t_1, micro mechanism accelerates with 49.05 m/s^2 and in order to stop at its workspace limit, decelerates with the same acceleration magnitude of the macro mechanism. As a result of this, the velocity of the end-effector is kept constant while the micro mechanism decelerates and comes to a stop.

During the deceleration of end-effector, the micro mechanism moves in the reverse direction of the end-effector motion with its maximum acceleration initiating from the limit of its workspace. This results in a faster deceleration of the end-effector, and the end-effector reaches the traveling segment's termination location. However, at t_6, while the end-effector completes its designated motion, the macro and micro mechanisms

still move. The motion on each mechanism from t_6 to t_7 is described to hold the end-effector position constant while retracting the micro mechanism to its workspace's mid-point. This is achieved by demanding 1 g acceleration from both mechanisms in different directions. Macro mechanism velocity is designed to have a trapezoidal profile with maximum acceleration (1 g) and maximum speed (200 m/min) between t_0-t_7.

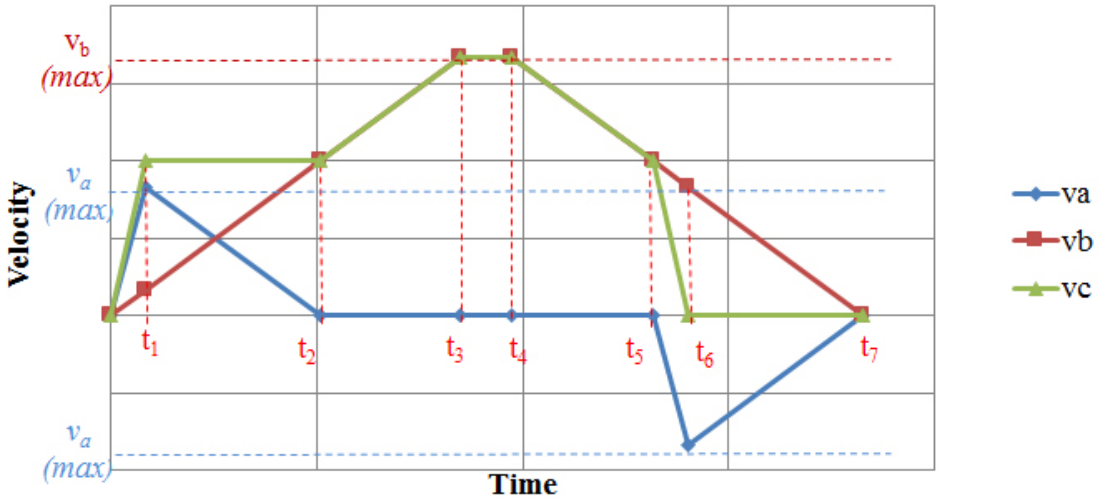

Figure 4.8. VLPA motion generation for traveling segment.

At the end of the motion described in Figure 4.8., there is a duration defined from t_6 to t_7 when the end-effector is not moving and reaches its motion termination location. This may be seen as a loss of time. However, for any machining operation, there should be a time interval to cut into the workpiece, and this dead time can be utilized for this purpose.

For the numerical example, motion planning of a traveling segment with a travel of 0.5 meters of the end-effector is presented. The calculations show that the traveling segment task is completed in 0.4515 seconds with a maximum velocity of 132.88 m/min for macro mechanism. It is deduced that there are 0.17 seconds of time gain (dead time) that can be used for initiation of the cutting process of the tool. As a result, there will be time reduction from total completion of sequences of MMM's process.

The generated algorithm is devised to distribute the global motion demand to the macro and micro mechanisms. Advantage of the algorithm is proved by numerical examples conducted for both machining and traveling segments.

4.4. Contour Shaping Algorithm (CSA)

The primary purpose of the Counter Shaping Algorithm (CSA) is to derive a continuous motion of the macro mechanism using geometrical features of the contour. This means that the macro mechanism never comes to a full stop during the process since its acceleration capabilities are limited. The offsets between desired trajectory and continuous trajectory of the macro mechanism are sent online as motion demands to the micro mechanism. The derivation of the continuous motion of the macro mechanism's trajectory is to be accomplished with respect to the workspace limitation of micro mechanism and motion limitations of both mechanisms. This interpreter makes use of the geometric approach in the generation of macro manipulators trajectory and semi-online motion generation process. As a result, the algorithm has the macro mechanism's motions to be planned without a full stop with its acceleration and jerk limitations throughout the process, while the precise and fast acceleration motions are carried out with micro mechanism.

4.4.1. Semi-Online Motion Generation

A new method is proposed for offline continuous motion generation for the macro mechanism taking into account the motion capabilities (velocity, acceleration, and jerk) of both mechanisms and the desired end-effector motion. The information flow for the new method is illustrated in Figure 4.9.

In this scheme, the trajectory of end-effector is configured to achieve jerk-bounded highest combined accelerations of the mechanisms throughout the task. Later, this trajectory is used to extract the macro mechanism's motion demands in X- and Y-axes. Micro mechanism's motion demands, in *u*-*v* axes, are generated online by calculating offset between the global trajectory and the macro mechanism's measured position. The reason for this offset is that smoothened motion trajectory developed for the macro mechanism excludes the sharp edges in the trajectory. In the next subsections, continuous motion generation for macro mechanism and point reduction steps are explained.

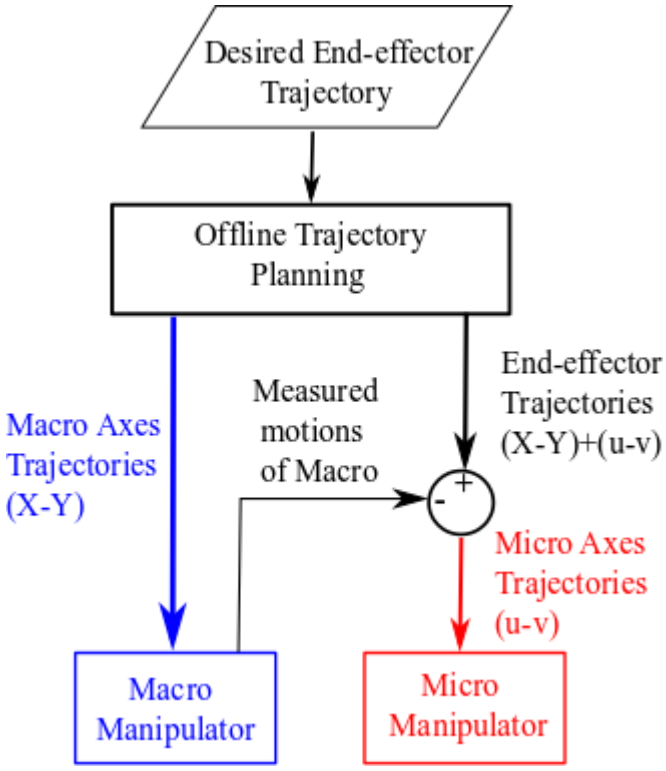

Figure 4.9. Information flow for semi-online generation.

4.4.2. Extracting the Motion of Macro Mechanism in CSA

The proposed method takes into account the workspace limitation of micro mechanism and optimizes the end-effector's global trajectory to obtain the continuous set of motions for macro mechanism while excluding the sharp and discontinuous motions to be achieved by the micro mechanism. The algorithm utilizes the Ramer-Douglas and Pecker algorithm (RDP) described in (Wu and Marquez, 2003). RDP is used to reduce the number of points in a curve that is approximated by a set of points. The trajectory for the macro mechanism is generated with the steps shown in the flowchart presented in Figure 4.10.

In the first step, trajectory information is extracted from G-codes as sequential traveling and cutting contours. Each cutting contour represents a closed or open contour of cutting (machining) trajectory, where the end effector (machining tool) is demanded to track. Traveling contours represents the motions that the end effector should travel between cutting contours without any motion limitation with respect to the cutting speed.

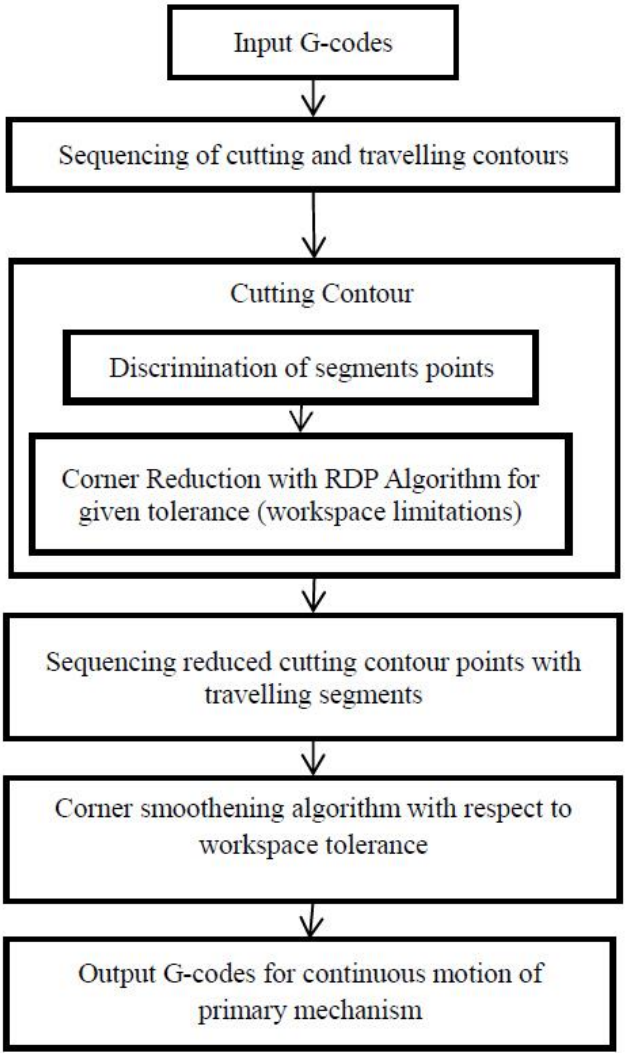

Figure 4.10. Continuous motion commands generation for macro mechanism.

In the next step, a set of points, which define the segments in a G-code sequence, for the desired trajectory of end-effector is generated for trajectory planning algorithm. Points extracted from the cutting contours are subjected to corner reduction algorithm. RDP algorithm is run for reducing the number of points in discontinuous trajectory with the tolerance defined by the limited workspace of the micro mechanism. This tolerance in this study is chosen regarding the workspace of micro manipulator which is 100 x150 mm.

For the next step, reduced points of each cutting contour are combined with traveling points to derive overall trajectory points with the same sequence as in the G-code list. Points are combined with lines in between. As a result of this, there are velocity level discontinuities at each point. This discontinuity is smoothened by increasing the

radii of curvature at these sharp edges so that continuous motion is generated for macro mechanism. Finally, continuous motion demands for the macro mechanism are generated in G-code language, as motion demands.

Corner reduction and trajectory smoothening process used in the derived algorithm is based on RDP and a corner curve-fitting algorithm. The basic principle of the corner reduction algorithm is illustrated in Figure 4.9 as follows:

(a) A basic trajectory for the end-effector composed of points is sequenced starting from P_0 to P_5, and it is illustrated with the green line in the following steps with the associated nodes.

(b) For a set of given points, the algorithm first combines the initiation and termination point to construct the line. The created line $\overline{\mathbf{P_0P_5}}$ drawn with dashed blue line in Figure 4.9. The distances of points, in between P_0 and P_5, to line $\overline{\mathbf{P_0P_5}}$ are calculated, and the distance which has the highest magnitude is marked as maximum distance, d_{max}. Later, the algorithm checks if d_{max} is higher than given tolerance, which is the workspace limitation of the secondary mechanism. For line, $\overline{\mathbf{P_0P_5}}$, d_{max} is calculated to be higher than the tolerance and the algorithm determines that the corner reduction for P_0 and P_5 point are out of bounds.

(c) In this step, the algorithm excludes the point P_5 and searches the distances of points P_2 and P_3 to $\overline{\mathbf{P_0P_4}}$. d_{max}, in this case, is calculated again to be out of tolerance and point P_4 is excluded.

(d) Calculation procedure for maximum d_{max} is carried out again in between P_2 and P_3 and d_{max} is calculated to be out of bounds. Thus, the algorithm excludes point P_3.

(e) Finally, d_{max}, the distance of point P_1 to $\overline{\mathbf{P_0P_2}}$ the line is calculated to be below the tolerance and algorithm sets the first reduction by excluding P_1.

(f) In this step, the points from P_2 to P_5, are investigated with respect to the line $\overline{\mathbf{P_2P_5}}$ since the algorithm already fit a line between previous points. Calculating the magnitude of dmax below the tolerance value, the algorithm excludes points P3and P4. As a result of the implementation of RDP algorithm for a set of given points, corner reduction is completed, and the motion segment is reduced to 3 points as P_0, P_2, and P_5.

(g) After the points are reduced, the proposed method fits a curvature to each corner complying with the workspace limitations. In this case, a curve is fitted to $\widehat{\mathbf{P_0P_2P_5}}$ where the center of the curve is represented with P_c.

(h) As a result of corner reduction algorithm, segments that are necessary to be generated with G-codes, to be constructed with G0, G1, G2, and G3 line segments, are illustrated with the blue line from point P_0 to the new P_4.

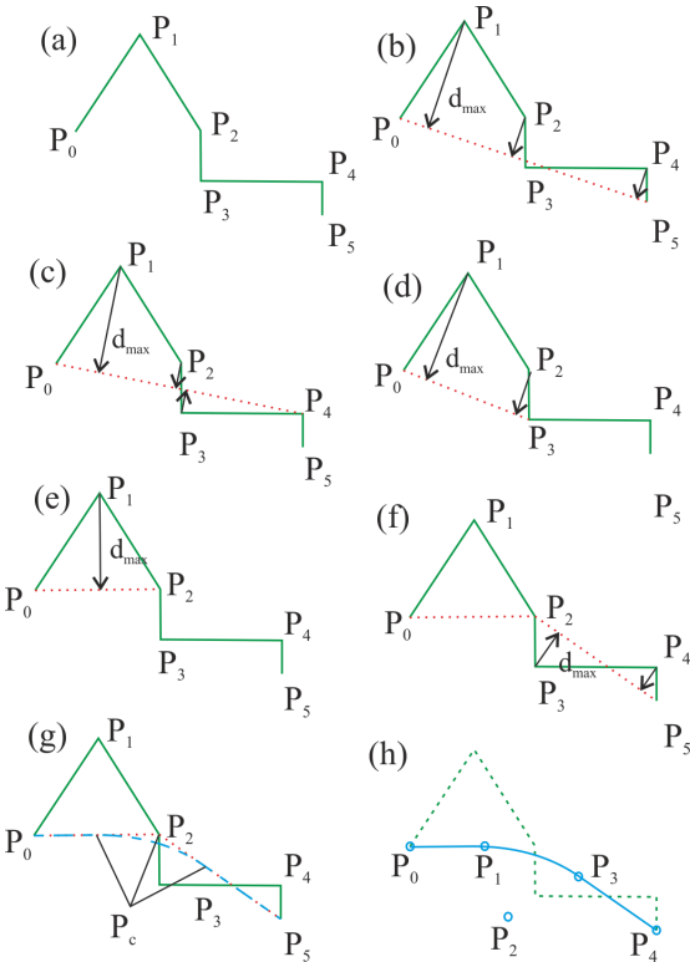

Figure 4.11. Corner reduction algorithm steps with an example.

The corner reduction process is carried out offline as proposed in continuous motion generation. It should be noted that circles and splines are represented with G2 and G3 commands in G-code language. The G2 and G3 commands generally include information about initiation, termination and center coordinates of the curve. In the corner reduction process given above, G2 and G3 segments are represented with these 3 points, which stands for clock-wise and counter-clockwise circular motions.

4.4.3. A Case Study: CSA

As an implementation and verification of this method, the proposed algorithm is applied for a relatively complex trajectory, and simulations are carried out with Matlab©. In this case study, the acceleration of the primary mechanism's axes are designated to be limited with 1 g, the acceleration of the micro mechanism is set to 5 g, and the end-effector velocity is limited with 40 m/min of maximum speed.

The desired trajectory of the end-effector and the reduced trajectory of the primary mechanism (*X*-*Y* axes) are presented in Figure 4.12 Desired end-effector trajectory is illustrated with the blue solid line while trajectory generated for the macro mechanism is illustrated with the dashed red line.

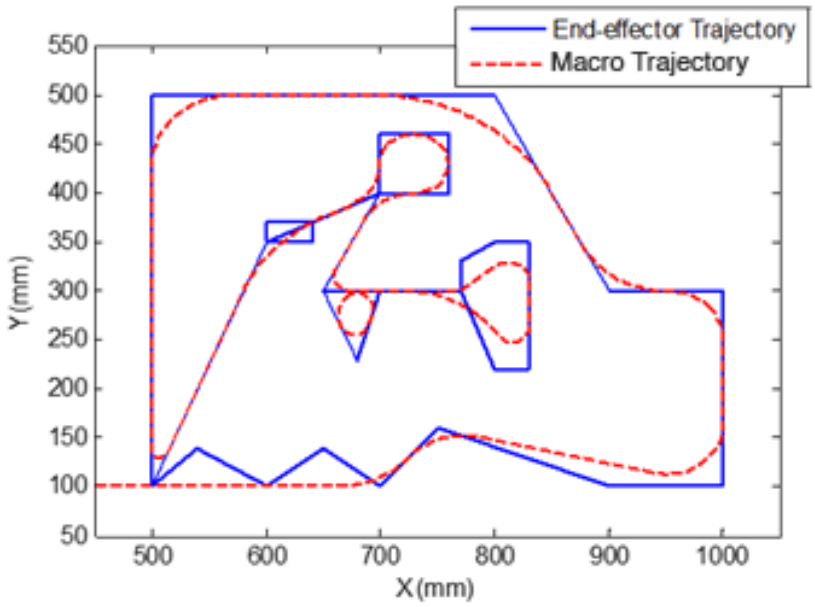

Figure 4.12. A case study for CSA.

Process duration for the case study is calculated to be 7.84 seconds when a conventional machine with the only *X*- and *Y*- axes and a 1 g acceleration limit was used. On the other hand, completion time with the proposed method is calculated to be 6.24 seconds. This means that there is a reduction of 20.41% in task completion duration.

Compared to the previous algorithm, in which both trajectories for the primary and secondary mechanisms are calculated offline, the problem of having limited jerks is

solved in the proposed control scheme by implementing an online control of the secondary mechanism. The macro mechanism is generated with a geometrical approach. Moreover, the online motion compensation with micro mechanism is expected to enhance the system accuracy. However, this method is highly iterative and has high computation load. In general, matching the derived macro mechanisms, trajectory and end-effector trajectory concerning time is hard to implement.

4.5. Motion Planning with Filtering Algorithm (MPFA)

The final algorithm is developed to expose the capabilities of both macro mechanism or otherwise called as the macro manipulator, which operates in x- and y-axes and micro mechanism or otherwise called as secondary/micro mechanism, which operates in u-v-axes. In this new algorithm, the continuous and smoothened motion (motion never coming to a full stop) is derived for macro mechanism's trajectory in global space while high accelerated motions are reserved for the micro mechanism. This is the offline part of the implemented algorithm in which the output is the jerk-bounded trajectory of the macro mechanism.

The aim of the filtering function is to derive the trajectory of the macro mechanism's axes, which should have slowly varying velocity profile. As a result of jerk-bounded motion planning for the input in the form of a segment data, a time series of data, $\boldsymbol{s}$, is generated for the trajectory of the tool path. The tool trajectory, $\boldsymbol{s}$, is formulated to have both motions with slowly varying velocity for the macro mechanism, $\boldsymbol{x}$, and faster varying velocity with relatively small displacements for the micro mechanism, $\boldsymbol{u}$. When $\boldsymbol{x}$ is extracted from $\boldsymbol{s}$, then the macro mechanism will have a smooth and continuous motion.

To extract the smoothened component of the tool trajectory, $\boldsymbol{x} = \boldsymbol{s} - \boldsymbol{u}$, trend filtering is adapted. This filtering technique has been used mainly in macro-scale time series analysis. In this technique, $\boldsymbol{x}$ is derived by minimizing the weighted sum objective function represented in equation below.

$$argmin_x \left\{ \sum_{t=0}^{n} \big(s(t) - x(t)\big)^2 + \lambda \sum_{t=1}^{n-1} \big(x(t-1) - 2x(t) + x(t+1)\big)^2 \right\} \quad (4.1)$$

The objective can be rewritten in the form of:

$$\|\boldsymbol{s}-\boldsymbol{x}\|_2^2+\lambda\|\boldsymbol{D}\boldsymbol{x}\|_2^2 \tag{4.2}$$

where $\boldsymbol{x}=[x_1 \dots x_n]'$, $\boldsymbol{s}=[s_1 \dots s_n]'$, $\|\boldsymbol{u}\|_2^2=\sum_i(u_i{}^2)^{1/2}$ (Euclidean norm) and $\boldsymbol{D}$ is second-order difference matrix. The unique solution to this problem can be found as:

$$\hat{\mathbf{x}}=(\boldsymbol{I_n}+\lambda\boldsymbol{F})^{-1}\boldsymbol{s} \tag{4.3}$$

where $\boldsymbol{I_n}$ is an *nxn* identity matrix and $\boldsymbol{F}$ is the pentadiagonal *nxn* matrix extracted from second order difference matrix, $\boldsymbol{F}=\boldsymbol{D^T D}$.

$\lambda \geq 0$ is the weighing parameter used to regulate the trade-off between the smoothness of $\boldsymbol{x}$ and the size of the residual $\boldsymbol{u}$. As λ approaches to zero, the outcome converges to original data $\boldsymbol{s}$, and as it approaches infinity, the outcome is more like least square approximation.

The residual is denoted by, $\boldsymbol{s}$-$\boldsymbol{x}$, macro mechanisms trajectory subtracted from end-effector trajectory which is designated to be the micro mechanism motions. The cyclical component features the second-order discrete differential of data which is in fact related to the macro mechanisms acceleration. Regularization parameter used to control the trade-off between the smoothness of $\boldsymbol{x}$ and the size of the residual $\boldsymbol{u}$. As a result, this filtering function does the regulization wanted in the trajectory generation problem proposed in this thesis.

The size of the residual should be kept inside the workspace limitation of the micro mechanism. The trend value, λ, is selected after iterations for every time the filtering function runs, in which the workspace limitation of the micro mechanism and acceleration limits of both mechanisms are checked whether they are within the range of the related physical capabilities of both mechanisms. The change in the workspace of the micro mechanism also changes the maximum acceleration expectations from the micro mechanism during the operation.

4.6. Conclusions

In this Chapter, three different algorithms devised for MMM concept are introduced. The first method makes use of velocity level trajectory planning in which all the motion planning is pre-processed and later to be used in the CNC controller. Although this algorithm is proved to be useful for task duration shortening, the algorithm has a

practical disadvantage that in real-life conditions as jerks are not infinite as utilized in this algorithm.

Within the second algorithm also, the semi-online control strategy is introduced, in which the micro manipulators demands are extracted from end-effector trajectory and realized macro manipulator's motion feedback. In this strategy, micro manipulator compensates the motion of the macro manipulator. The difference between CSA and MPFA is that the former one uses geometric methods, while the latter uses the smoothening function.

In the end, the third algorithm, MPFA, is found to be the most feasible option for industrial application. The superiority of the proposed method with respect to the previously developed methods is that this tuning capability, which brings much flexibility in distributing the accelerations between the macro and micro mechanism. Proper division of acceleration limits with this tuning capability, the accuracy of the total system can be improved. The chosen algorithm is also more flexible (allowing concatenation, over-fly, punching time, lead-in, lead-out processes) and easier to integrate.

.

CHAPTER 5

INDUSTRIAL APPLICATION AND VALIDATION

In this Chapter, the industrial case study is presented which comprises of MMM and laser cutting process. First, the scope of the project is introduced along with the system specifications and overall system scheme. Second, validation of positioning accuracy of the system and validation is made. Later the controller validation for the micro manipulator is given with the embedded controllers inside the motor drivers.

The SANTEZ project consists of the design, production and verification tests of a planar laser cutting machine. Conventional planar laser cutting machines cannot achieve high accelerations because of the high inertial characteristics of the long reach conventional axes in *X*- and *Y*-directions for movement in the XY plane (Figure 5.1). Conventional machines in the industry have an acceleration limitation of 2 g at most. However, with the aid of MMM, this limitation can be increased to 5-6 g acceleration. In addition to the conventional structure that moves in *X*- and *Y*- direction, two relatively smaller axes are added parallel to *X*- and *Y*-direction which are called *u*-*v* (Figure 5.1). In this way, it is possible to perform high accelerations with a combined motion of axes.

The aim of this project is to have a redundant laser cutting manipulator with at least the same sensitivity and high acceleration values compared to the conventional systems. Creating a unique mechanical structure based on subsystems and optimizing the system-specific trajectory and operating the system at its highest performance were other objectives of the project. The numerical targets at the proposal of the project were given as follows: positioning accuracy ± 0.03 mm/m, repeatability ± 0.015 mm/m.

As a result of the conducted investigations, the scope of this project, a novel design MMM design is introduced, which can reach high acceleration levels (3.5g) while having at least the same precision that ta conventional machine has. In addition, in the scope of this project, a kinematically redundant robot controller that optimizes the actuator motion for the highest acceleration that can be achieved by the mechanism is developed. The details on macro-micro mechanism design are shown in Figure 5.1, where macro and micro mechanism's axes are denoted respectively by X-Y and u-v.

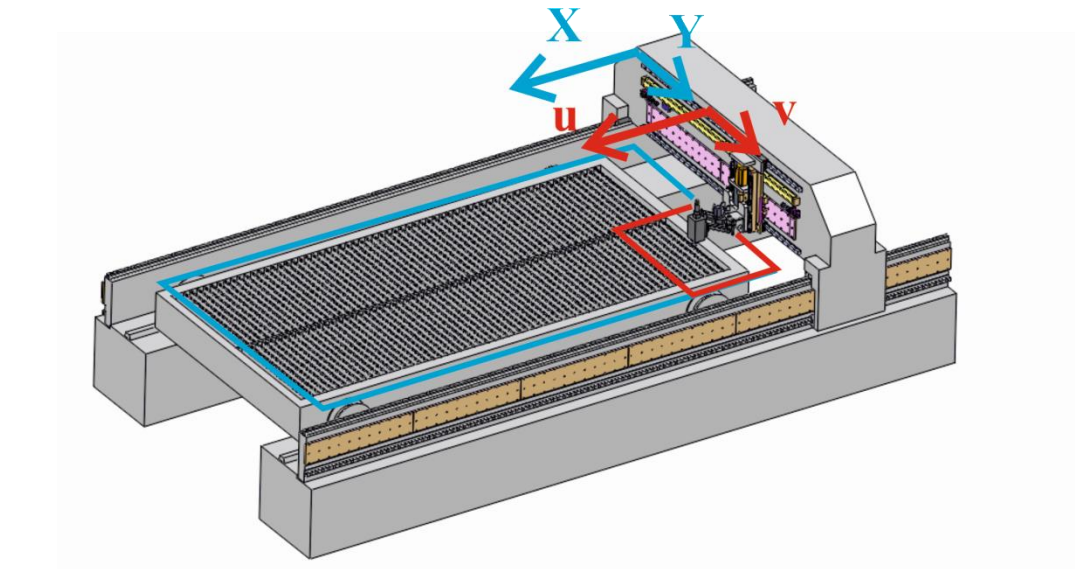

Figure 5.1. Macro-micro laser cutting machine design.

In the project, apart from traditional machine design and production, both parallel mechanism design and kinematically redundant robot controller/redundancy resolution algorithm design were studied. Mechanical, electronic and software designs and integrations have been revealed as a result of analysis, modeling, and simulation studies made by using various software. Production of designs and supply of materials have been completed. The project team decompose the components/functionalities of the overall system, address and validate each issue individually in detail with novel and feasible methods, and validate the overall system with experiments. The design of the machine is accomplished, confirming the standards listed in Appendix A. Hence, the system integration was performed. Before the commissioning of the integrated system, hardware online tests were performed, and calibration procedures were performed. The calibrated manipulator was put into operation with the laser cutting system. Comparative cutting tests and final cutting tests were performed on the commissioned system for benchmark parts.

The technical specifications of the manipulator as results of the project are listed below:

1. Micro axes accuracy: ±0.037 mm/m
2. Micro axes repeatability: ±0.026 mm/m
3. Macro axes accuracy: ±0.014 mm/m
4. Macro axes repeatability: ±0.011 mm/m
5. Maximum combined acceleration of MMM: 3.5 g

6. Laser power: 2 kW
7. Maximum sheet thickness: 8 mm mild steel
8. The combined workspace of MMM: 3 m x 1,5 m

The overall system scheme is described along with the hardware used and the information flow in Figure 5.2. The desired workpiece cutting trajectories are entered to the CNC interface via G-codes, which are derived from the CAM program. Then, the G-codes are converted into two time series data. One time series data are the motion demands ready to be delivered to the servo drivers of the macro mechanism. The other time-series data are the desired motions of the end-effector. The motion demand for the micro-mechanism is calculated online, as described in Section 4.3.1, and the resultant motion demands are directed to the servo drivers of the micro-mechanism after the motion is mapped from the workspace of the micro-mechanism to the joint space of the micro-mechanism. The motion demands are generated and fed forward to the servo drivers of the actuators with a sampling rate of 2 kHz.

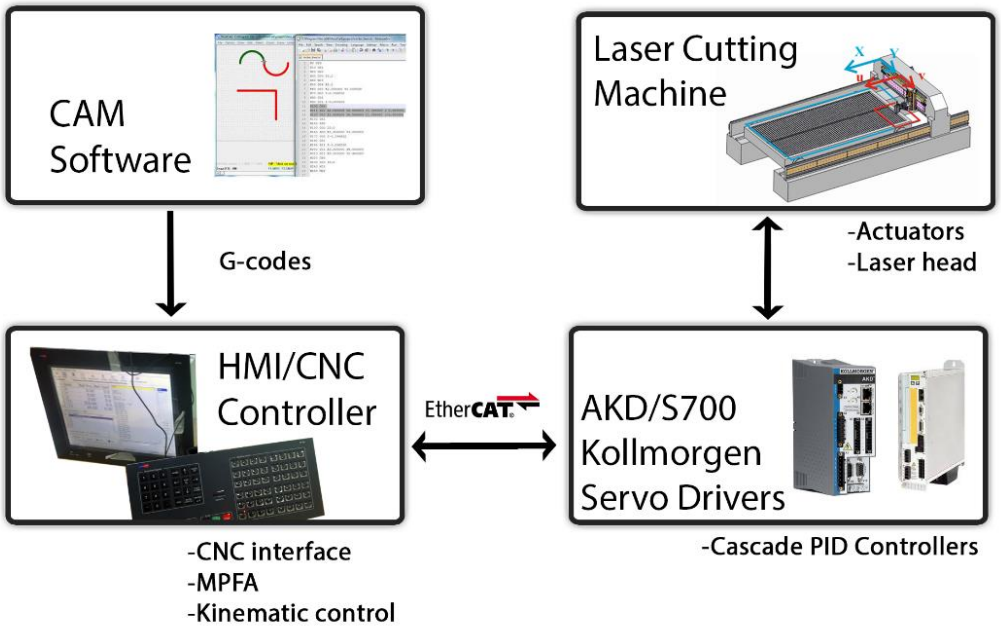

Figure 5.2. Hardware description.

The trajectory generation algorithm was designed and tested first in simulations using Matlab and Simulink software packages. To use the algorithms in the CNC,

functions of the trajectory planning algorithm are compiled and embedded in a UNIX-based real-time operating system (RTLinux). The test results with the constructed system working with the CNC system are presented in the experimental results section. Macro mechanism's trajectory is designed with a finite jerk to be used in the CNC machine controller in terms of time series data with a sampling rate of 0.5 ms. This sampling rate is determined with respect to the capabilities of the CNC used in this work. LYNCA CNC, which is a PC based open architecture general-purpose multi-axis CNC control unit developed by BİLKO, is used as CNC in this MMM.

5.1. Validation of Positioning Accuracy of MMM

This section describes the work done to measure the end-effector accuracy of manipulator axes separately and gives a summary of the calibration process. First, the calibration of the micro manipulator was carried out. To achieve this, end-effector measurements were performed with FARO Laser Tracker ION interferometer (IFM). The technical characteristics of the FARO IFM device are given in Table 5.1.

Table 5.1. FARO IFM specifications.

FARO IFM	
Resolution	0.5 μm
Accuracy	4 μm+0.8 μm
Maximum radial velocity	4 m/sec
Angular accuracy	10 μm + 2.5 μm/m
Sample rate	10,000 /sec

The test setup for measuring the accuracy and repeatability is presented in Figure 5.3 on the MMM system with the FARO IFM and the reflective apparatus attached to the laser cutting tool. The tests were carried out by the FARO IFM and the coordinates of the measured points were recorded according to the reference point. For the measurements, motion demands are sent to the actuators with the inverse kinematic function embedded inside the CNC unit. Measurements made with the FARO IFM are compared with the trajectory requirements given to the system to assess the performance and proceed with calibration.

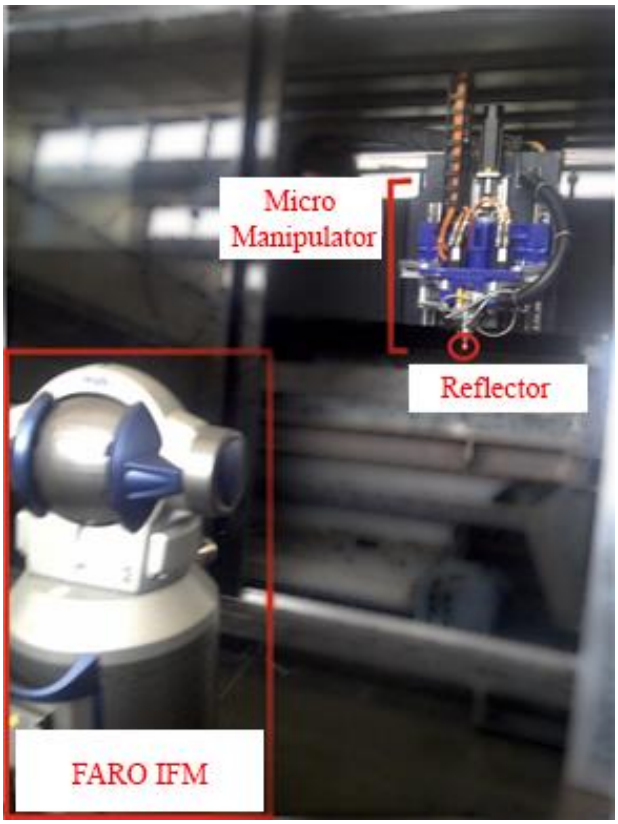

Figure 5.3. Test setup for measuring positioning accuracy.

First, the calibration on the micro manipulator was carried out. For a given measured motor and end-effector location data, the model estimation problem is a path generation synthesis problem along with the hidden robot analogy (Kiper et al., 2015). In polynomial approximation synthesis, the link lengths of the mechanism are determined so that the function/path/motion of the end-effector is exactly satisfied at certain precision points. In Figure 5.4, the points measured for enhancing the kinematic parameters are presented. The calibration process made in this study is explained in the work of Kiper et al. (2015a) in detail.

In the beginning, the link lengths of the manufactured micro manipulator were designated as 150 mm. After the measurements are done on the micro manipulator, the calibration is carried out and as a result, the new link lengths are calculated as a = 149.959 mm, b = 150.013 mm, c = 150.033 mm and d = 150.040 mm. With the modified link lengths, the positioning error decreased from about 1500 μm to about 700 μm. As a result, additional calibration of the micro mechanism is realized with an error correction matrix. Error correction matrix makes use of a calibration method with bilinear interpolation.

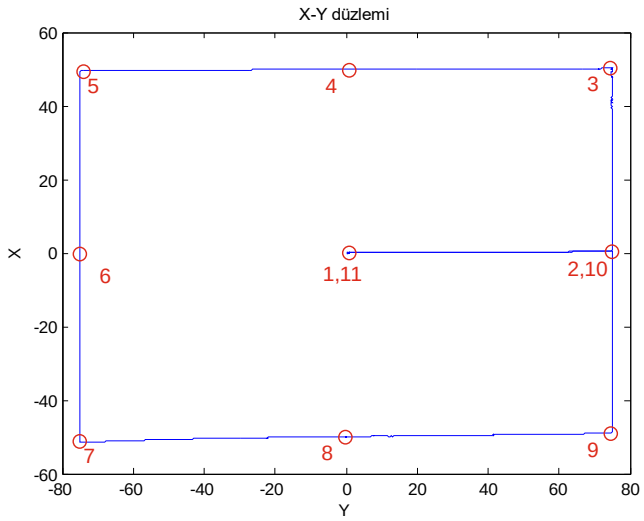

Figure 5.4. Measured points inside the workspace of micro manipulator for polynomial approximation synthesis.

After recalculating the kinematic parameters with the measurements made on the FARO device, the laser interferometer device Renishaw XL80, which have higher precision, is used. In this stage, the calibration was performed with the methodology stated in (Kiper et al., 2015) with bilinear interpolation. Iterations were made in the compensation values , and the accuracy value was reduced to ±37 µm. In this study, the micro mechanism was moved from one end of the workspace to the other end with 5 mm intervals in both + direction and - direction, and two measurements were taken at each point.

The measurement results are given in Appendix B. According to the results, the accuracy of the local mechanism was measured as ±37 µm, while the bidirectional repeatability was measured as ±26 µm (according to VDI/DGQ 3441 standard). The repeatability value was measured by the device as the most significant difference between the + and - approaches to the same point.

For the macro manipulator, the axes of the micro manipulator were locked and position measurements were made. As a result of the measurements, the process known as linear compensation was performed. For this operation, errors were taken every 25 mm in the + and - directions. A straightforward linear fit was made and the compensations of the axes were made. For the positions between the measured points, the linear approach was used and embedded in the CNC. Following linear compensation, accuracy and repeatability measurements were taken. As a result of the measurements, the accuracy

was measured as 14 µm and the bidirectional repeatability was 11 µm. The report of the measurement results re given in Appendix B.

5.2. Validation of the Controller

In this section, the cascade controllers embedded inside motor drivers and the performance of micro manipulator control is presented. This cascade structure has three closed-loop control stages, which are position, velocity, and current loop (Figure 5.5).

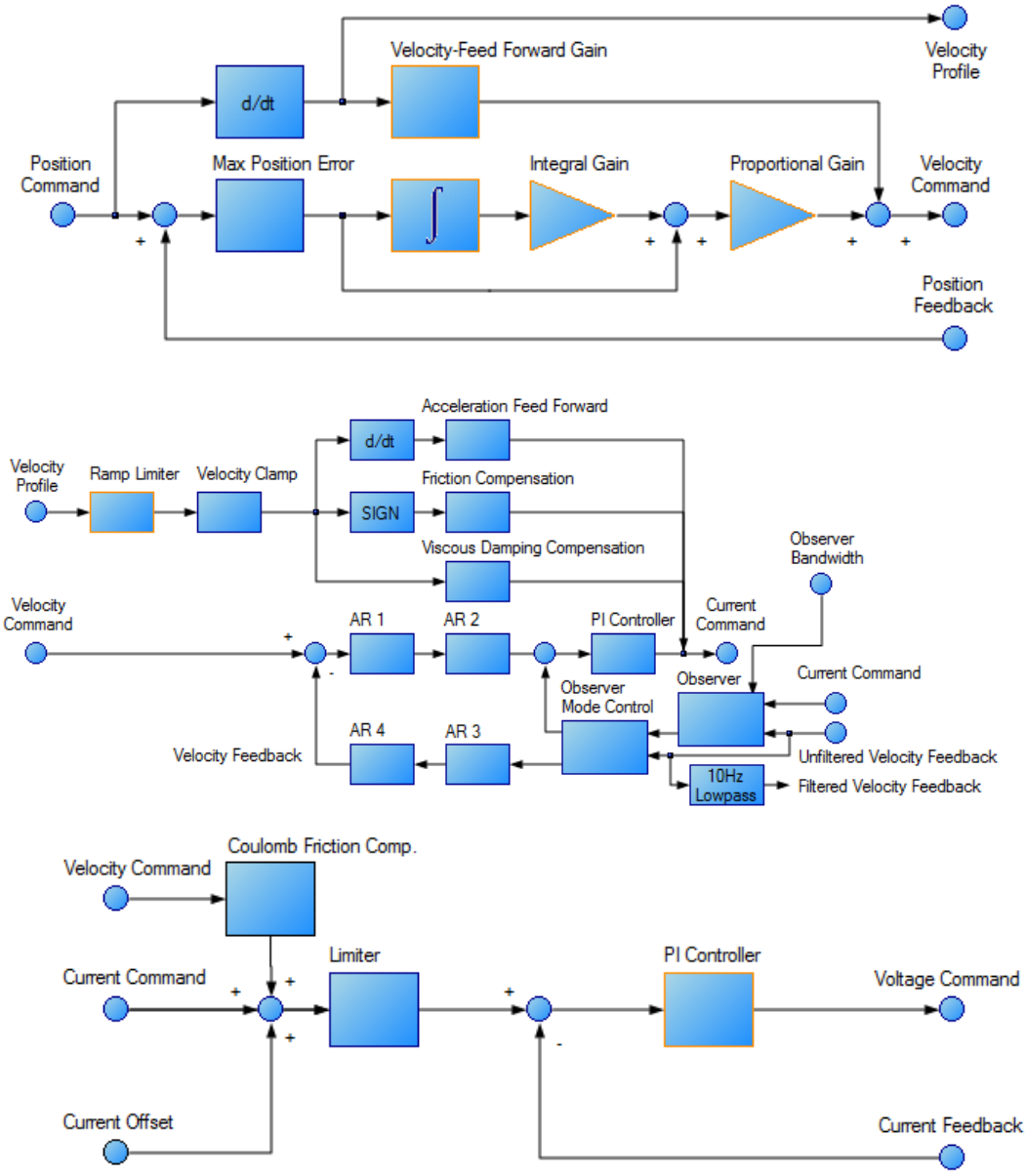

Figure 5.5. Cascade controller for micro manipulator.

The position loop consists of a PI controller with feedforward velocity term which is delivered to the velocity loop as velocity commands. Position feedback is delivered from the encoder readings on the motor. In the second loop, velocity control is realized with filtered velocity feedback and acceleration feedforward term. The velocity loop also includes friction and viscous damping compensation which are to be added to the current command. Observers and filters are utilized in the velocity loop to overcome the noise generated in the feedback. There are optional four filters in the velocity feedback. Lastly, the commands generated in the velocity loop are used in the PI controller for current. In addition a compensation term is added to the current command, which is to overcome Coulomb friction.

The tuning of the controllers are done separately for macro and micro manipulators separately. Moreover, the tuning procedure is carried out for each axis and the parameters are tuned with respect to their transient and steady-state response.

For the end-effector trajectory tracking performance, different trajectories have been designated to test the system with 1 g to 3.5 g at 40 m/min. Experimental tests with 3.5 g (maximum end-effector acceleration) are presented in this section. This limitation was demarked considering the maximum torque capability of harmonic reducer and AC servo motors used on the MMM.

The trajectory for controller performance was chosen as in Figure 5.6, in which the end-effector follows a path on the borders of the micro manipulator. The motion demands and current demands generated and realized for each actuator and end-effector errors are given in the Figures 5.7 and 5.8. These figures are plotted with the feedback acquired from motor encoders. Hence, the effects such as vibration and backlash cannot be seen, which also affects the dynamic trajectory tracking performance. However, in the previous section, such effects can be observed with measurements made with external hardware.

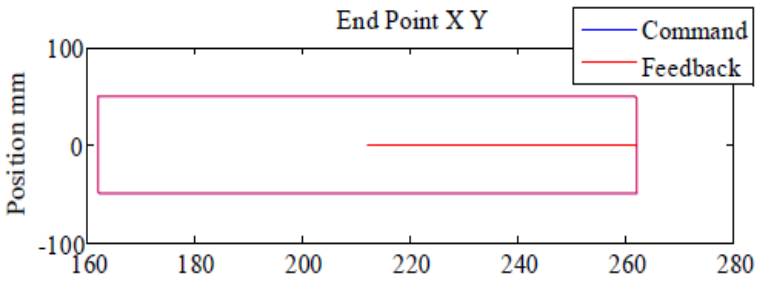

Figure 5.6. Generated path and tracking performance.

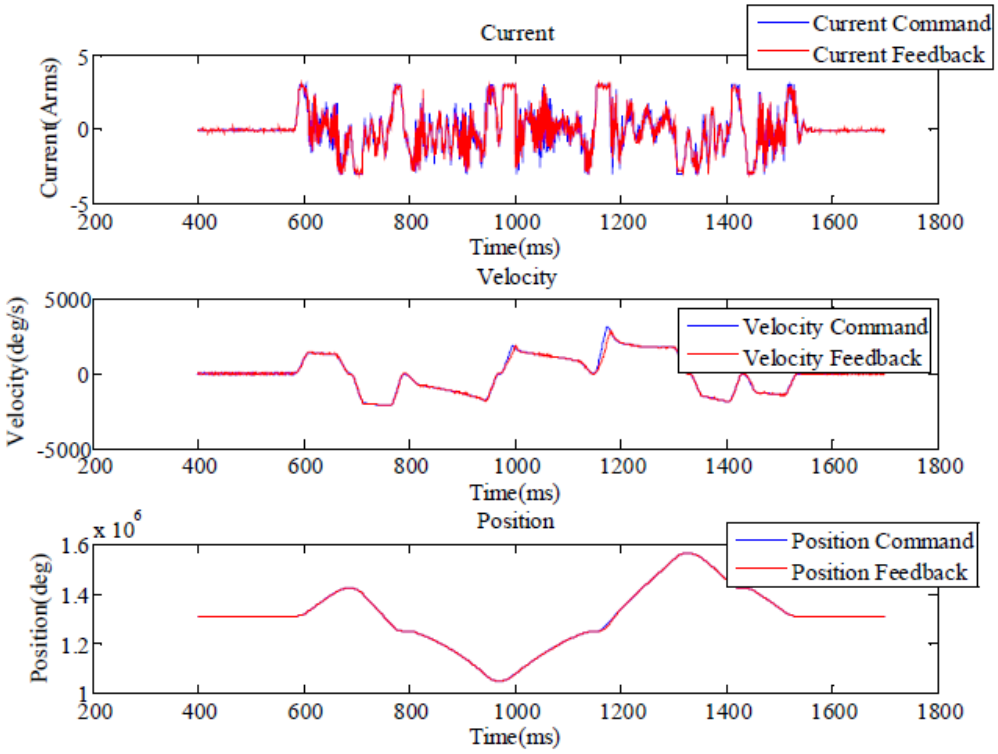

Figure 5.7. Motion and current tracking performance in motor 1 (q_1).

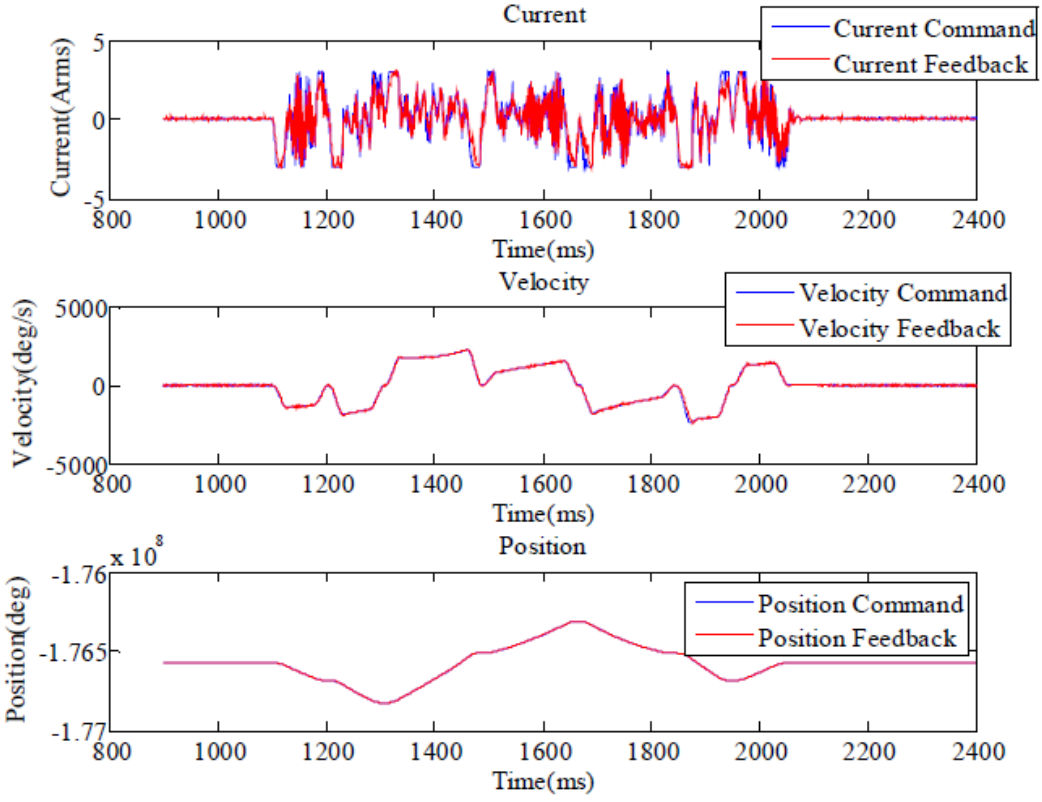

Figure 5.8. Motion and current tracking performance in motor 2 (q_2).

5.3. Implementation

The algorithm intended to be applied on the machine is MPFA as mentioned in the previous Chapter 4 (in Section 4.4). Integration of the algorithm and the derivation of both mechanism's trajectories are explained in detail in this Section. The aim of the system developed is to output as trajectories to be utilized in the CNC unit, in terms of time series data with a sampling rate of 0.5 ms. This sampling rate was determined with respect to the capabilities of the CNC used in this work. Flowline of trajectory information is given in Figure 5.9. Each step of the trajectory generation algorithm is explained as follows. It should be noted that another algorithm was devised in this application for the CNC unit to interpret conventional G-code in the industry for MPFA.

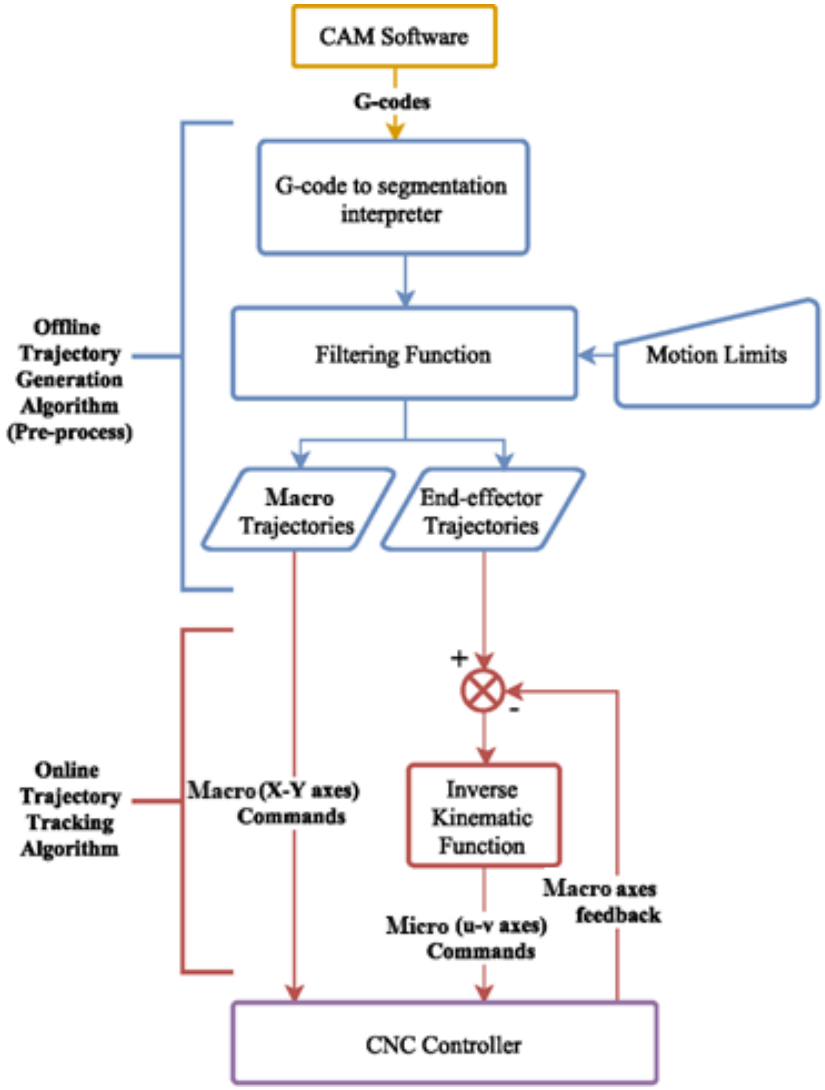

Figure 5.9. Flowline of the new trajectory generation algorithm.

Offline trajectory generation flow starts with registering function inputs. The necessary inputs consist of segment data extracted from G-codes and manually entered inputs, which are the motion limitations. As the motions are generated in jerk-bounded S-shaped profiles, both acceleration and jerk limits should be specified within motion limitations. Moreover, the function enables inputting different limitations for traveling, cutting and leading/piercing processes. After referencing the workpiece inside the workspace of the machine, initial coordinates should also be entered as an input with respect to the global workspace. In this study, no leading or piercing process is used, but the developed algorithm allows the user to enter piercing time or leading if required. The segment data are obtained from G-codes for trajectory generation and converted to sequential format in the "G-code to segmentation interpreter" function block. This sequential format is later used as input in MPFA's functions.

The segment data received from the G-code in the array format is in the given form, *[N G M X Y Z I J]*, where the letters in the array denoted as follows:

N: number of line

G: Contour description

M: Function

X,Y,Z: x, y, and z motion coordinates

I,J: Circular motion centre coordinates

Regarding this interpreter, *G* command and *M* command are further defined with the next number on the line. In which their interpretations are listed below for *G* and *M* command line:

G0: traveling, G1: line cutting

G2: Clockwise circular cutting, G3: Counter-clockwise circular cutting

M3: Laser on, M5: Laser off

M30: Program done, M34: lead in, M35: lead out, M4: piercing

The trajectory of the tool is planned in S-shaped segments with a time step of 0.5 ms. Traveling process is divided into seven phases with respect to distance *S(t)*, velocity *V(t)*, acceleration *A(t)*, and jerk *J(t)* as shown in Figure 5.10. In Figure 5.10, T_i is the total time of each phase, *S* is the total distance traveled, *V* is the velocity, *A* is the acceleration, and *J* is the jerk. The phases are the increasing acceleration phase (T_1), the constant acceleration phase (T_2), the decreasing acceleration phase (T_3), the constant velocity phase (T_4), the decreasing deceleration phase (T_5), the constant deceleration phase (T_6) and the increasing deceleration phase (T_7).

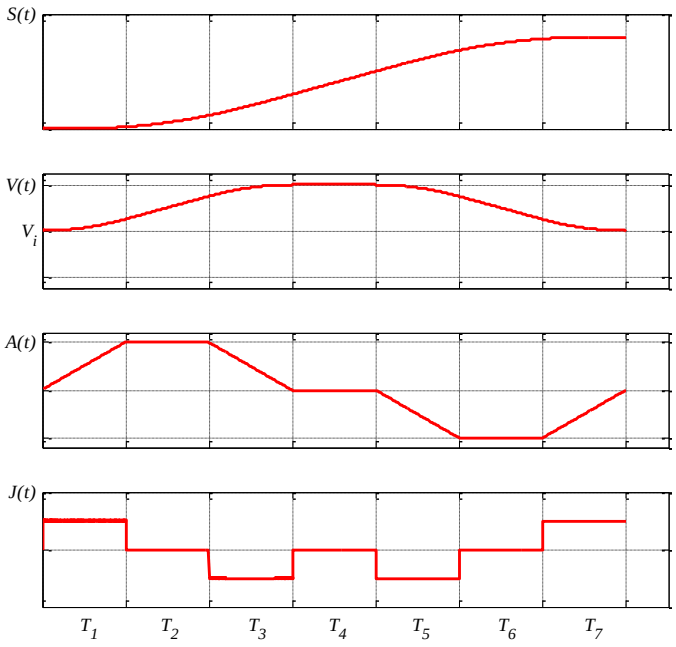

Figure 5.10. Distance, velocity, acceleration, and jerk profiles of S-shaped motion planning.

The expression for calculating the motions in acceleration, velocity, and displacement levels are presented equations 1, 2, and 3.

t_i—the terminating duration of stage T_i, where i=0, 1, …, 7.

τ_i—the relative time within the phase, where i=0, 1, …, 7.

$$A(t) = \begin{cases} J\tau_1 & 0 \le t < t_1 \\ JT_1 & t_1 \le t < t_2 \\ JT_1 - J\tau_3 & t_2 \le t < t_3 \\ 0 & t_3 \le t < t_4 \\ -J\tau_5 & t_4 \le t < t_5 \\ -JT_5 & t_5 \le t < t_6 \\ -JT_5 + J\tau_7 & t_6 \le t < t_7 \end{cases} \tag{5.1}$$

$$V(t) = \begin{cases} V_i + J{\tau_1}^2/2 & 0 \le t < t_1 \\ V_1 + JT_1\tau_2 & t_1 \le t < t_2 \\ V_2 + JT_1\tau_3 - J{\tau_3}^2/2 & t_2 \le t < t_3 \\ V_3 & t_3 \le t < t_4 \\ V_4 - J{\tau_5}^2/2 & t_4 \le t < t_5 \\ V_5 - JT_5\tau_6 & t_5 \le t < t_6 \\ V_6 - JT_5\tau_7 + J{\tau_7}^2/2 & t_6 \le t < t_7 \end{cases} \tag{5.2}$$

$$V_1 = V_i + JT_1{}^2/2$$

$$V_2 = V_1 + JT_1T_2$$

$$V_3 = V_2 + JT_1T_3 - JT_3{}^2/2 \tag{5.3}$$

$$V_4 = V_3 = V_{max}$$

$$V_5 = V_4 - JT_5{}^2/2$$

$$V_6 = V_5 - JT_5T_6$$

Hence, the displacements of the motion can be given as:

$$S(t) = \begin{cases} V_i\tau_1 + J\tau_1{}^3/6 & 0 \le t < t_1 \\ S_1 + V_1\tau_2 + JT_1\tau_2{}^2/2 & t_1 \le t < t_2 \\ S_2 + V_2\tau_3 + JT_2\tau_3{}^2/2 - J\tau_3{}^3/6 & t_2 \le t < t_3 \\ S_3 + V_3\tau_4 & t_3 \le t < t_4 \\ S_4 + V_4\tau_5 - J\tau_5{}^3/6 & t_4 \le t < t_5 \\ S_5 + V_5\tau_6 + JT_5\tau_6{}^2/2 & t_5 \le t < t_6 \\ S_6 + V_6\tau_7 - JT_5\tau_7{}^2/2 - J\tau_7{}^3/6 & t_6 \le t < t_7 \end{cases} \tag{5.4}$$

$$S_1 = V_iT_1 + JT_1{}^3/6$$

$$S_2 = S_1 + V_1T_2 + JT_1T_2{}^2/2$$

$$S_3 = S_2 + V_2T_3 + JT_2T_3{}^2/2 \; - JT_3{}^3/6 \tag{5.5}$$

$$S_4 = S_3 + V_3T_4$$

$$S_5 = S_4 + V_4T_5 - JT_5{}^3/6 \; S_6$$

$$S_6 = S_5 + V_5T_6 + JT_5T_6{}^2/2$$

The motion profile for each traveling distance is calculated, and time series data are generated within the combined macro-micro mechanism's limits. Motion profiles may not have the constant velocity or constant acceleration phases in short traveling ranges which is accounted for in the algorithm.

After the offline trajectory generation phase, the generated data are fed to the online process, which directs the motion commands to the CNC controller that includes the drivers for the servomotors actuating all the axes. Macro manipulator's motion is derived using MPFA to the time series data. The smoothened macro mechanism's motion commands are directly used as inputs to the drivers that actuate the macro manipulator's

servo motors. On the other hand, the micro manipulator's motion commands are to be calculated in a higher-level control loop before delivering these commands to the drivers of the micro manipulator's servo motors. This semi-online method is devised to compensate for the offsets in tool trajectory that may occur in between the macro mechanism's motion and tool trajectory. Motion demands for the micro mechanism in *u-v* axes are generated online by calculating offset, $U(t) = S(t) - X(t)$, in real-time between the tool trajectory and the macro mechanism's measured position via absolute position encoders. This offset forms as a result of the exclusion of the sharp edges in the smoothened motion trajectory of the macro mechanism and possible control errors of the macro mechanism axes. The motion demands calculated for u-v-axes is later converted to the joint motion commands using the inverse kinematics function developed for the micro mechanism's parallel robot structure.

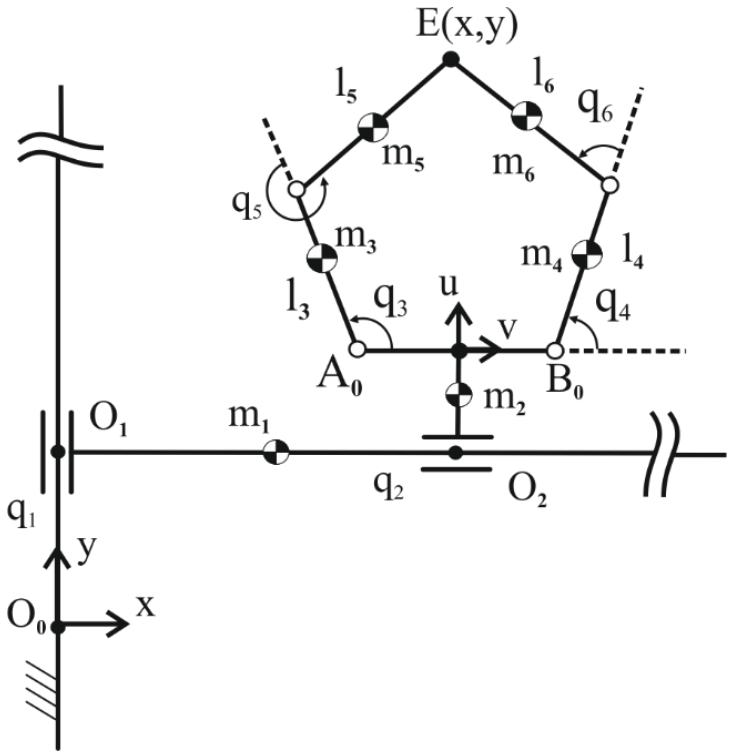

Figure 5.11. Model of the macro-micro manipulator (MMM).

The devised structure comprises a Cartesian prismatic planar macro manipulator and a five-bar parallel micro manipulator. The Cartesian manipulator has a workspace of 3000 mm x 1500 mm and a planar mechanism devised to use 100x150 mm free from kinematic singularities. The mechanism's kinematic structure is represented in Figure 5.11. It should be noted that micro mechanism kinematics are extracted from the case

when A_0 and B_0 points are concurrent. $\boldsymbol{q_1}$ and $\boldsymbol{q_2}$ are Cartesian macro mechanism's prismatic joints and $\boldsymbol{q_3}$ and $\boldsymbol{q_4}$ are micro mechanisms active revolute joints of five-bar. Due to the closed chain, parallel mechanism's $\boldsymbol{q_5}$ and $\boldsymbol{q_6}$ joints are passive. Consequently, given the desired trajectory on planar space, the manipulator has two extra degrees-of-freedom.

The direct and inverse kinematics of the kinematically equivalent five-bar mechanism are found as below to be utilized in the control algorithm. *E(x,y)* is the designated trajectory of tool/end-effector, and the micro mechanism axes are denoted by *u* and *v*, which are to be extracted by using the semi-online control algorithm explained in Section 4.5 with MPFA.

Inverse kinematics are given with the following set of equations:

$$\begin{aligned} s &= \sqrt{u^2 + v^2} \\ \varphi &= atan2(v, u) \\ \gamma_1 &= \operatorname{acos}\left(\frac{l_3^2 + s^2 - l_5^2}{2 l_3 s}\right) \\ \gamma_2 &= \operatorname{acos}\left(\frac{l_4^2 + s^2 - l_6^2}{2 l_4 s}\right) \\ q_3 &= \varphi + \gamma_1 \\ q_4 &= \varphi - \gamma_2 \end{aligned} \tag{5.6}$$

Direct kinematics are given with the following equations:

$$\begin{aligned} s &= \sqrt{(l_3 \cos(q_3) - l_4 \cos(q_4))^2 + (l_3 \sin(q_3) - l_4 \sin(q_4))^2} \\ \varphi &= atan2(l_3 \sin(q_3) - l_4 \sin(q_4)\, l_3 \cos(q_3) - l_4 \cos(q_4)) \\ \gamma &= acos\left(\frac{l_3^2 + s^2 - l_5^2}{2 l_3 s}\right) \\ q_5 &= \varphi + \gamma \\ q_6 &= atan2(l_3 \sin(q_3) + l_5 \sin(q_5) - l_4 \sin(q_4)\,, l_3 \cos(q_3) + l_5 \cos(q_5) \\ &\quad - l_4 \cos(q_4)) \\ u &= l_3 \sin(q_3) + l_5 \sin(q_5) \\ v &= l_3 \cos(q_3) + l_5 \cos(q_5) \end{aligned} \tag{5.7}$$

In the end, motion profile for each traveling distance is calculated and time series data are generated for combined macro and micro manipulators' limits.

5.4. Experiments

The experiments on the physical system were done in the industrial site with the machine designed and manufactured during the SANTEZ project. Prior to the experiments with a laser cutting tool, laser cutting parameters were adjusted for the workpiece. These parameters are laser power, assistive gas type and flow rate, the focal length of the tool, and cutting tool speed. The laser cutting scenario was prepared for on-the-fly-cutting of a thin sheet metal scenario, in which no time is spent for piercing workpiece. In addition lead-in and lead-out functions of the process were not utilized in the process for thin material cutting. Regarding the controller on the servo drivers, the cascade PID controllers are tuned with conventional methods by targeting the minimum positioning errors.

As an implementation and verification, the proposed algorithm is used in MMM, planar laser-cutting machine, to cut a benchmark piece that has a total of 100 consecutive holes with a 3 mm diameter, which are placed with 4 mm offset from each other. The experimentation was conducted on a galvanized steel sheet with 3 mm thickness as the workpiece. To compare the developed method, the same benchmark was cut with the conventional cutting procedure by using only the macro mechanism's axes. In this scenario, the micro manipulator's axes are locked at their homing position, which is at the middle of its workspace.

Complying with the limitations of the experimental system, the acceleration of the macro axes are limited with 1.5 g, the maximum acceleration of the overall system is set to 3.5 g, and the tool velocity is limited with 40 m/min, which is the maximum cutting speed due to the laser power and workpiece material specifications.

As proposed, the tool trajectory generated for benchmark cut is illustrated in Figure 5.12 with blue lines. This trajectory is generated from the tool path developed from G-codes complying with the motion limitations explained above. After the tool trajectory is generated, it is processed with the filtering function that is described in the previous section. The macro mechanism's trajectory is indicated in red color in Figure 5.12. It can be clearly observed that the red line has no sharp edges when the tool is cutting out the square outer boundary. Also, the macro mechanism flows on top of the circular cuts without following the circle trajectories, which means that the circular trajectories are filtered out to be executed by the micro mechanism.

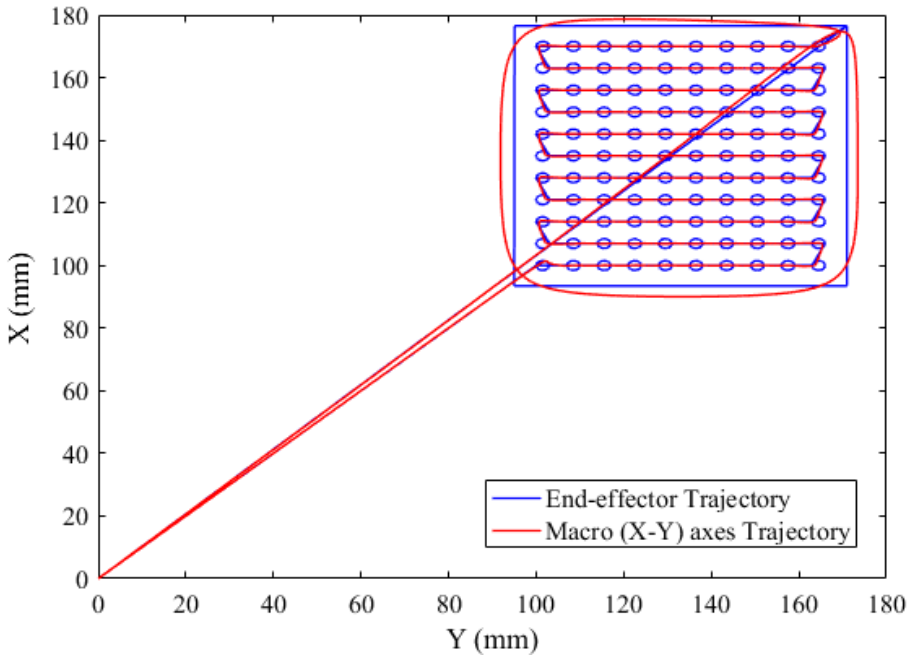

Figure 5.12. Motion trajectories generated for benchmark piece (100 circle cut).

In Figure 5.13, motion demands for benchmark piece along two planar axes are shown. The motion demand for the macro mechanism's *X*- and *Y*-axes (macro manipulator trajectories) are indicated with red color and the tool trajectories (*x*-*u*) and (*y*-*v*) are drawn in blue color, which represent tool trajectories. A focused view is provided in Figure 5.13 (b) to clearly show the smoothened trajectory of the macro mechanism. Relatively smaller displacements that can be observed in Figure 5.13 (b) in blue color are reserved for micro mechanism. The total task completion time is calculated as 26.04 s for 100 consecutive holes and their square frame contour.

After the pre-processing of G-codes and extracting the necessary motion demands both for the macro mechanism and the tool, these demands are exported to the online part of the algorithm. Micro manipulator's motion demands are calculated online by subtracting the measured macro mechanism's motion from previously generated time-series data of the tool trajectory as mentioned in Section 4.4.1.

In Figure 5.14, motion demands that are calculated online for the micro mechanism along *u*- and *v*- axes are given. These demands are processed online with the inverse kinematics formulation, presented in the previous section, to calculate the motion demand for each actuated axis of the micro mechanism's parallel structure. The kinematic functions are built in the online process generation algorithm.

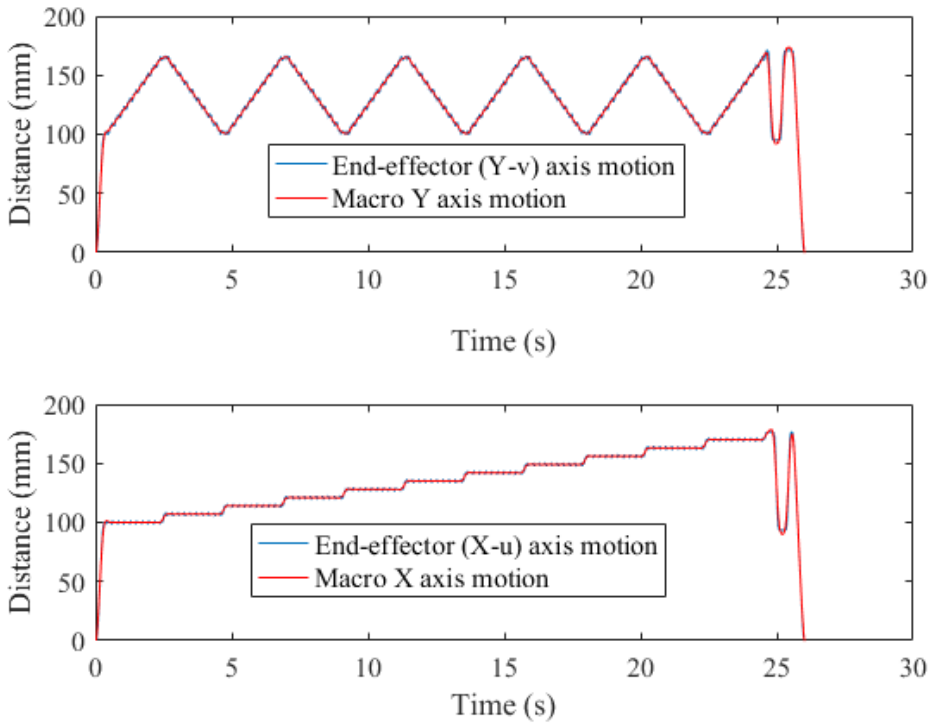

(a)

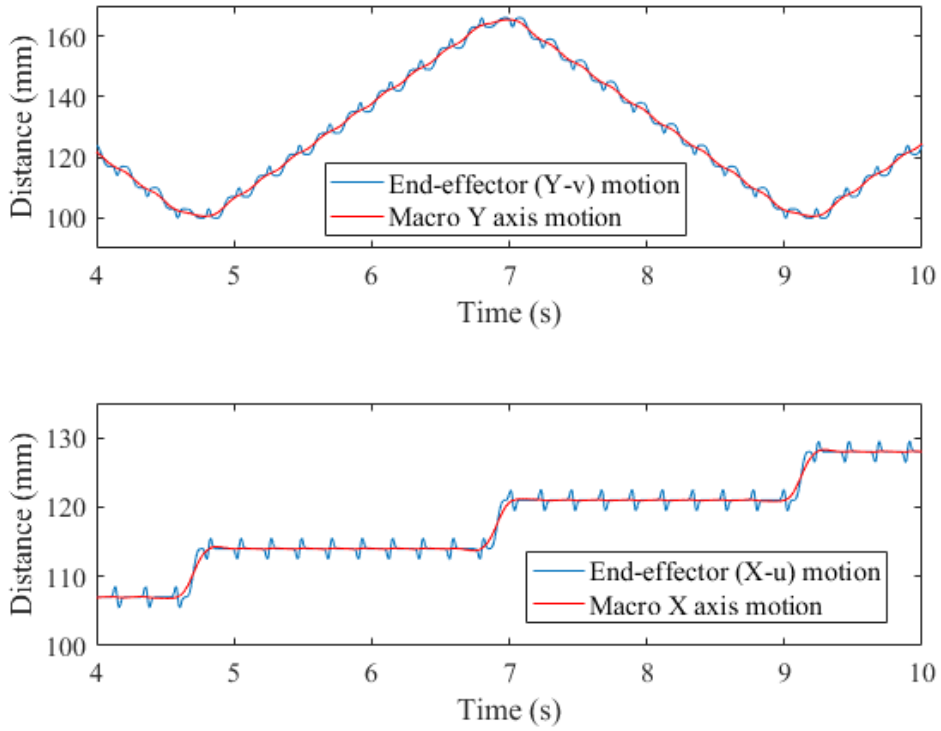

(b)

Figure 5.13. (a) Motion demands generated using proposed algorithm (b) Zoomed in version of the motion demands.

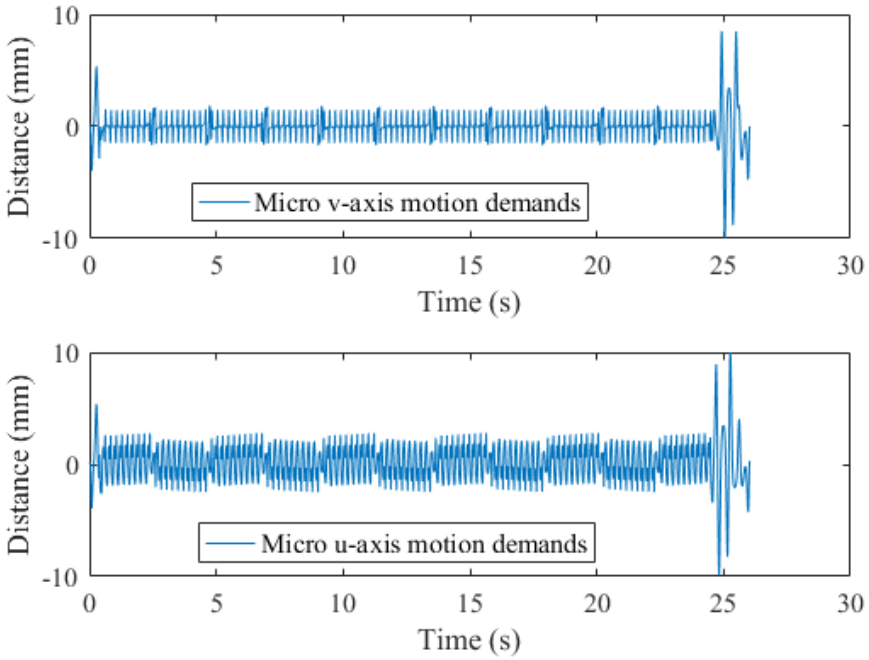

Figure 5.14. Calculated motion of the micro mechanism's (u-v) axes.

To compare the results in terms of improvement in task completion duration, the same benchmark piece is cut by only using a macro mechanism's axes which have acceleration limits at 1 g and limited jerk. It takes about 119 s to complete the same task by using the motion profile generated for the conventional machine, which is shown in Figure 5.15.

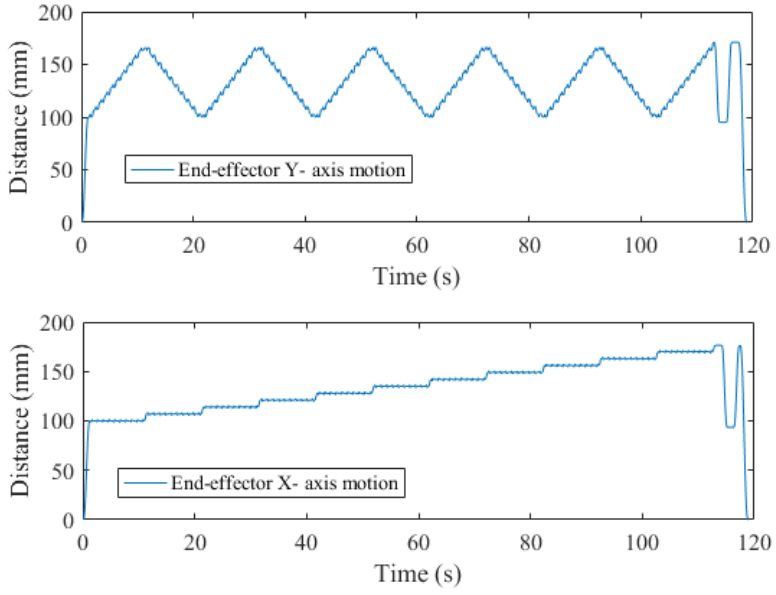

Figure 5.15. Motion profile generated for conventional machine's axes.

Another benchmark piece is cut with the proposed algorithm, which has relatively more complex contours that consist of a double-headed eagle shape with crescent and star. The end-effector trajectory generated for benchmark cut is illustrated with blue lines and trajectory for the macro mechanism is represented with red lines in Figure 5.6. It takes about 82.53 s to complete the task by using the motion profile generated for the conventional machine and 13.50 s with the proposed method. As a result, there is an 83.64% reduction in process duration for this complex and small contour.

In Figure 5.17, the end-effector trajectory generated for another benchmark part is drawn in red color and simplified trajectory for the macro mechanism, which is extracted in motion planning, is indicated with blue lines. During the process, motion demands for the micro-mechanism are generated online, as explained in the previous section. During the tests using the presented benchmark part, the task completion duration for the conventional machine is calculated to be 87.28 seconds while the machine with the macro-micro manipulator completed the cutting process in 14.70 seconds. In total, there is an 83.16% reduction in process duration for this complex and small contour.

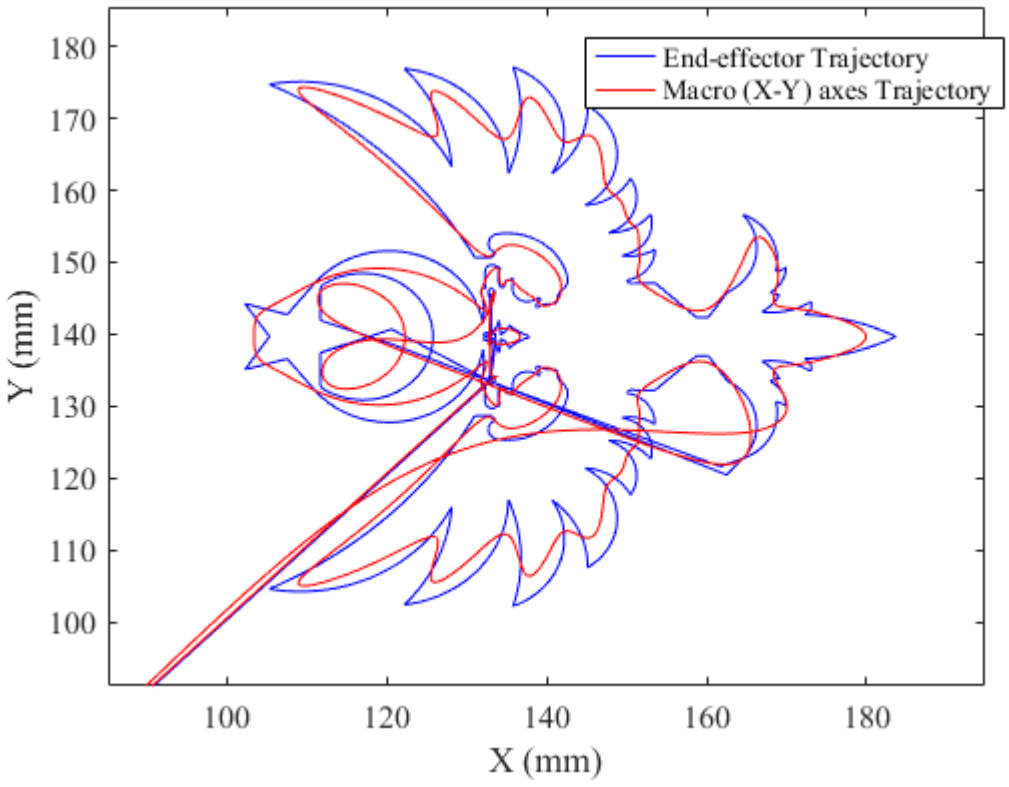

Figure 5.16. Motion trajectories generated for benchmark cut with the eagle and the crescent-star shaped piece.

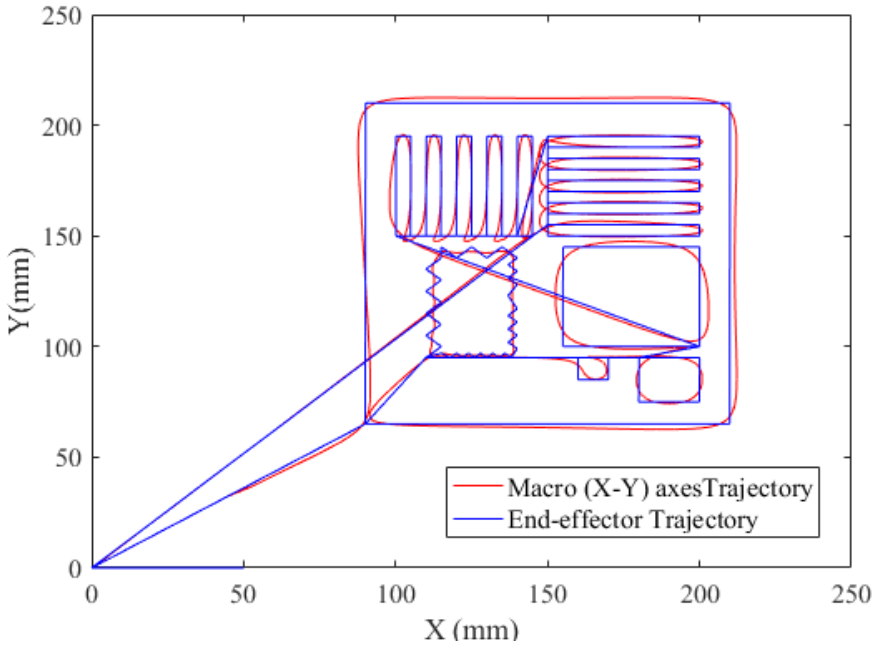

Figure 5.17. Third benchmark part's trajectory.

The pictures of processed workpieces for the 100-circle benchmark part and eagle with the crescent-star part are shown in Figure 5.18. These pieces are cut with the real planar laser cutting machine by using the motion profiles generated for MMM, which are presented in Figures 5.12, 5.17, and 5.18.

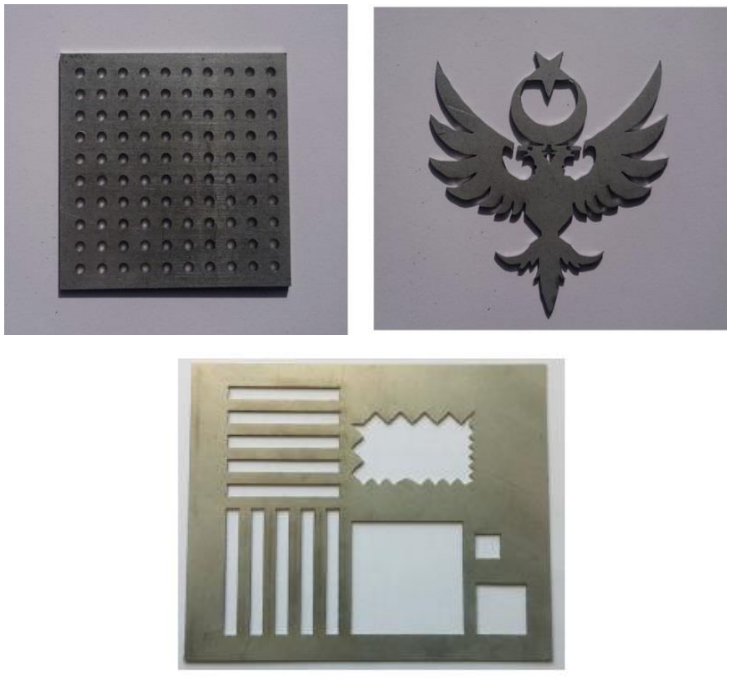

Figure 5.18. Pictures of manufactured benchmark parts.

5.5. Conclusions and Discussions

To summarize the work done, a new control method and motion planning algorithm are developed to reduce the task completion duration of a planar macro-micro mechanism laser cutting machine is proposed. The novel method deals with practical limitations by integrating a semi online trajectory generation with the offline method, and it is designed to be compatible with the industrial CNC systems.

The planar redundant laser-cutting machine, which is constructed within a funded project, is used in experimentation. A benchmark workpiece is chosen to have a relatively larger number of small circular cuts. The experiment to cut out the workpiece is carried out with both MMM and conventional machine. The results indicate that with the new trajectory planning algorithm, the same piece can be cut out in less than a third of the duration it took to cut it out with the conventional machine. It can be argued that the precision of the operation can be improved especially by tuning the controller of the macro mechanism's actuators. However, the critical observation as a result of the tests is that the error range is about the same for both types of operation while the macro–micro mechanism machine decreased the task completion duration drastically.

The macro–micro machine developed in this study takes advantage of the larger workspace of the macro mechanism and the agility of the micro mechanism. The proposed concept including the machine and the algorithm can be used in CNC systems that have relatively large workspaces and manufacture workpieces, which have trajectories with relatively higher amount of smaller-radius curvature and small distance motions. In such CNC systems, time to reach maximum manufacturing speed gains importance to complete the manufacturing job in shorter duration. On the other hand, the maximum manufacturing speed is determined by the type of manufacturing (laser cutting, conventional machining processes, additive manufacturing) and the workpiece properties (material, thickness). The proposed concept does not improve or degrade the maximum manufacturing speed of the process but reduces the total task completion time.

For laser cutting, YLS-2000-TR model Yterbium laser manufacturer system and LaserMech company Fiber Mini RA model laser head cutter were integrated into the system. This laser head will be able to withstand acceleration up to a maximum of 4g, thus it is understood that the already purchased cutting head cannot be used to cut 6g acceleration between the project targets. Nevertheless, the mechanical design of the machine was made to withstand accelerations of the order of 6g. It has been determined

that competitor companies, which can reach acceleration values of 5g and above, have designed a special laser head for these machines.

The outcome of the SANTEZ project is the first redundant laser cutting machine in the Turkish Machine Industry, and third of its kind in the world that can reach higher accelerations using redundancy. For the conventional cutting experiment, 1g acceleration limit is set for each of the macro mechanism's axes. During the test with the proposed algorithm, trajectory for the end-effector are generated with 3.5 g acceleration limits however, the macro mechanism's axes are limited with a maximum acceleration of 1 g. For a laser cutting process, the laser head/end-effector velocity limitations are determined with the laser power and workpiece specifications (material and thickness). Increasing the acceleration of the end-effector's motion is one way to reduce the task completion duration.

To enhance the positioning of micro manipulator, by making use of inverse kinematics and the Jacobian matrix for the hidden robot, error compensation values for the motor inputs are calculated. The errors for the points inside the grids are estimated via bilinear interpolation. The details of the calculations are presented in Kiper et al. (2015a). After implementing the error compensation values, positioning tests are repeated for the macro and micro mechanisms separately. The positioning errors are found to be bounded to ±37 μm and bi-directional repeatability is determined as ±26 μm for micro axis, shown in Appendix B. The positioning errors are found to be bounded to ±14 μm and bi-directional repeatability is determined as ±10 μm for micro axis, given in Appendix B. It should be noted that the calibration process is terminated and the results are given for only one axis. These values are determined according to VDI Standard no VDI/DGQ 3441 - Statistical Testing of the Operational and Positional Accuracy of Machine Tools; Basis. However, dynamic effects prove to be worse due to some faults causing noise and gear's unexpected low dynamic performance. The accuracy and repeatability of the machine are to be enhanced to a level that the machine can compete with conventional machines in the industry, with the completion of the calibration process, and iterations in design and production. The experimental results, given in Section 5.4., indicate that with the proposed algorithm the same piece can be cut out in less than a third of the duration it took to cut it out with the conventional machine. It can be argued that the precision of the operation can be improved especially by tuning the controller and calibrating the complete mechanism. During higher acceleration motions of the micro mechanism, deformation of the links is observed due to the relatively larger inertial properties of the

machining tool (e.g. a laser head). For future work, the stiffness model, calibration, and balancing of the micro mechanism are to be studied to increase the accuracy and repeatability of the machining process.

CHAPTER 6

NONLINEAR CONTROLLER DEVELOPMENT

This Chapter is divided into two sections regarding the control studies carried out. First, dynamic modeling and control of micro mechanism are given for controller development. In this section, computed torque based and adaptive nonlinear controllers are developed for the control of the micro manipulator, using the reduced model. The nonlinear controllers developed for micro manipulator are based on the study of Tatlıcıoğlu (2008). This controller is developed for future studies, to be utilized in the project called "Methodologies for Increasing the Positioning Accuracy of High-Acceleration Parallel Robots Used in Industrial Applications". Briefly, this project has emerged from the necessary need of increasing the accuracy of micro manipulator structure used in SANTEZ Project. In the previous project, it is proven that dynamic positioning accuracy of the system should be improved. To achieve this the over-constrained mechanism is redesigned and assembled in Iztech Modeling and Prototyping Laboratory. The positioning accuracy of the system is planned to be enhanced with better design and control methodology. The controllers, in this section, are developed and proven with numeric simulations, and they are aimed to be used on this new manipulator in future studies. Exact model knowledge and adaptive controller to deal with the uncertainties in the mass and inertia parameters of the micro manipulator are devised and tested in simulations. Since the dynamic model, the over-constrained mechanism parameters are lumped to the five-bar mechanism (using the hidden robot analogy), the adaptive controller is expected to decrease the positioning errors in the real-world application.

In the second section, a multi-priority controller is devised for MMM, in which a pseudo-Jacobian based controller is devised and tested with simulation. Manipulator task is divided into primary/main and secondary priority tasks. The main/first priority is used for end-effector trajectory tracking. Acceleration distribution and workspace limitation are realized in the second priority of the controller. The aim of this controller is the same as the MMM developed in industrial laser cutting machine and manipulator model is reconstructed with the parameters of the previously developed manipulator. This

controller is a novel approach for model-based control of the MMM which can be a framework for such systems.

6.1. Controller Development for Micro Mechanism

Before presenting the controller, it is necessary to describe the new micro manipulator system which is aimed to be used with the controller developed in this section. The manufactured and assembled parallel mechanism is presented in Figure 6.1. Similar to micro manipulator developed in the previous project, the kinematic structure is chosen as 6R over-constrained mechanism. This structure is inherited from the micro manipulator used in the industrial case stud. This manipulator is designed to hold a tool in the end-effector with a maximum payload of 5 kg. In the manipulator, Sumitomo Fine Cyclo F1C-A15 gearbox and Kollmorgen AKM33E series AC servo motors with their AKD drivers are used.

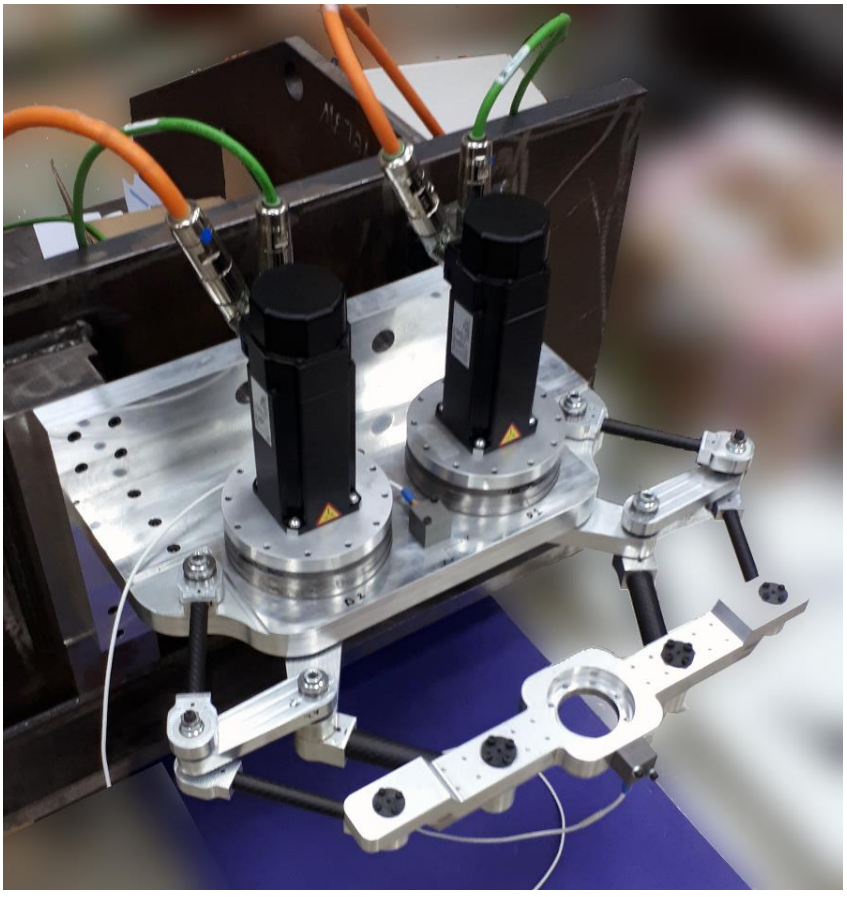

Figure 6.1. Over-constrained manipulator.

One of the scopes of this project is nonlinear controller development along with stiffness model of the mechanism. This section consists of modeling and nonlinear controller development of this system. The aim of this section is the introduction of controller algorithms that may be utilized regarding this scope.

There is no analytical solution of kinematic and static equilibrium equations since in over-constrained mechanism (Figure 6.2 b) the number of equations needed to be solved is less than the number of unknowns. To overcome this hardship, in the modeling of over-constrained mechanism, the parallelograms introduced in the mechanism are considered as a single limb, the offset in between fixed axes and axes on the platform are accepted as zero and the mechanism is transformed to the 5R in Figure 6.2 a. In this case, the two mechanisms are kinematically identical. Hence, the dynamic parameters of the 6R mechanism are lumped into the 5R mechanism in the dynamic model.

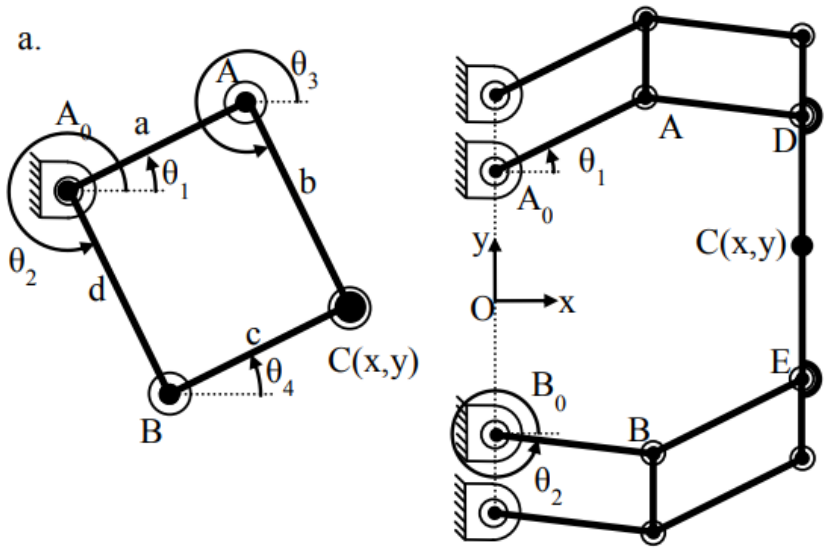

(a) (b)

Figure 6.2. Over-constrained mechanism and 5R kinematically identical model.

(Source: Kiper et al., 2015)

In the following part dynamic model of the micro mechanism, exact model controller, adaptive controller, and the simulation results are presented. The model of the closed chain mechanical system can be designed by subjecting constraints to the open-loop model. The 2-DoF five-bar linkage closed-loop mechanism (Figure 6.3) is constructed from two open-chain serial links. The respective numbers for kinematic parameters of the mechanism are denoted in Figure 6.3.

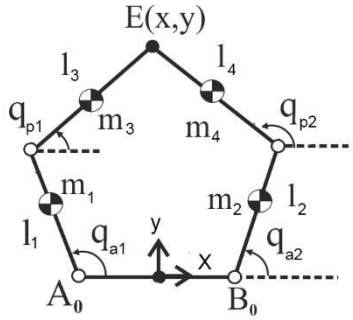

Figure 6.3. 5R mechanism used in the derivation of the dynamic model.

First, the dynamic model of each planar 2-DoF serial manipulator can be formulated as:

$$\boldsymbol{\tau_i} - \boldsymbol{f_i} = \boldsymbol{M_i}\ddot{\boldsymbol{q}}_\boldsymbol{i} + \boldsymbol{N_i}\dot{\boldsymbol{q}}_\boldsymbol{i} + \boldsymbol{G_i} \tag{6.1}$$

$$\boldsymbol{q_i} = [\boldsymbol{q_{ai}} \quad \boldsymbol{q_{pi}}]^{\boldsymbol{T}}$$

$$\boldsymbol{\tau_i} = [\boldsymbol{\tau_{ai}} \quad \boldsymbol{\tau_{pi}}]^{\boldsymbol{T}}$$

$$\boldsymbol{f_i} = [\boldsymbol{f_{ai}} \quad \boldsymbol{f_{pi}}]^{\boldsymbol{T}}$$

where $\boldsymbol{q_i}$, for i= 1,2, is the vector of generalized coordinates of the open-chain manipulator including the passive joints $\boldsymbol{q_{pi}}$ and active joints $\boldsymbol{q_{ai}}$on the five-bar and $\boldsymbol{\tau_i}$ is the corresponding computed torques. $\boldsymbol{M_i} \in \mathbb{R}^{\mathbf{2x2}}$ is the generalized inertia matrix, $\boldsymbol{N_i} \in \mathbb{R}^{\mathbf{2x2}}$ is a matrix including centrifugal and Coriolis terms, and $\boldsymbol{G_i} \in \mathbb{R}^{\mathbf{2}}$ is the gravity term. After obtaining equations of open chain dynamics, a reduced model in the form of equations can be extracted by subjecting it to constraints as follows.

$$\boldsymbol{M_i} = \begin{bmatrix} \boldsymbol{a_i} & \boldsymbol{b_i}\,\boldsymbol{cos}(\boldsymbol{q_{ai}} - \boldsymbol{q_{pi}}) \\ \boldsymbol{b_i}\,\boldsymbol{cos}(\boldsymbol{q_{ai}} - \boldsymbol{q_{pi}}) & \boldsymbol{d_i} \end{bmatrix} \tag{6.2}$$

$$\boldsymbol{N_i} = \begin{bmatrix} \mathbf{0} & \dot{\boldsymbol{q}}_{\boldsymbol{pi}}\,\boldsymbol{h_i}\,\boldsymbol{sin}(\boldsymbol{q_{ai}} - \boldsymbol{q_{pi}}) \\ -\dot{\boldsymbol{q}}_{\boldsymbol{ai}}\,\boldsymbol{k_i}\,\boldsymbol{sin}(\boldsymbol{q_{ai}} - \boldsymbol{q_{pi}}) & \mathbf{0} \end{bmatrix} \tag{6.3}$$

where $\boldsymbol{a_i}, \boldsymbol{b_i}, \boldsymbol{d_i}, \boldsymbol{h_i}, \boldsymbol{k_i}$ includes the dynamic parameters. $\boldsymbol{M_i}$ is a symmetric and positive and $\dot{\boldsymbol{M}}_\boldsymbol{i} - \mathbf{2}\boldsymbol{N_i}$ is a skew-symmetric matrix.

Combining the dynamic models of two 2-DOF serial manipulators, uniting the active joint equation and the passive joint equation respectively, then the dynamic model of the open-chain system can be expressed as:

$$\begin{bmatrix}\boldsymbol{\tau_a}\\ \boldsymbol{\tau_p}\end{bmatrix} - \begin{bmatrix}\boldsymbol{f_a}\\ \boldsymbol{f_p}\end{bmatrix} = \boldsymbol{M'}\begin{bmatrix}\ddot{\boldsymbol{q}}_{\boldsymbol{a}}\\ \ddot{\boldsymbol{q}}_{\boldsymbol{p}}\end{bmatrix} + \boldsymbol{N'}\begin{bmatrix}\dot{\boldsymbol{q}}_{\boldsymbol{a}}\\ \dot{\boldsymbol{q}}_{\boldsymbol{p}}\end{bmatrix} \tag{6.4}$$

$$\boldsymbol{q_a} = [q_{a1} \quad q_{a2}]^T$$

$$\boldsymbol{q_b} = [q_{b1} \quad q_{b2}]^T$$

$$\boldsymbol{\tau_a} = [\tau_{a1} \quad \tau_{a2}]^T$$

$$\boldsymbol{\tau_b} = [\tau_{b1} \quad \tau_{b2}]^T = [0 \quad 0]^T$$

where $\boldsymbol{M'}$and $\boldsymbol{N'}$are defined as:

$$\boldsymbol{M'} = \begin{bmatrix} a_1 & 0 & b_1\cos(q_{a1} - q_{p1}) & 0 \\ 0 & a_2 & 0 & b_2\cos(q_{a2} - q_{p2}) \\ b_1\cos(q_{a1} - q_{p1}) & 0 & d_1 & 0 \\ 0 & b_2\cos(q_{a2} - q_{p2}) & 0 & d_2 \end{bmatrix} \tag{6.5}$$

$$\begin{bmatrix} 0 & 0 & \dot{q}_{p1}\, h_1\, sin(q_{a1} - q_{p1}) & 0 \\ 0 & 0 & 0 & \dot{q}_{p2}\, h_2\, sin(q_{a2} - q_{p2}) \\ -\dot{q}_{a1}\, k_1\, sin(q_{a1} - q_{p1}) & 0 & 0 & 0 \\ 0 & -\dot{q}_{a2}\, k_2\, sin(q_{a2} - q_{p2}) & 0 & 0 \end{bmatrix} \tag{6.6}$$

$\boldsymbol{M'}$ is a symmetric and positive and $\boldsymbol{\dot{M}' - 2N'}$ is skew-symmetric. The angular velocity relation between the active joints and passive joints can be written as:

$$\boldsymbol{\dot{q}_p = \sigma\dot{q}_a},\ \boldsymbol{\ddot{q}_p = \dot{\sigma}\dot{q}_a + \sigma\ddot{q}_a} \tag{6.7}$$

Using the mentioned relation, $\boldsymbol{J_{ap}}$ is the velocity relation matrix defined as:

$$\boldsymbol{J_{ap}} = \begin{bmatrix}\mathbf{I}\\ \boldsymbol{\sigma}\end{bmatrix} \tag{6.8}$$

Redefining the combined dynamic models Equation 6.9 is constructed.

$$\begin{bmatrix}\boldsymbol{\tau_a}\\ \boldsymbol{\tau_p}\end{bmatrix} - \begin{bmatrix}\boldsymbol{f_a}\\ \boldsymbol{f_p}\end{bmatrix} = \boldsymbol{M'J_{ap}\ddot{q}_a} + (\boldsymbol{M'\dot{J}_{ap} + N'J_{ap}})\boldsymbol{\dot{q}_a} \tag{6.9}$$

When the constraint forces due to the closed-loop constraints are introduced, the dynamic model of the parallel manipulator can be formulated as:

$$\begin{bmatrix}\boldsymbol{\tau_a}\\ \boldsymbol{\tau_p}\end{bmatrix} - \begin{bmatrix}\boldsymbol{f_a}\\ \boldsymbol{f_p}\end{bmatrix} + \boldsymbol{Q^T\lambda} = \boldsymbol{M'J_{ap}\ddot{q}_a} + (\boldsymbol{M'\dot{J}_{ap} + N'J_{ap}})\boldsymbol{\dot{q}_a} \tag{6.10}$$

$\boldsymbol{Q^T\lambda}$ represents the constraint force vector, where constraint matrix $\boldsymbol{Q}$ is the differential of the closed-loop constrained equation, and $\boldsymbol{\lambda}$ is a multiplier representing the magnitude of the constraint forces. The closed-loop constraint equations of the parallel manipulator can be determined by:

$$\boldsymbol{\varphi(q)} = \begin{bmatrix} l_1\cos(q_{a1}) + l_3\cos(q_{b1}) - l_2\cos(q_{a2}) - l_4\cos(q_{b2}) - l_{5x} \\ l_1\sin(q_{a1}) + l_3\sin(q_{b1}) - l_2\sin(q_{a2}) - l_4\sin(q_{b2}) - l_{5y} \end{bmatrix} \quad (6.11)$$

In this model, passive joints frictions are assumed zero to reduce the complexity of equation, $\boldsymbol{f_p = 0}$. Also compared to the actuator friction, they are predicted to be negligible. Passive joints torques, $\boldsymbol{\tau_p}$, are equal to zero. After differentiating the $\boldsymbol{\varphi(q)}$ as:

$$\frac{\boldsymbol{d\varphi(q)}}{\boldsymbol{dt}} = \frac{\boldsymbol{\partial\varphi(q)}}{\boldsymbol{\partial q}}\boldsymbol{\dot{q}} = \boldsymbol{Q\dot{q}} = \boldsymbol{0} \quad (6.12)$$

$\boldsymbol{Q}$ is obtained as:

$$\boldsymbol{Q} = \begin{bmatrix} -l_1\sin(q_{a1}) & l_2\sin(q_{a2}) & -l_3\sin(q_{b1}) & l_4\sin(q_{b2}) \\ l_1\cos(q_{a1}) & -l_2\cos(q_{a2}) & l_3\cos(q_{b1}) & -l_4\cos(q_{b2}) \end{bmatrix} \quad (6.13)$$

Using the constraint equation $\boldsymbol{Q\dot{q} = 0}$, then one can have $\boldsymbol{Q\dot{q} = QJ_{ap}{}^T\dot{q}_a = 0}$ with the Jacobian matrix $\boldsymbol{J_{ap}}$.With this equality, the term of $\boldsymbol{J_{ap}{}^TQ^T\lambda = 0}$ can be eliminated.

$$\boldsymbol{Q^TJ_{ap}{}^T\dot{q}_a = 0} \quad (6.14)$$

$$\boldsymbol{J_{ap}{}^TQ^T\lambda = 0} \quad (6.15)$$

Multiplying both sides with $\boldsymbol{J_{ap}{}^T}$the equation becomes as follows:

$$\boldsymbol{\tau_a - f_a + J_{ap}{}^TQ^T\lambda = J_{ap}{}^TM'J_{ap}\ddot{q}_a + J_{ap}{}^T(M'\dot{J}_{ap} + N'J_{ap})\dot{q}_a}$$

$$\boldsymbol{\tau_a - f_a = J_{ap}{}^TM'J_{ap}\ddot{q}_a + J_{ap}{}^T(M'\dot{J}_{ap} + N'J_{ap})\dot{q}_a}$$

$$\boldsymbol{M = J_{ap}{}^TM'J_{ap}} \quad (6.16)$$

$$\boldsymbol{N = J_{ap}{}^T(M'\dot{J}_{ap} + N'J_{ap})\dot{q}_a}$$

$$\boldsymbol{\tau_a - f_a = M\ddot{q}_a + N\dot{q}_a}$$

where $\boldsymbol{M}$ is symmetric and positive and $\dot{\boldsymbol{M}} - \mathbf{2}\boldsymbol{N}$ is a skew-symmetric matrix. Proof of this can be given with the following properties:

- $\boldsymbol{A}^T$=-$\boldsymbol{A}$ (skew symmetry)
- $(\boldsymbol{AB})^T$=$\boldsymbol{B}^T\boldsymbol{A}^T$
- $(\boldsymbol{A}+\boldsymbol{B})^T$=$\boldsymbol{B}^T$+$\boldsymbol{A}^T$

$$\dot{\boldsymbol{M}} - \mathbf{2}\boldsymbol{N} = \dot{\boldsymbol{J}}_{\boldsymbol{ap}}{}^{\boldsymbol{T}}\boldsymbol{M}'\boldsymbol{J}_{\boldsymbol{ap}} + \boldsymbol{J}_{\boldsymbol{ap}}{}^{\boldsymbol{T}}\boldsymbol{M}'\boldsymbol{J}_{\boldsymbol{ap}} + \boldsymbol{J}_{\boldsymbol{ap}}{}^{\boldsymbol{T}}\dot{\boldsymbol{M}}'\boldsymbol{J}_{\boldsymbol{ap}} - \mathbf{2}\boldsymbol{J}_{\boldsymbol{ap}}{}^{\boldsymbol{T}}\boldsymbol{M}'\dot{\boldsymbol{J}}_{\boldsymbol{ap}} - \mathbf{2}\boldsymbol{J}_{\boldsymbol{ap}}{}^{\boldsymbol{T}}\boldsymbol{N}'\boldsymbol{J}_{\boldsymbol{ap}}$$

$$\dot{\boldsymbol{M}} - \mathbf{2}\boldsymbol{N} = \boldsymbol{J}_{\boldsymbol{ap}}{}^{\boldsymbol{T}}(\dot{\boldsymbol{M}}' - \mathbf{2}\boldsymbol{N}')\boldsymbol{J}_{\boldsymbol{ap}} + \dot{\boldsymbol{J}}_{\boldsymbol{ap}}{}^{\boldsymbol{T}}\boldsymbol{M}'\boldsymbol{J}_{\boldsymbol{ap}} - \boldsymbol{J}_{\boldsymbol{ap}}{}^{\boldsymbol{T}}\boldsymbol{M}'\dot{\boldsymbol{J}}_{\boldsymbol{ap}} \tag{6.17}$$

Since $\dot{\boldsymbol{M}}' - \mathbf{2}\boldsymbol{N}'$ and $\dot{\boldsymbol{J}}_{\boldsymbol{ap}}{}^{\boldsymbol{T}}\boldsymbol{M}'\boldsymbol{J}_{\boldsymbol{ap}} - \boldsymbol{J}_{\boldsymbol{ap}}{}^{\boldsymbol{T}}\boldsymbol{M}'\dot{\boldsymbol{J}}_{\boldsymbol{ap}}$ have skew-symmetric property so $\dot{\boldsymbol{M}} - \mathbf{2}\boldsymbol{N}$ is also skew-symmetric.

Adaptive control methods are used when the parameters of the system model with uncertainties are linearly separable. In cases where uncertainties cannot be measured it has been proved that the error analysis and the derivative used to measure controller performance lead to asymptotically zero.

The general dynamic equation of the second order, two degrees of freedom system, can be defined by the generalized coordinate system $\boldsymbol{q}, \dot{\boldsymbol{q}}, \ddot{\boldsymbol{q}} \in \mathbb{R}^{\mathbf{2}}$ according to Equation 6.18 and system matrices $\boldsymbol{M}(\boldsymbol{q}) \in \mathbb{R}^{\mathbf{2x2}}$, $\boldsymbol{N}(\boldsymbol{q}, \dot{\boldsymbol{q}}) \in \mathbb{R}^{\mathbf{2x2}}$, $\boldsymbol{G}(\boldsymbol{q}) \in \mathbb{R}^{\mathbf{2}}$.

$$\boldsymbol{\tau} = \boldsymbol{M}(\boldsymbol{q})\ddot{\boldsymbol{q}} + \boldsymbol{N}(\boldsymbol{q}, \dot{\boldsymbol{q}})\dot{\boldsymbol{q}} + \boldsymbol{G}(\boldsymbol{q}) \tag{6.18}$$

Before starting the design of adaptive controller on second-order dynamic systems, the position error should be specified as follows to evaluate the performance.

$$\boldsymbol{e} \triangleq \boldsymbol{x}_{\boldsymbol{d}} - \boldsymbol{x} \tag{6.19}$$

$\boldsymbol{x}_{\boldsymbol{d}} \in \mathbb{R}^{\mathbf{2}}$,$\boldsymbol{x} \in \mathbb{R}^{\mathbf{2}}$ are end-effector desired and measured motion. The Jacobian matrix $\boldsymbol{J} \in \mathbb{R}^{\mathbf{2x2}}$ is obtained by the relationship between the working space of the mechanism and the generalized coordinate system.

$$\dot{\boldsymbol{x}} = \boldsymbol{J}\dot{\boldsymbol{q}} \tag{6.20}$$

A filtered error signal is generated by the $\boldsymbol{\alpha} \in \mathbb{R}$ scalar coefficient.

$$\dot{\boldsymbol{e}} = \boldsymbol{J}\boldsymbol{r} - \boldsymbol{\alpha}\boldsymbol{e}$$

$$\boldsymbol{J}\boldsymbol{r} = \dot{\boldsymbol{x}}_{\boldsymbol{d}} - \dot{\boldsymbol{x}} + \boldsymbol{\alpha}\boldsymbol{e} \tag{6.21}$$

$$\boldsymbol{r} = \boldsymbol{J}^{-\mathbf{1}}(\dot{\boldsymbol{e}} + \boldsymbol{\alpha}\boldsymbol{e})$$

If time dependent equation $\boldsymbol{r} \in \mathbb{R}^2$ vector can be drawn to zero, $\boldsymbol{e} \in \mathbb{R}^2$, error vector is also drawn to the desired values. The following expression is obtained by taking the time derivative of $\boldsymbol{r}$.

$$\dot{\boldsymbol{r}} = \frac{\boldsymbol{d}}{\boldsymbol{dt}}(\boldsymbol{J^{-1}})(\dot{\boldsymbol{x}}_{\boldsymbol{d}} + \boldsymbol{\alpha e}) + (\boldsymbol{J^{-1}})(\ddot{\boldsymbol{x}}_{\boldsymbol{d}} + \boldsymbol{\alpha}\dot{\boldsymbol{e}}) - \ddot{\boldsymbol{q}} \tag{6.22}$$

The controller design is continued by introducing the vector containing the error functions.

$$\boldsymbol{M}\dot{\boldsymbol{r}} = \boldsymbol{M}\frac{\boldsymbol{d}}{\boldsymbol{dt}}(\boldsymbol{J^{-1}})(\dot{\boldsymbol{x}}_{\boldsymbol{d}} + \boldsymbol{\alpha e}) + \boldsymbol{M}(\boldsymbol{J^{-1}})(\ddot{\boldsymbol{x}}_{\boldsymbol{d}} + \boldsymbol{\alpha}\dot{\boldsymbol{e}}) - \boldsymbol{M}\ddot{\boldsymbol{q}} \tag{6.23}$$

With the filtered error, the addition of the expressions in the dynamic equation is derived from Equation 6.23 and Equation 6.22.

$$\boldsymbol{M}\ddot{\boldsymbol{q}} = \boldsymbol{N}\dot{\boldsymbol{q}} + \boldsymbol{G} - \boldsymbol{\tau} \tag{6.24}$$

$$\dot{\boldsymbol{q}} = \boldsymbol{J^{-1}}(\dot{\boldsymbol{x}}_{\boldsymbol{d}} + \boldsymbol{\alpha e}) - \boldsymbol{r} \tag{6.25}$$

$\boldsymbol{M}\dot{\boldsymbol{r}}$ can be found as:

$$\boldsymbol{M}\frac{\boldsymbol{d}}{\boldsymbol{dt}}(\boldsymbol{J^{-1}})(\dot{\boldsymbol{x}}_{\boldsymbol{d}} + \boldsymbol{\alpha e}) + \boldsymbol{M}(\boldsymbol{J^{-1}})(\ddot{\boldsymbol{x}}_{\boldsymbol{d}} + \boldsymbol{\alpha}\dot{\boldsymbol{e}}) + \boldsymbol{N}(\boldsymbol{J^{-1}})(\ddot{\boldsymbol{x}}_{\boldsymbol{d}} + \boldsymbol{\alpha}\dot{\boldsymbol{e}}) - \boldsymbol{Nr} + \boldsymbol{G} - \boldsymbol{\tau} \tag{6.26}$$

In particular, where the non-linear terms are not known, the $\boldsymbol{W}$ matrix is designated to be used in the adaptive controller.

$$\boldsymbol{W} \triangleq \boldsymbol{M}\frac{\boldsymbol{d}}{\boldsymbol{dt}}(\boldsymbol{J^{-1}})(\dot{\boldsymbol{x}}_{\boldsymbol{d}} + \boldsymbol{\alpha e}) + \boldsymbol{M}(\boldsymbol{J^{-1}})(\ddot{\boldsymbol{x}}_{\boldsymbol{d}} + \boldsymbol{\alpha}\dot{\boldsymbol{e}}) + \boldsymbol{N}(\boldsymbol{J^{-1}})(\dot{\boldsymbol{x}}_{\boldsymbol{d}} + \boldsymbol{\alpha e}) \tag{6.27}$$

Therefore, system equations can be rewritten as:

$$\boldsymbol{M}\dot{\boldsymbol{r}} = \boldsymbol{W} - \boldsymbol{Nr} - \boldsymbol{\tau} \tag{6.28}$$

6.1.1. Exact Model Knowledge Control

The controller is defined as follows, for the case when all parameters are known before the adaptive controller design. With Equation 6.26 and stability analysis, the input, $\boldsymbol{\tau}$, is designed.

$$\boldsymbol{\tau} = \boldsymbol{W} + \boldsymbol{K_r r} + \boldsymbol{J^T e} \tag{6.29}$$

$\boldsymbol{K_r}$ is a positive diagonal gain matrix. Summing Equation 6.28 and 6.29, closed dynamic equation is obtained as follows:

$$\boldsymbol{M\dot{r} = -Nr - K_r r - J^T e} \tag{6.30}$$

For stability analysis of proposed controller design positive $\boldsymbol{V_{emk}(t)} \in \mathbb{R}$ time-dependent function is analyzed.

$$\boldsymbol{V_{emk} = \frac{1}{2} r^T M r + \frac{1}{2} e^T e} \tag{6.31}$$

Thereby the derivative of Lyapunov function is investigated.

$$\boldsymbol{\dot{V}_{emk} = \frac{1}{2} r^T \dot{M} r + r^T M \dot{r} + e^T \dot{e}}$$

$$\boldsymbol{= \frac{1}{2} r^T \dot{M} r + r^T (-Nr - K_r r - J^T e) + e^T (Jr - \alpha e)} \tag{6.32}$$

$$\boldsymbol{= \frac{1}{2} r^T (\dot{M} - 2N) r + r^T K_r r - r^T J^T e - e^T \alpha e + e^T J r}$$

$$\boldsymbol{= -r^T K_r r - e^T \alpha e}$$

As a result of the stability analysis, the error asymptotically reaches to zero when the time deviates of function are defined with positive gains in the condition of limited closed-loop signal inputs. $\boldsymbol{V_{emk}(t)}$ function for $\boldsymbol{t \geq 0}$ goes exponentially fast to the zero.

6.1.2. Adaptive controller

After the controller has been designed for the situation where the system parameters are known where there is no uncertainty in the system. Thereby, it is aimed to design the adaptive where there are uncertainties in the model. This controller is devised for uncertainties in the dynamic parameters of the model-based controller, namely the parameters used in the generalized inertia matrix. For this adaptation, it is important to state that these parameters should be linearly separable in $\boldsymbol{W}$. $\boldsymbol{W}$ matrix contains nonlinear terms and can be defined with known parameters $\boldsymbol{Y}$ (regression) matrix and unknown parameter $\boldsymbol{\phi}$ vector.

$$\boldsymbol{W = Y\phi} \tag{6.33}$$

Since $\boldsymbol{\phi}$ vector is unknown the estimation of this vector is defined with $\boldsymbol{\hat{\phi}}$.

$$\boldsymbol{\tau = Y\hat{\phi} + K_r r + J^T e} \tag{6.34}$$

With Equations given, the dynamic equation is redefined as:

$$\boldsymbol{M\dot{r} = Y\phi - Y\hat{\phi} - Nr - K_r r - J^T e} \tag{6.35}$$

The performance of the estimation vector, $\boldsymbol{\hat{\phi}}$, can be given with $\boldsymbol{\tilde{\phi}}$.

$$\boldsymbol{\tilde{\phi} \triangleq \phi - \hat{\phi}} \tag{6.36}$$

Then, the time derivative of the vector, $\dot{\boldsymbol{\tilde{\phi}}}$, cane be defined with negative of $\dot{\boldsymbol{\hat{\phi}}}$.

$$\boldsymbol{\dot{\tilde{\phi}} = -\dot{\hat{\phi}}} \tag{6.37}$$

For stability analysis, $\boldsymbol{V_{adp}(t)} \in \mathbb{R}$ time-dependent Lyapunov function is designed.

$$\boldsymbol{V_{adp} = \frac{1}{2} r^T M r + \frac{1}{2} e^T e + \frac{1}{2} \tilde{\phi}^T \Gamma \tilde{\phi}} \tag{6.38}$$

Positive symmetric diagonal gain matrix $\boldsymbol{\Gamma}$ is defined in previous Equation. The time derivative of the Lyapunov function is then found as:

$$\boldsymbol{\dot{V}_{adp} = \frac{1}{2} r^T \dot{M} r + r^T M \dot{r} + e^T \dot{e} + \tilde{\phi}^T \Gamma^{-1} \dot{\tilde{\phi}}} \tag{6.39}$$

With summation of equations $\boldsymbol{\dot{V}_{adp}(t)} \in \mathbb{R}$ function can be written as:

$$\boldsymbol{\dot{V}_{adp} = \frac{1}{2} r^T \dot{M} r + r^T \left(Y\tilde{\phi} - Nr - K_r r - J^T e \right) + e^T (Jr - \alpha e) + \tilde{\phi}^T \Gamma^{-1} \dot{\tilde{\phi}}} \tag{6.40}$$

$$\boldsymbol{= -r^T K_r r - e^T \alpha e + r^T Y \tilde{\phi} + \tilde{\phi}^T \Gamma^{-1} \dot{\tilde{\phi}}}$$

$$\boldsymbol{= -r^T K_r r - e^T \alpha e + \tilde{\phi}^T \left(Y^T r + \Gamma^{-1} \dot{\tilde{\phi}} \right)}$$

The update rule of $\boldsymbol{\hat{\phi}}$ in Equation 6.37 can be defined with $\boldsymbol{\dot{\hat{\phi}} = \Gamma Y^T r}$ so as with $\boldsymbol{\dot{\tilde{\phi}} = \Gamma Y^T r}$. When inserted in Equation 6.40 with $\boldsymbol{Y^T r - \Gamma^{-1} \Gamma Y^T r}$=0, $\boldsymbol{\dot{V}_{adp}(t)}$ the function can be represented with:

$$\boldsymbol{\dot{V}_{adp} = -r^T K_r r - e^T \alpha e} \tag{6.41}$$

When the error is bounded (Barbalat's Lemma), filtered error and position error $r(\boldsymbol{t})$ $\boldsymbol{\dot{e}(t)}$ goes to zero asymptotically fast when $\boldsymbol{t}$ goes to zero.

6.1.3. Validation of Controllers with Simulations

A case study is presented to show the performance and viability of the proposed controller. The simulation model is constructed by using Matlab™ Simscape™ Multibody™ blocks. Initially, a dynamic analysis of the manipulator is carried out and validated with the results of the model constructed with Matlab™ Simscape™ Multibody™ blocks. This validated model is used in computing the respective matrices (e.g., generalized inertia matrix).

Simulations are run with 2 kHz sampling rate and with ode4 (Runge-Kutta) solver. Desired task space motions are given in position, velocity, and acceleration level in Figure 6.4.

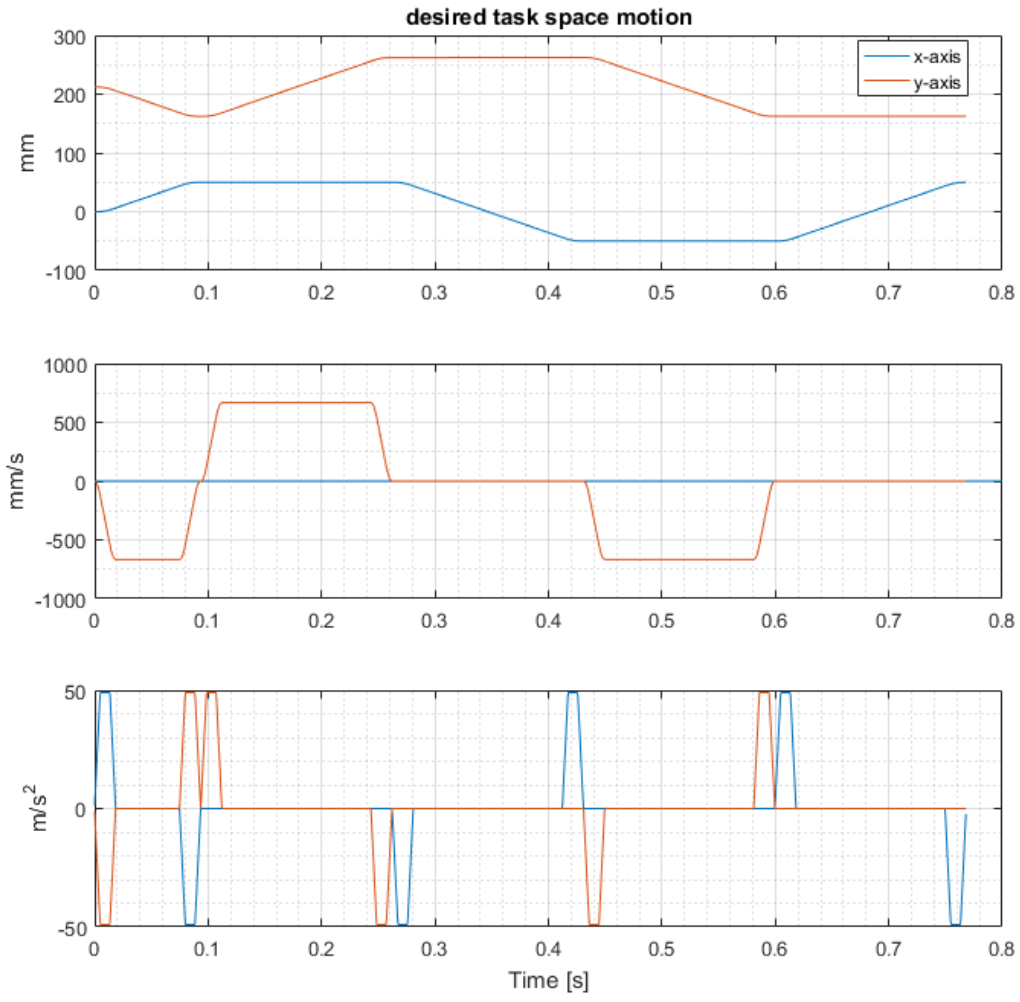

Figure 6.4. Desired task-space motion.

Therefore, first, the exact model knowledge controller is tested in the given conditions and with the parameters given in Table 6.1., which are obtained from the design of the robot. The tracking errors $\boldsymbol{e}, \dot{\boldsymbol{e}}$ are given in Figure 6.5. for performance evaluation. In all of the simulations, the control gains are chosen as $\alpha = 1, \boldsymbol{K} = diag(10,10)$ for consistency. The results are presented to compare the performance of the adaptive controller with respect to the exact model knowledge controller. It should be noted that better tuning results in better performance.

The $\widehat{\boldsymbol{\phi}} = [\boldsymbol{m_1} \quad \boldsymbol{m_2} \quad \boldsymbol{m_3} \quad \boldsymbol{m_4} \quad \boldsymbol{I_1} \quad \boldsymbol{I_2} \quad \boldsymbol{I_3} \quad \boldsymbol{I_4}]$ vector contains the uncertain parameters used in the adaptive controller. $\widehat{\boldsymbol{\phi}}(\mathbf{0})$, represent the initial condition of these parameters and may vary with the degree of knowledge one has about the system model in means of link's mass and inertia values.

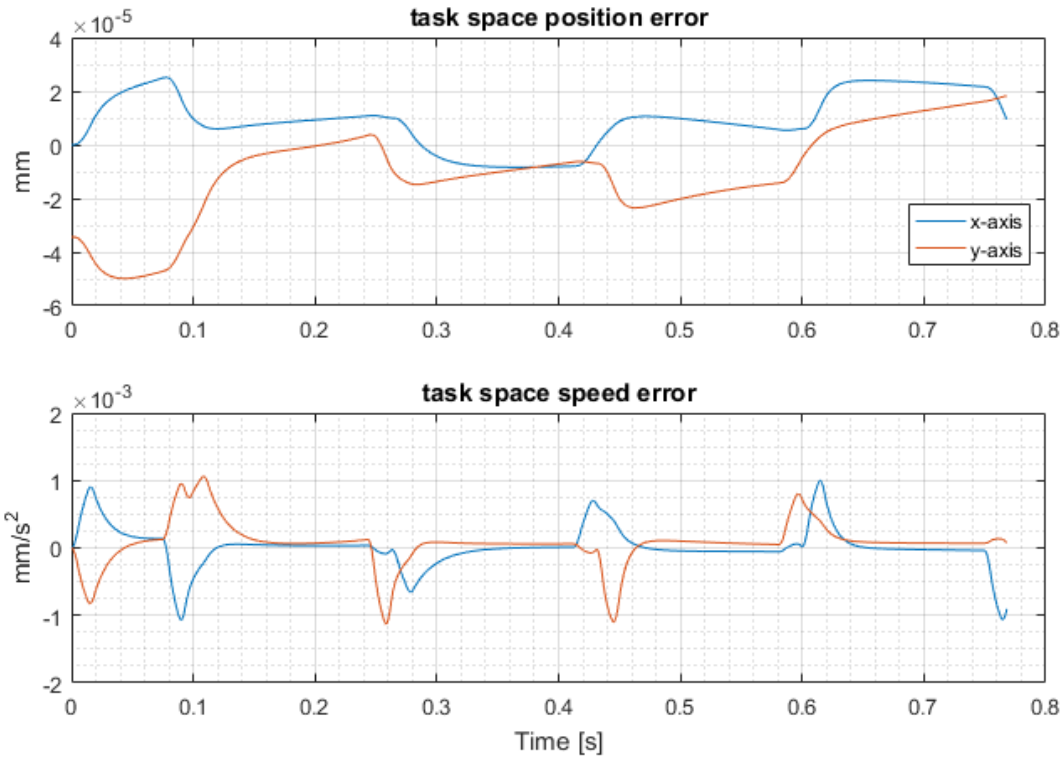

Figure 6.5. EMK controller simulation results.

In Figures 6.7 to 6.10 task space motion tracking errors are given for the results of the adaptive controller. In each figure different initial condition $\widehat{\boldsymbol{\phi}}(\mathbf{0})$ are used. The initial conditions of the estimated parameters and gain matrix, $\boldsymbol{\Gamma}$, are presented in Table 6.1. The maximum positioning errors for each case are also given in Table 6.1. These

trials are presented here to show the performance of adaptive controller for different cases of uncertainty.

Table 6.1. The conditions used in simulation of the adaptive controller for each case.

	Initial Condition	$\boldsymbol{\Gamma}$, Update Law Gain Matrix	Positioning Error
Figure 6.6	Exact model values	$\boldsymbol{diag}[\mathbf{1} \quad \mathbf{1} \quad \mathbf{1} \quad \mathbf{1} \quad \mathbf{1} \quad \mathbf{1} \quad \mathbf{1} \quad \mathbf{1}]$	$< \lvert \mathbf{0.01} \rvert \boldsymbol{\mu m}$
Figure 6.7	Initial conditions are 80% lower than the exact model	$\boldsymbol{diag}[\mathbf{10} \quad \mathbf{10} \quad \mathbf{10} \quad \mathbf{10} \quad \mathbf{1} \quad \mathbf{1} \quad \mathbf{1}$	$< \lvert \mathbf{13} \rvert \boldsymbol{\mu m}$
Figure 6.8	Unknown 5 kg payload	$\boldsymbol{diag}[\mathbf{10} \quad \mathbf{10} \quad \mathbf{100} \quad \mathbf{100} \quad \mathbf{1} \quad \mathbf{1}$	$< \lvert \mathbf{250} \rvert \boldsymbol{\mu m}$
Figure 6.10	Initial conditions are 80% lower than the exact model With feedback noise	$\boldsymbol{diag}[\mathbf{10} \quad \mathbf{10} \quad \mathbf{10} \quad \mathbf{10} \quad \mathbf{1} \quad \mathbf{1} \quad \mathbf{1}$	$< \lvert \mathbf{16} \rvert \boldsymbol{\mu m}$

As presented in Table 6.1., the initial condition, $\widehat{\boldsymbol{\phi}}(\mathbf{0})$, for results in Figure 6.6 is chosen equal to exact model parameters. The initial condition, $\widehat{\boldsymbol{\phi}}(\mathbf{0})$, for results in Figure 6.7 is chosen 80 percent lower than the exact model parameters. In Figure 6.8, a case is presented when the payload of 5 kg (designated mass of laser cutting head) is not known, and it is assumed that only the link's dynamic parameters are known. It can be seen that the positioning error is worst in magnitude for the case presented in Figure 6.8 in which the uncertainty is inserted for the case of an unknown robot payload. The errors, in this case, are bounded below 250 μm. On the other hand, errors are bounded below 16 μm for other initial conditions.

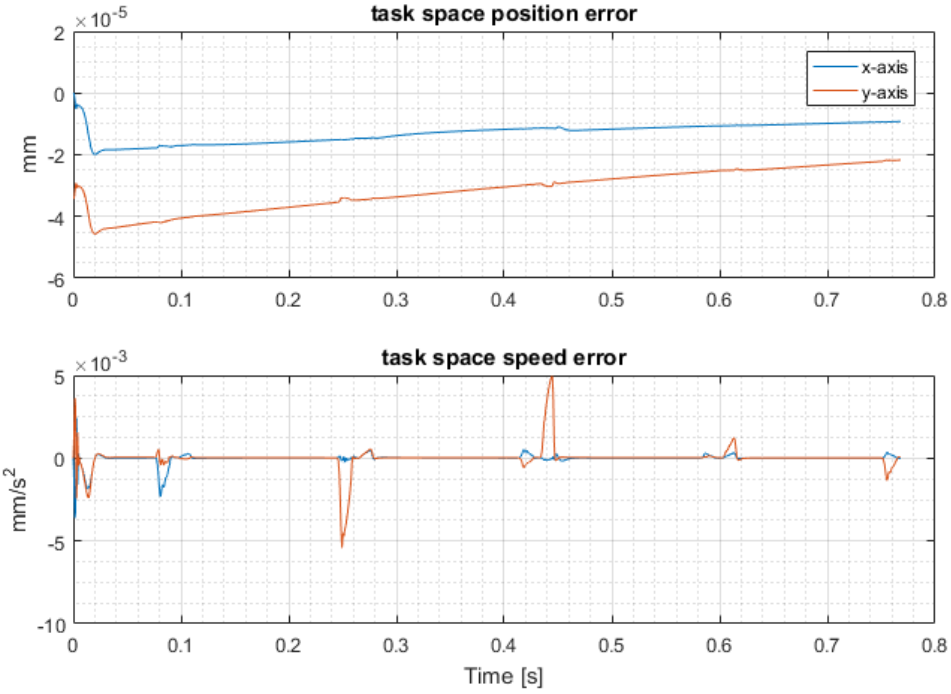

Figure 6.6. Adaptive controller result with exact model parameters.

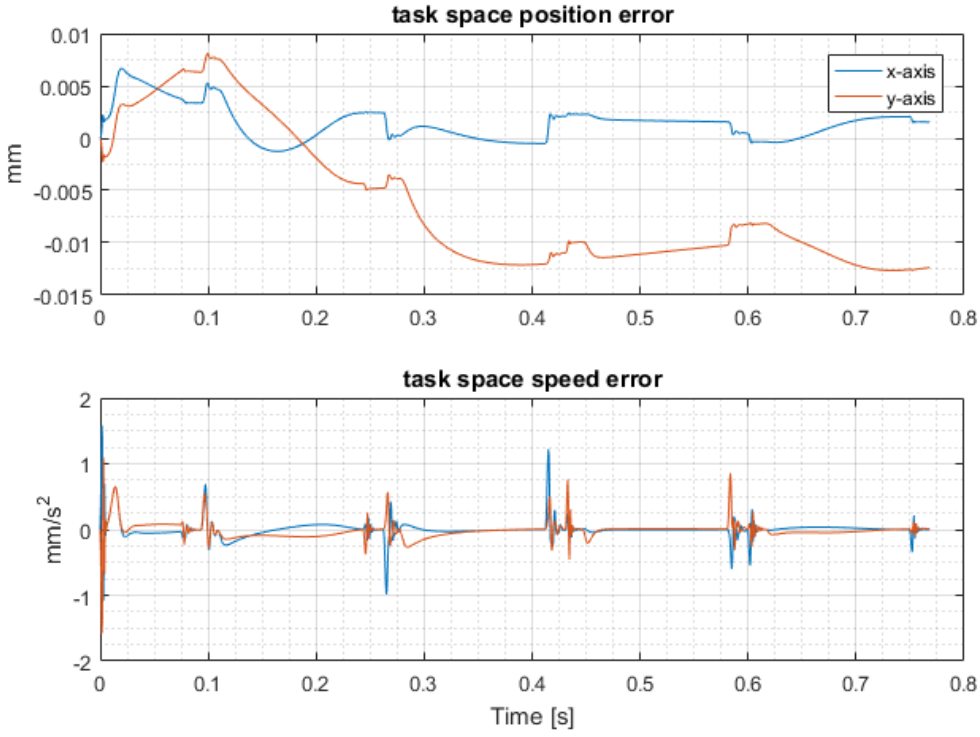

Figure 6.7. Adaptive controller result with 80 percent lower than exact model parameters.

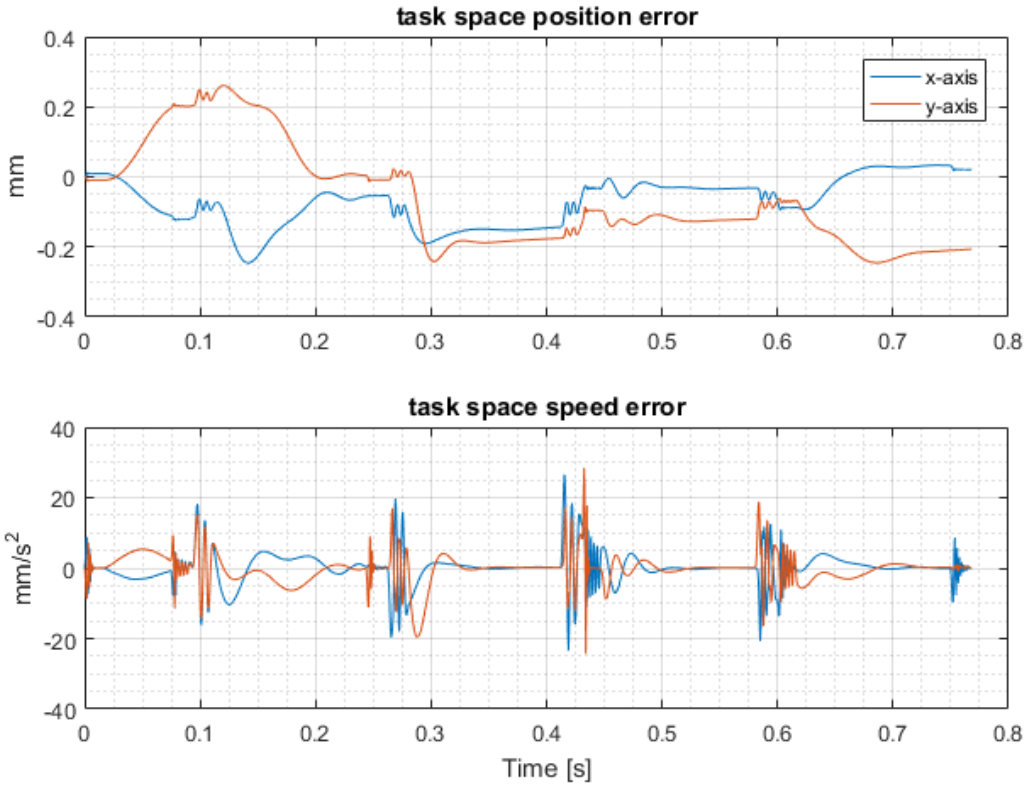

Figure 6.8. Adaptive controller result when the payload of 5kg is not added to the initial model parameters.

For the last case, virtual (white) noise is generated in the feedback of the simulation model for evaluation of the performance of the controller in the presence of feedback noise. In Figure 6.9, the noise-induced and raw feedback data are given for actuator feedback. In Figure 6.10 task space motion tracking errors are given for the results of the adaptive controller in case of feedback noise.

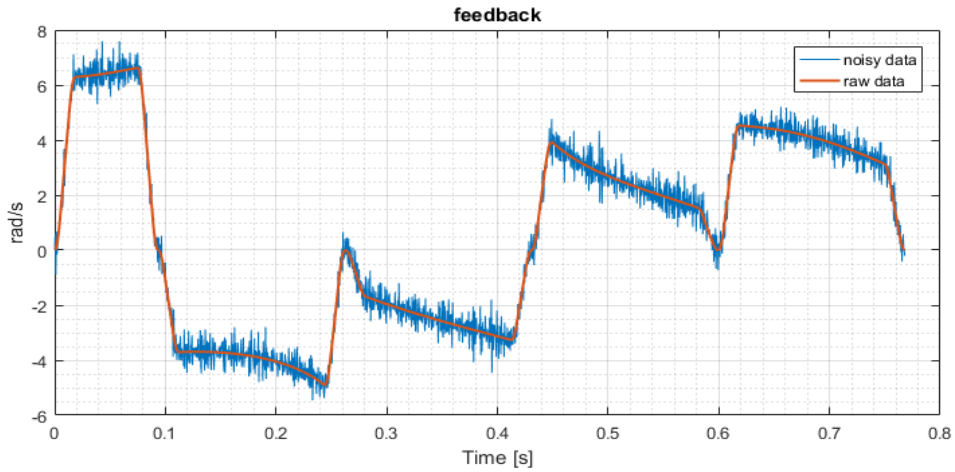

Figure 6.9. The noise introduced in actuator feedback.

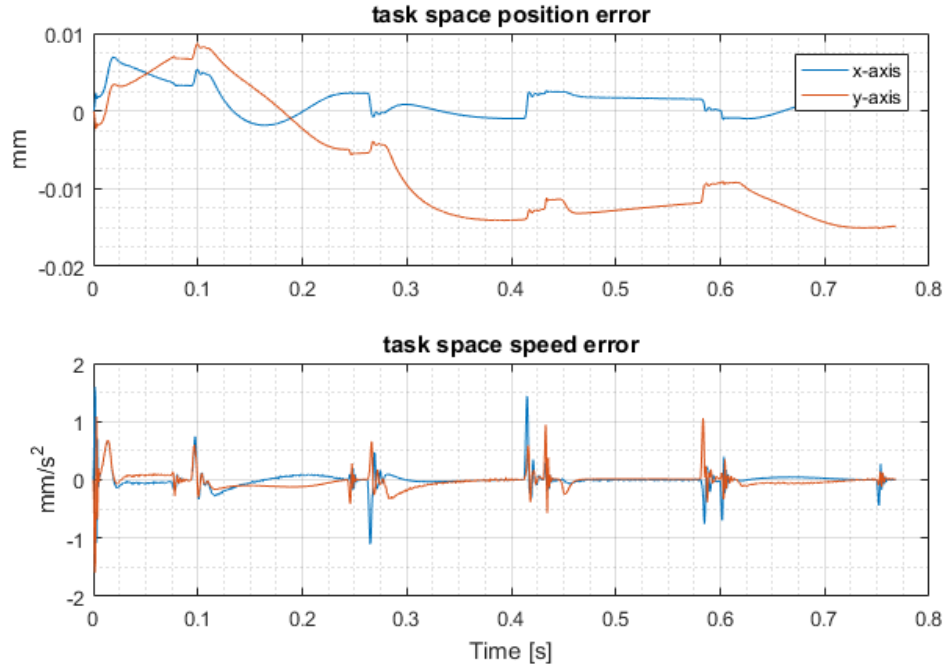

Figure 6.10. Adaptive controller result with noise in feedback and 80 percent lower than exact model parameters.

6.1.4. Conclusions

Consequently, exact model knowledge and adaptive controller for micro manipulator are derived and tested in simulations for future studies. The performance of these controllers proves their applicability. The adaptive controller could present an advantage for uncertainties in the model parameters. These algorithms can be applied in the real system using the current control loop of the servo drivers; however the torque reflecting the capability of the system should be tested with experiments.

It is advised that the torque control of the industrial servo motors should be investigated thoroughly with a test setup which includes a torque sensor. Considering the application, it is foreseen that a look-up table or more complex mathematical expressions for torque/ current characteristic of used industrial AC servo motors should be adjusted with empirical data. For future studies, the motor model could also be integrated into the controller. It is also suggested that machine learning methodologies can be tested with the developed system for modeling and control of this nonlinear system.

6.2. Multi-priority Controller for MMM

In Chapter 3, a semi-online control strategy and motion planning algorithm employed on an industrial laser cutting machine is presented. In addition to these studies, it is possible to develop better control strategies by making use of fully online controllers. The method introduced here is a multi-priority online controller which does not need an iterative procedure or pre-processing motion division algorithm as presented in previous Chapters. The nonlinear controller will diminish errors generated by nonlinearity in the physical system. The proposed methodology also results in the minimization of the total actuation effort. This method introduced in this Section is inspired from human upper-limb motion, in which it is observed that arm and wrist-hand motion can be identified as macro and micro manipulation especially for handling delicate tasks that would require precise motion; e.g., writing.

The proposed method is a multi-priority control where the first priority is end-effector's motion trajectory tracking, and the second priority is limiting the maximum acceleration of the macro manipulator to the desired limits while not violating the workspace boundaries of the micro manipulator. Redundancy is resolved by designing the null-space controller utilizing a simplified dynamic model of the proposed MMM.

In the previous Section, the derivation of the dynamic model of the micro manipulator is given. Also, the kinematic and dynamic properties of the model are listed. In the following section, the controller designed for the MMM is explained. The redundancy resolution algorithm to regulate the acceleration and workspace of the macro and micro manipulators is proposed along with the optimization of the parameters of this algorithm. A simulation test is prepared that has MMM model parameters similar to experiments in industrial application and the same trajectory as the previous experimental study. Proposed redundancy resolution algorithm is tested in simulations, and the obtained test results are discussed in the conclusions section.

The MMM devised in the study comprises the same workspace limitations as in planar laser cutting machine case study. The mechanism's kinematic structure is represented in Figure 6.11. $\boldsymbol{q_1}$ and $\boldsymbol{q_2}$ are Cartesian macro mechanism's prismatic joints and $\boldsymbol{q_3}$ and $\boldsymbol{q_4}$ are micro mechanisms active revolute joints of five-bar. Due to the closed chain, parallel mechanism's $\boldsymbol{q_5}$ and $\boldsymbol{q_6}$ joints are passive. Consequently, given the desired trajectory on planar space, the manipulator has two extra degrees-of-freedom. Therefore,

in addition to the main objective, which is to follow the end-effector trajectory, a secondary objective can be planned by making use of extra degrees-of-freedom. The dynamic model developed is defined in a compact and structured form and is used to implement a computed torque control method with the novel secondary-task definition for redundancy resolution. However, the computation of the dynamics of the parallel micro mechanism is more complicated than serial macro mechanisms because of their closed-form structure. The model of the mechanism with constraints is derived utilizing reduced-order model method for micro manipulator, proposed in the previous section, and a straightforward model for macro manipulator.

For the model is given in Figure 6.11, kinematic and dynamic parameters of the MMM are listed in Table 6.2. Link 1 and Link 2 are the macro manipulator's links in Cartesian configuration, which is a conventional x-y table in planar laser cutting machines. In the micro manipulator, five-bar parallel mechanism's Link 3 and Link 6 are identical to Link 4 and Link 5 respectively, which shows that they have the same kinematic and dynamic parameters. The length, $\boldsymbol{A_0B_0}$, given in Figure 6.11 is chosen to be zero in simulations to be consistent with the actual MMM in the case study. Global axes are represented by *E(x, y)* where end-effector's motions are defined, while the micro manipulator's axes are indicated with u and v on its base frame. According to given link parameters, the five-bar mechanism's (micro manipulator) middle position in its effective workspace is chosen as [0 0.212] m with respect to its base frame.

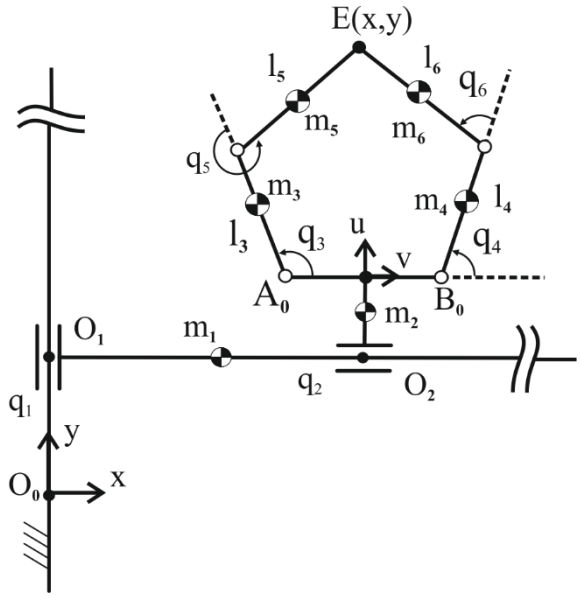

Figure 6.11. Model of the macro-micro manipulator (MMM).

Table 6.2. Kinematic and dynamic parameters of MMM used in simulations.

	Link length/maximum travel distance (mm)	Center of Mass (mm)	Mass (kg)	Moment of Inertia about the z-axis (kgmm^2)
Link 1 (Macro)	1500 (max)	750.2	422.49	1020718.61
Link 2 (Macro)	1000 (max)	100	29.87	36363.92
Link 3/4 (Micro)	150	80.35	3.40	1800.02
Link 5/6 (Micro)	150	82.66	3.91	1312.99

The model of the closed chain mechanical system can be designed by subjecting constraints to the open-loop model. The 2 DoF five-bar linkage closed-loop mechanism is constructed from two open-chain serial links, and the holonomic system is governed as given in Section 6.1. However, this time with the addition of prismatic joints for Cartesian macro manipulator the vector of generalized coordinates $\boldsymbol{q}'$ is represented as:

$$\boldsymbol{q}' = [q_1 \quad q_2 \quad q_3 \quad q_4 \quad q_5 \quad q_6]^{\boldsymbol{T}}, \ \dot{\boldsymbol{q}}' = [\dot{\boldsymbol{q}}_{\boldsymbol{1}} \quad \dot{\boldsymbol{q}}_{\boldsymbol{2}} \quad \dot{\boldsymbol{q}}_{\boldsymbol{3}} \quad \dot{\boldsymbol{q}}_{\boldsymbol{4}} \quad \dot{\boldsymbol{q}}_{\boldsymbol{5}} \quad \dot{\boldsymbol{q}}_{\boldsymbol{6}}]^{\boldsymbol{T}} \quad (6.42)$$

$\boldsymbol{\tau}$, corresponding computed torques are computed in expressions below where $\boldsymbol{M}(\boldsymbol{q}') \in \mathbb{R}^{\boldsymbol{4x4}}$ is the generalized inertia matrix, $\boldsymbol{N}(\boldsymbol{q}', \dot{\boldsymbol{q}}') \in \mathbb{R}^{\boldsymbol{4x4}}$ is a matrix including centrifugal and Coriolis terms, and $\boldsymbol{G}(\boldsymbol{q}') \in \mathbb{R}^{\boldsymbol{4}}$ is gravity term that is acquired using the Lagrangian method. After obtaining equations of open chain dynamics, a reduced model in the form of Equation below can be extracted by subjecting it to constraints as mentioned in the previous section.

$$\boldsymbol{\tau} = \boldsymbol{M}(\boldsymbol{q}')\ddot{\boldsymbol{q}} + \boldsymbol{N}(\boldsymbol{q}', \dot{\boldsymbol{q}}')\dot{\boldsymbol{q}} + \boldsymbol{G}(\boldsymbol{q}') \quad (6.43)$$

$$\boldsymbol{q} = \begin{bmatrix} q_1 \\ q_2 \\ q_3 \\ q_4 \end{bmatrix}, \dot{\boldsymbol{q}} = \begin{bmatrix} \dot{q}_1 \\ \dot{q}_2 \\ \dot{q}_3 \\ \dot{q}_4 \end{bmatrix}, \ddot{\boldsymbol{q}} = \begin{bmatrix} \ddot{q}_1 \\ \ddot{q}_2 \\ \ddot{q}_3 \\ \ddot{q}_4 \end{bmatrix} \quad (6.44)$$

Redundant manipulator has a Jacobain matrix $\mathbf{J} \in \mathbb{R}^{\boldsymbol{2x4}}$.

$$\boldsymbol{J} = \begin{bmatrix} 0 & 1 & -\frac{l_3 \sin(q_4+q_6)\sin(q_5)}{\sin(q_3+q_5-q_4-q_6)} & \frac{l_3 \sin(q_3+q_5)\sin(q_6)}{\sin(q_3+q_5-q_4-q_6)} \\ 1 & 0 & \frac{l_4 \cos(q_4+q_6)\sin(q_5)}{\sin(q_3+q_5-q_4-q_6)} & \frac{-l_4 \cos(q_3+q_5)\sin(q_6)}{\sin(q_3+q_5-q_4-q_6)} \end{bmatrix} \quad (6.45)$$

The task space motion of MMM is represented in Cartesian space with $\boldsymbol{x}$. The relationships of manipulator end-effector velocity and acceleration are described as:

$$\begin{aligned} \dot{\boldsymbol{x}} &= \boldsymbol{J}\dot{\boldsymbol{q}} \\ \ddot{\boldsymbol{x}} &= \boldsymbol{J}\ddot{\boldsymbol{q}} + \dot{\boldsymbol{J}}\dot{\boldsymbol{q}} \\ \dot{\boldsymbol{q}} &= \boldsymbol{J}^{+}\dot{\boldsymbol{x}} + \dot{\boldsymbol{q}}_{\boldsymbol{N}} \\ \ddot{\boldsymbol{q}} &= \boldsymbol{J}^{+}\left(\ddot{\boldsymbol{x}} - \dot{\boldsymbol{J}}\dot{\boldsymbol{q}}\right) + \ddot{\boldsymbol{q}}_{\boldsymbol{N}} \end{aligned} \tag{6.46}$$

where $\dot{\boldsymbol{q}} \in \mathbb{R}^{\boldsymbol{4}}$, $\ddot{\boldsymbol{q}} \in \mathbb{R}^{\boldsymbol{4}}$ joint velocity and acceleration vectors, $\dot{\boldsymbol{q}}_{\boldsymbol{N}} \in \mathbb{R}^{\boldsymbol{4}}$,$\ddot{\boldsymbol{q}}_{\boldsymbol{N}} \in \mathbb{R}^{\boldsymbol{4x6}}$are joint space projections to the null-space and $\dot{\boldsymbol{x}} \in \mathbb{R}^{\boldsymbol{2}}$, $\ddot{\boldsymbol{x}} \in \mathbb{R}^{\boldsymbol{2}}$ are task space velocity and acceleration. The pseudo-inverse denoted by $\boldsymbol{J}^{+} \in \mathbb{R}^{\boldsymbol{4x2}}$ is defined when $\boldsymbol{J}$ has the full rank to be used in control law.

6.2.1. The Control Law

The computed-torque method is used to control the MMM. The control input torque, $\boldsymbol{\tau}$, is formulated previously in which the term $\boldsymbol{J}^{+}\left(\ddot{\boldsymbol{x}}_{\boldsymbol{d}} + \boldsymbol{K}_{\boldsymbol{v}}\dot{\boldsymbol{e}} + \boldsymbol{K}_{\boldsymbol{p}}\boldsymbol{e} - \dot{\boldsymbol{J}}\dot{\boldsymbol{q}}\right)$ ensures the primary objective, which is trajectory tracking. The vector $\boldsymbol{\phi}_{\boldsymbol{N}} \in \mathbb{R}^{\boldsymbol{4}}$ is in the null-space of the Jacobian matrix which is obtained by multiplying a secondary objective function with the null-space projection matrix, which is $(\boldsymbol{I} - \boldsymbol{J}^{+}\boldsymbol{J})$. It is proven (Nakamura, 1991) that the main task, which can be also named as the primary task, is not affected by any arbitrary demands associated with the null space vector. Also, gravitational terms are neglected since the planar mechanism does not make any motion against gravity.

$$\boldsymbol{\tau} = \boldsymbol{M}(\boldsymbol{q}')\left\{\boldsymbol{J}^{+}\left(\ddot{\boldsymbol{x}}_{\boldsymbol{d}} + \boldsymbol{K}_{\boldsymbol{v}}\dot{\boldsymbol{e}} + \boldsymbol{K}_{\boldsymbol{p}}\boldsymbol{e} - \dot{\boldsymbol{J}}\dot{\boldsymbol{q}}\right) + \boldsymbol{\phi}_{\boldsymbol{N}}\right\} + \boldsymbol{N}(\boldsymbol{q}', \dot{\boldsymbol{q}}') \tag{6.47}$$

where $\boldsymbol{K}_{\boldsymbol{v}} \in \mathbb{R}^{\boldsymbol{2x2}}$ and $\boldsymbol{K}_{\boldsymbol{p}} \in \mathbb{R}^{\boldsymbol{2x2}}$ are constant diagonal gain matrices. Error vectors $\boldsymbol{e}$ and $\dot{\boldsymbol{e}}$ are computed with the desired task trajectory $\boldsymbol{x}_{\boldsymbol{d}}$, $\dot{\boldsymbol{x}}_{\boldsymbol{d}} \in \mathbb{R}^{\boldsymbol{2}}$ and end-effector $\boldsymbol{x}, \dot{\boldsymbol{x}} \in \mathbb{R}^{\boldsymbol{2}}$ motions.

$$\boldsymbol{e} = \boldsymbol{x}_{\boldsymbol{d}} - \boldsymbol{x}, \dot{\boldsymbol{e}} = \dot{\boldsymbol{x}}_{\boldsymbol{d}} - \dot{\boldsymbol{x}} \tag{6.48}$$

It should be noticed that that in addition to primary objective controller commands which includes (task-space) command accelerations $\ddot{\boldsymbol{x}}_{\boldsymbol{d}}$ and the null-space command $\boldsymbol{\phi}_{\boldsymbol{N}}$, the components of Coriolis and centrifugal forces, $\boldsymbol{N}(\boldsymbol{q}', \dot{\boldsymbol{q}}')$, are completely compensated in the control to ensure stability. The stability proof of the overall control

algorithm is based on the task-priority based controllers using pseudo inverse, first used in (Hsu, 1988) to prove the stability of the overall system for any vector of $\boldsymbol{\phi_N}$ which is projected in null-space.

The closed-loop system is given is reduced to the equation below.

$$\boldsymbol{M(q')\ddot{q} + N(q', \dot{q}') = M(q')\{J^{+}(\ddot{x}_d + K_v\dot{e} + K_p e - \dot{J}\dot{q}) + \phi_N\} + N(q', \dot{q}')} \quad (6.49)$$

$$\boldsymbol{\ddot{q} = J^{+}(\ddot{x}_d + K_v\dot{e} + K_p e - \dot{J}\dot{q}) + \phi_N} \quad (6.50)$$

Equating 6.46 and 6.50 results in the following expression.

$$\boldsymbol{J^{+}(\ddot{e} + K_v\dot{e} + K_p e) = \ddot{q}_N - \phi_N} \quad (6.51)$$

where $\boldsymbol{\ddot{q}_N - \phi_N}$ belongs to the null space of $\boldsymbol{J}$ and $\boldsymbol{J}$ has full rank. Later this equation is multiplied with $\boldsymbol{J}$.

$$\boldsymbol{(\ddot{e} + K_v\dot{e} + K_p e) = 0} \quad (6.52)$$

Linear analysis tools can be used to show that primary error, $\boldsymbol{e}$, go to zero exponentially with the constant positive definite diagonal gain matrices. It should also be noted that the micro mechanism is singularity-free as long as the workspace boundary, which is set as 100 x150 mm, is not violated.

6.2.2. Secondary Control

The secondary control is realized by projecting a lower-priority dynamic characteristic into the null-space of the Jacobian. Previously, in (Sadeghian et al., 2013; Platt et al., 2011; Sharon et al. ,1993) a dynamic level secondary task called Cartesian impedance control was realized in null-space. A control law is devised for desired force and motion with a multi-priority impedance control in (Platt et al., 2011). In (Sharon et al. ,1993) the dynamic coupling of macro and micro manipulator is investigated and it is deduced that higher frequency force or motion demands can be allocated to micro manipulator which improves the accuracy of the overall system. The algorithm proposed in this study is inspired from these studies in terms of designing a Virtual Dynamic Model (VDM) for the MMM to carry out secondary tasks. A decoupled control law is used for primary and secondary tasks by making use of the null-space projection of the Jacobian. The algorithm is designed to make promote the distinct advantages of both manipulators. The VDM used for secondary tasks is used to regulate internal motions of manipulators

while the first task is carried out to track the desired end-effector trajectories. The VDM is presented in 6.53 by desired mass $\boldsymbol{M_d}$, damping $\boldsymbol{B_d}$, and stiffness $\boldsymbol{K_d}$ matrices and an external force vector, $\boldsymbol{f_e}$.

$$\boldsymbol{M_d}\ddot{\tilde{\boldsymbol{x}}} + \boldsymbol{B_d}\dot{\tilde{\boldsymbol{x}}} + \boldsymbol{K_d}\tilde{\boldsymbol{x}} - \boldsymbol{f_e} = \boldsymbol{0} \tag{6.53}$$

$$\tilde{\boldsymbol{x}} = \boldsymbol{x_{Md}} - \boldsymbol{x_M}, \dot{\tilde{\boldsymbol{x}}} = \boldsymbol{x_{Md}} - \dot{\boldsymbol{x}}_{\boldsymbol{M}}, \ddot{\tilde{\boldsymbol{x}}} = \ddot{\boldsymbol{x}}_{\boldsymbol{Md}} - \ddot{\boldsymbol{x}}_{\boldsymbol{M}} \tag{6.54}$$

where $\tilde{\boldsymbol{x}} \in \mathbb{R}^{\boldsymbol{4}}, \dot{\tilde{\boldsymbol{x}}} \in \mathbb{R}^{\boldsymbol{4}}$, and $\ddot{\tilde{\boldsymbol{x}}} \in \mathbb{R}^{\boldsymbol{4}}$ error signal vectors are computed by subtracting the planar motions of the macro and micro manipulators, $\boldsymbol{x_M} \in \mathbb{R}^{\boldsymbol{4}}, \dot{\boldsymbol{x}}_{\boldsymbol{M}} \in \mathbb{R}^{\boldsymbol{4}}$, and $\ddot{\boldsymbol{x}}_{\boldsymbol{M}} \in \mathbb{R}^{\boldsymbol{4}}$, from the desired planar motions, $\boldsymbol{x_{Md}} \in \mathbb{R}^{\boldsymbol{4}}, \dot{\boldsymbol{x}}_{\boldsymbol{Md}} \in \mathbb{R}^{\boldsymbol{4}}$, and $\ddot{\boldsymbol{x}}_{\boldsymbol{Md}} \in \mathbb{R}^{\boldsymbol{4}}$.

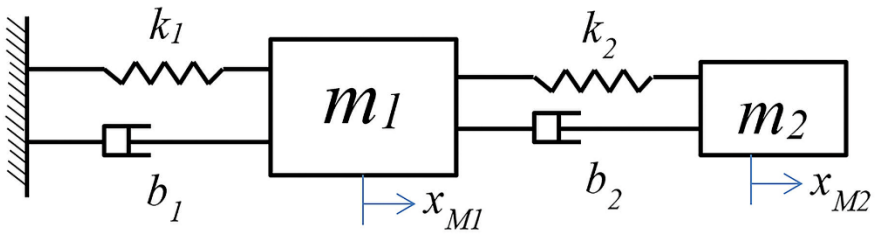

Figure 6.12. Double mass-spring-damper model representation for secondary dynamics.

A double mass-spring-damper model is used to describe the dynamic behavior of secondary task as shown in Figure 6.12. The subscript 1 denotes the macro manipulator and the subscript 2 denotes the micro manipulator. The m_1 mass, k_1 spring constant,b_1 damping constant and $\boldsymbol{x_{M1}}$motion is used to represent the macro manipulator's VDM, while m_2 mass, k_2 spring constant,b_2 damping constant and $\boldsymbol{x_{M2}}$ motion is used to represent the VDM of the micro manipulator. For each Cartesian axis (x and y axes in Fig. 1), a double mass-spring-damper model is used with the selected parameters that are discussed in the next section. With respect to this VDM presented in Figure 6.12 and its above-mentioned parameters, the parameter matrices in 6.53 are calculated as follows:

$$\boldsymbol{M_d} = \begin{bmatrix} m_1 & 0 \\ 0 & m_2 \end{bmatrix}$$

$$\boldsymbol{K_d} = \begin{bmatrix} k_1 + k_2 & -k_2 \\ -k_2 & k_2 \end{bmatrix} \tag{6.55}$$

$$\boldsymbol{B_d} = \begin{bmatrix} b_1 + b_2 & -b_2 \\ -b_2 & b_2 \end{bmatrix}$$

Secondary joint acceleration demands are computed from VDM introduced in Equation 6.53. First of all, 6.53 is reshaped as shown in Equation 6.56.

$$\ddot{\boldsymbol{x}}_{\boldsymbol{M}} = \ddot{\boldsymbol{x}}_{\boldsymbol{Md}} + \boldsymbol{M_d^{-1}}\left[\left(\boldsymbol{B_d}\dot{\tilde{\boldsymbol{x}}} + \boldsymbol{K_d}\tilde{\boldsymbol{x}}\right) - \boldsymbol{f_e}\right] \tag{6.56}$$

An augmented Jacobian, $\boldsymbol{J_s} \in \mathbb{R}^{\boldsymbol{4x4}}$, presented below is formulated to relate the MMM's joint space motion to VDM's task space motion.

$$\boldsymbol{J_s} = \begin{bmatrix} 0 & 1 & 0 & 0 \\ 1 & 0 & 0 & 0 \\ 0 & 0 & -\frac{l_3 \sin(q_4+q_6)\sin(q_5)}{\sin(q_3+q_5-q_4-q_6)} & \frac{l_3 \sin(q_3+q_5)\sin(q_6)}{\sin(q_3+q_5-q_4-q_6)} \\ 0 & 0 & \frac{l_4 \cos(q_4+q_6)\sin(q_5)}{\sin(q_3+q_5-q_4-q_6)} & \frac{-l_4 \cos(q_3+q_5)\sin(q_6)}{\sin(q_3+q_5-q_4-q_6)} \end{bmatrix} \tag{6.57}$$

Inverse kinematics is used to calculate the secondary joint acceleration demands, $\ddot{\tilde{\boldsymbol{\theta}}}$ in 6.58. Finally, the null space vector is calculated by using null-space mapping in 6.58. With this simplified model, the null space vector, $\boldsymbol{\phi_N}$, to be used in the controller is found by computing secondary joint acceleration demands, $\ddot{\tilde{\boldsymbol{\theta}}}$.

$$\begin{aligned} \ddot{\boldsymbol{x}}_{\boldsymbol{M}} &= \boldsymbol{J_s}\ddot{\tilde{\boldsymbol{\theta}}} + \dot{\boldsymbol{J}}_{\boldsymbol{s}}\dot{\tilde{\boldsymbol{\theta}}} \\ \ddot{\tilde{\boldsymbol{\theta}}} &= \boldsymbol{J_s^{-1}}\left\{\ddot{\boldsymbol{x}}_{\boldsymbol{Md}} + \boldsymbol{M_d^{-1}}\left[\left(\boldsymbol{B_d}\dot{\tilde{\boldsymbol{x}}} + \boldsymbol{K_d}\tilde{\boldsymbol{x}}\right) - \boldsymbol{f_e}\right] - \dot{\boldsymbol{J}}_{\boldsymbol{s}}\dot{\tilde{\boldsymbol{\theta}}}\right\} \\ \boldsymbol{\phi_N} &= (\boldsymbol{I} - \boldsymbol{J}^{+}\boldsymbol{J})\ddot{\tilde{\boldsymbol{\theta}}} \end{aligned} \tag{6.58}$$

In particular, secondary task demands represents a dynamic equation (mass-sping-damper system), expressed in terms of task space variables projected to joint space with $\boldsymbol{J_s}$. By proper choice of the null-space dynamic matrices $\boldsymbol{M_d}$, $\boldsymbol{B_d}$, and $\boldsymbol{K_d}$, it is possible to achieve a desired dynamic behavior with secondary task objectives, without affecting the task-space dynamics and stability of the system.

The overall control scheme is illustrated in Figure 6.13, where primary and secondary tasks and their information flow are distinctively shown. The primary task is created according to the trajectory generation of desired end-effector/cutting path and motion limits designated for the end-effector motion. The trajectory for the given path is planned by using the algorithm presented in the previous section, which generates S-shaped velocity profiles to ensure finite jerk limits. The motion demands created from the primary task along with the position and velocity feedback of the end-effector are used to generate error signals to be fed into the controller, which is explained in Equation 6.47. The motion demand in acceleration level is fed forward directly to the controller.

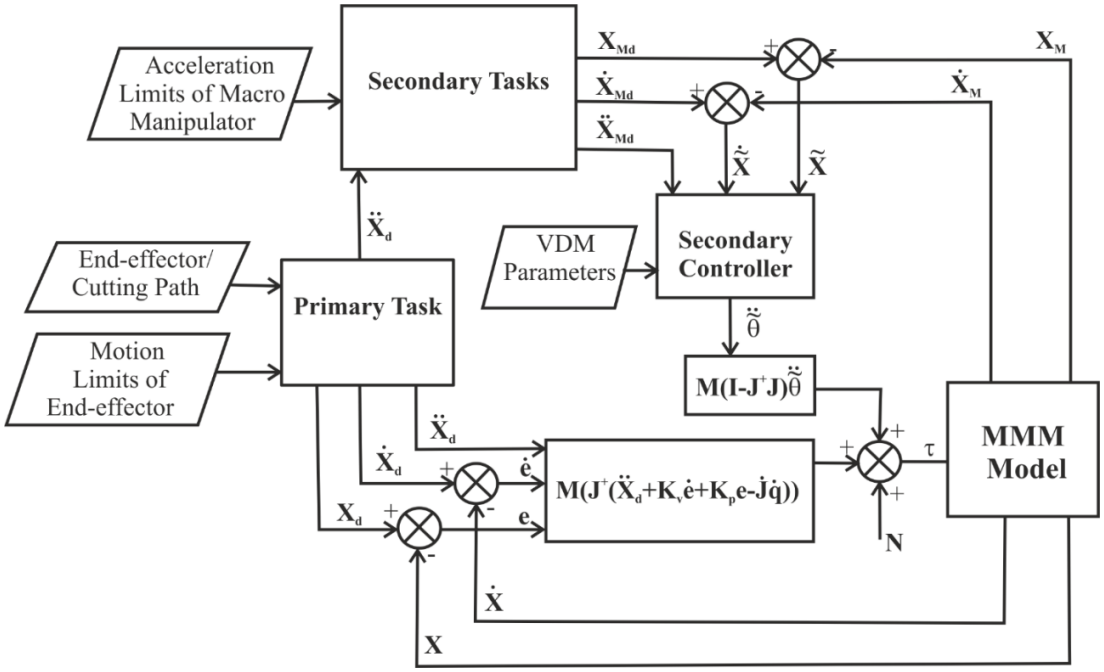

Figure 6.13. The overall control scheme for the MMM.

The secondary task block in Figure 6.13 is used to distribute motion demands according to the acceleration and workspace capabilities of the macro and micro manipulators. In this secondary task, the acceleration of the macro manipulator is constrained by complying with the workspace limitation of the micro manipulator. The algorithm for such a distribution of motion demands is explained in detail in the next section.

A designed VDM, represented in Equation 6.53, is used to formulate the secondary controller which is given in Equation 6.58. The optimization of VDM parameters is described in the next section. The secondary controller's outputs, $\ddot{\tilde{\boldsymbol{\theta}}}$, are projected to null-space, and $\boldsymbol{\phi_N}$ is issued as a controlled input to the actuators of the MMM model along with the other control inputs issued by the primary task's controller and the nonlinearity effects cancellation term $\boldsymbol{N}$.

In this case, the design of the VDM is considered to make use of MMM concept. Designing the system in this way allows adjusting the desired dynamic behaviors of MMM in a redundant configuration. The VDM parameters can be optimized depending on the acceleration and workspace capabilities of the macro and micro manipulators. Moreover, the desired control tasks for this secondary controller and parameter optimization of the proposed VDM are presented in the next subsections.

6.2.3. Secondary Control Tasks

Aforementioned secondary control tasks are achieved by designing the desired Cartesian space motions of macro and micro manipulator separately. For this application, the external forces, $\boldsymbol{f_e}$, acting on the secondary control is chosen to be zero in VDM parameters, because the algorithm is developed for a laser cutting machine in which tool is never in physical interaction with its environment. Parameters matrices of VDM ($\boldsymbol{M_d}, \boldsymbol{B_d}, \boldsymbol{K_d}$) should be optimized for the selected secondary tasks and the motion demands of this system $\ddot{\boldsymbol{x}}_{\boldsymbol{M1d}}, \ddot{\boldsymbol{x}}_{\boldsymbol{M2d}}$ should be accordingly set to achieve these secondary tasks. These tasks are selected as limiting the maximum acceleration of macro manipulator's axes and the workspace for micro manipulator.

Maximum acceleration limitation of the macro manipulator is achieved by saturating the desired end-effector acceleration demands set in the primary task. The primary task acceleration should be selected complying with the combined acceleration capabilities of the MMM. A saturation law is devised for secondary task acceleration demands for the macro manipulator $\ddot{\boldsymbol{x}}_{\boldsymbol{M1d}}, \ddot{\boldsymbol{y}}_{\boldsymbol{M1d}}$ by saturating the motion demands for the end-effector's desired acceleration demands, $\ddot{\boldsymbol{x}}_{\boldsymbol{d}}$ along *x* and *y* axes. In 6.59 and 6.60, $\ddot{\boldsymbol{x}}^{+}_{\boldsymbol{sat}}, \ddot{\boldsymbol{y}}^{+}_{\boldsymbol{sat}}$ and $\ddot{\boldsymbol{x}}^{-}_{\boldsymbol{sat}}\ \ddot{\boldsymbol{y}}^{-}_{\boldsymbol{sat}}$ are acceleration limits of macro mechanism which are set to accomplish +9.81 m/s^2 (+1g) and -9.81 m/s^2 (-1g) limitations, respectively.

$$\ddot{\boldsymbol{x}}_{\boldsymbol{M1d}} = \begin{cases} \ddot{\boldsymbol{x}}^{+}_{\boldsymbol{sat}} \ , \ddot{\boldsymbol{x}}_{\boldsymbol{d}} \geq \ddot{\boldsymbol{x}}^{+}_{\boldsymbol{sat}} \\ \ddot{\boldsymbol{x}}^{-}_{\boldsymbol{sat}} \ , \ddot{\boldsymbol{x}}_{\boldsymbol{d}} \leq \ddot{\boldsymbol{x}}^{-}_{\boldsymbol{sat}} \\ \ddot{\boldsymbol{x}}_{\boldsymbol{d}} \ , \quad \boldsymbol{else} \end{cases}, \ddot{\boldsymbol{y}}_{\boldsymbol{M1d}} = \begin{cases} \ddot{\boldsymbol{y}}^{+}_{\boldsymbol{sat}} \ , \ddot{\boldsymbol{y}}_{\boldsymbol{d}} \geq \ddot{\boldsymbol{y}}^{+}_{\boldsymbol{sat}} \\ \ddot{\boldsymbol{y}}^{-}_{\boldsymbol{sat}} \ , \ddot{\boldsymbol{y}}_{\boldsymbol{d}} \leq \ddot{\boldsymbol{y}}^{-}_{\boldsymbol{sat}} \\ \ddot{\boldsymbol{y}}_{\boldsymbol{d}} \ , \quad \boldsymbol{else} \end{cases} \tag{6.59}$$

On the other hand, the micro manipulator's acceleration demands are generated to compensate for the difference between the primary task's assigned motion and the motion of macro manipulator. This is done by extracting the saturated macro manipulator demands from MMM's desired task trajectories in Cartesian space.

$$\ddot{\boldsymbol{x}}_{\boldsymbol{M2d}} = \begin{cases} \ddot{\boldsymbol{x}}_{\boldsymbol{d}} - \ddot{\boldsymbol{x}}^{+}_{\boldsymbol{sat}} \ , \ddot{\boldsymbol{x}}_{\boldsymbol{d}} \geq \ddot{\boldsymbol{x}}^{+}_{\boldsymbol{sat}} \\ \ddot{\boldsymbol{x}}_{\boldsymbol{d}} - \ddot{\boldsymbol{x}}^{-}_{\boldsymbol{sat}} \ , \ddot{\boldsymbol{x}}_{\boldsymbol{d}} \leq \ddot{\boldsymbol{x}}^{-}_{\boldsymbol{sat}} \\ \mathbf{0} \quad , \quad \boldsymbol{else} \end{cases}, \ddot{\boldsymbol{y}}_{\boldsymbol{M2d}} = \begin{cases} \ddot{\boldsymbol{x}}_{\boldsymbol{d}} - \ddot{\boldsymbol{y}}^{+}_{\boldsymbol{sat}} \ , \ddot{\boldsymbol{x}}_{\boldsymbol{d}} \geq \ddot{\boldsymbol{y}}^{+}_{\boldsymbol{sat}} \\ \ddot{\boldsymbol{x}}_{\boldsymbol{d}} - \ddot{\boldsymbol{y}}^{-}_{\boldsymbol{sat}} \ , \ddot{\boldsymbol{x}}_{\boldsymbol{d}} \leq \ddot{\boldsymbol{y}}^{-}_{\boldsymbol{sat}} \\ \mathbf{0} \quad , \quad \boldsymbol{else} \end{cases} \tag{6.60}$$

Hence, the secondary control task's acceleration demands, $\ddot{\boldsymbol{x}}_{\boldsymbol{Md}}$, are formed as shown in Equation 6.61, which are the input signals of the secondary controller in

Equation 6.54. The velocity demands are calculated by integrating the acceleration demands for both manipulators, respectively.

$$\ddot{\boldsymbol{x}}_{\boldsymbol{Md}} = \begin{bmatrix} \ddot{x}_{M1d} \\ \ddot{y}_{M1d} \\ \ddot{x}_{M2d} \\ \ddot{y}_{M2d} \end{bmatrix} \tag{6.61}$$

Although saturation on acceleration level is implemented by using the above-mentioned methods, the algorithm still needs to guarantee that workspace limitation of the five-bar planar micro manipulator is not violated. To ensure this, the VDM spring constants and springs' neutral position should be adjusted. For this study, to comply with the workspace limitation of the micro manipulator, the neutral position of the spring in between the micro and macro manipulator is chosen at the middle position of the micro manipulator's workspace by designing the position demand of the secondary control.

Designing the secondary task with VDM based secondary control allows adjusting parameters to achieve both tasks at the same time. Also, by integrating a dynamic model, a continuous behavior of the secondary tasks is targeted in the presence of the discontinuity imposed by the saturation function.

6.2.4. Parameter Optimization of Secondary Control Objective

The VDM presented in Equation 6.53 is designed to impose saturated accelerations and not to violate the workspace of micro manipulator. In this section, the optimization of the VDM parameters is discussed. Parameters are optimized to meet the secondary control task explained in the previous section. To explain the optimization procedure, the VDM is analytically represented for only one Cartesian axis, which is, in the end, applied to both *x*- and *y*- axes.

Parameter optimization for the proposed model is realized by constructing a state-space representation of the VDM and running VDM parameter optimization with the selected performance index.

The VDM in state-space representation is given as follows.

$$\dot{\boldsymbol{z}} = \boldsymbol{A}\boldsymbol{z} + \boldsymbol{B}\boldsymbol{u} \tag{6.62}$$

The state vector, $\boldsymbol{z}$, and system matrix, $\boldsymbol{A}$, is defined as:

$$\boldsymbol{z} = \begin{bmatrix} x_{M1} \\ \dot{x}_{M1} \\ x_{M2} \\ \dot{x}_{M2} \end{bmatrix}, \boldsymbol{A} = \begin{bmatrix} 0 & 1 & 0 & 0 \\ -(k_1 + k_2)/M_1 & -(b_1 + b_2)/M_1 & k_2/M_1 & b_2/M_1 \\ 0 & 0 & 0 & 1 \\ k_2/M_2 & b_2/M_2 & -k_2/M_2 & -b_2/M_2 \end{bmatrix} \quad (6.63)$$

Optimization of VDM parameters consists of determining parameters $\boldsymbol{k_1}$, $\boldsymbol{k_2}$, $\boldsymbol{b_1}$, and $\boldsymbol{b_2}$, by minimizing the selected performance index, $\boldsymbol{W}$. For this problem, $\boldsymbol{W}$ penalizes state variables. In the conventional form, $\boldsymbol{W}$ would be formulated as follows:

$$\boldsymbol{W} = \int_0^\infty (\boldsymbol{z^T Q z}) \boldsymbol{dt} \quad (6.64)$$

where $Q \in \mathbb{R}^{\boldsymbol{4x4}}$is a positive definite weighting matrix. In conventional form, the Q matrix is given as:

$$\boldsymbol{z^T Q z} \triangleq -\frac{\boldsymbol{d}}{\boldsymbol{dt}} \boldsymbol{z^T R z} \quad (6.65)$$

$$-\boldsymbol{Q} = \boldsymbol{A^T R} + \boldsymbol{RA} \quad (6.66)$$

where $\boldsymbol{R} \in \mathbb{R}^{\boldsymbol{4x4}}$ is a symmetric matrix. In this work, $\boldsymbol{J}$ is modified so that accelerations of masses are included with the term, $\ddot{\boldsymbol{z}}$.

$$\boldsymbol{W} = \int_0^\infty (\boldsymbol{z^T Q z} + \ddot{\boldsymbol{z}}^{\boldsymbol{T}} \boldsymbol{S} \ddot{\boldsymbol{z}}) \boldsymbol{dt} \quad (6.67)$$

Based on the VDM, accelerations are calculated by $\begin{bmatrix} \ddot{\boldsymbol{x}}_{\boldsymbol{M1}} \\ \ddot{\boldsymbol{x}}_{\boldsymbol{M2}} \end{bmatrix} = \boldsymbol{Vz}$, where the matrix $\boldsymbol{V}$ is defined as follows:

$$\boldsymbol{V} = \begin{bmatrix} -(\boldsymbol{k_1} + \boldsymbol{k_2})/\boldsymbol{M_1} & -(\boldsymbol{b_1} + \boldsymbol{b_2})/\boldsymbol{M_1} & \boldsymbol{k_2}/\boldsymbol{M_1} & \boldsymbol{b_2}/\boldsymbol{M_1} \\ \boldsymbol{k_2}/\boldsymbol{M_2} & \boldsymbol{b_2}/\boldsymbol{M_2} & -\boldsymbol{k_2}/\boldsymbol{M_2} & -\boldsymbol{b_2}/\boldsymbol{M_2} \end{bmatrix} \quad (6.68)$$

Making use of the above-mentioned relation, is re-written as follows:

$$\mathbf{W} = \int_0^\infty \boldsymbol{z^T} (\boldsymbol{Q} + \boldsymbol{V^T S V}) \boldsymbol{z}\, \boldsymbol{dt} \quad (6.69)$$

At this moment, we can define a new weighting matrix $\boldsymbol{Q_s}$ in Equation (38).

$$\boldsymbol{Q_s = Q + V^T S V} \tag{6.70}$$

where $\boldsymbol{S}$ is a weighting matrix which is chosen to impose minimization for only macro manipulator's acceleration.

$$\boldsymbol{-Q_s = A^T R + RA} \tag{6.71}$$

The $\boldsymbol{R}$ matrix is a function of VDM parameters. Finally, the optimal solution is found by minimization of $\boldsymbol{W}$.

$$\boldsymbol{W = z^T R z} \tag{6.72}$$

The penalty function, $\boldsymbol{W}$, is subjected to the Nelder-Mead optimization method using Matlab functions to find the minimum of a constrained nonlinear multivariable function. A local minimum is found for parameters given in Table 6.3 with initial conditions and constraints with upper and lower bounds of parameters as: $\boldsymbol{0 < k_1 < 10}$, $\boldsymbol{0 < k_2 < 100}$, $\boldsymbol{0 < b_1 < 100}$, $\boldsymbol{0 < b_2 < 100}$. It is known that with different initial parameters the parameters for resultant minima changes, because of this the initial values are set manually by trial and error by making use of simulation test results to accomplish secondary tasks with more precision.

Table 6.3. VDM parameters.

	Initial values of parameters	Optimized values of parameters
$\boldsymbol{k_1}$	0	1.61
$\boldsymbol{k_2}$	12	10.28
$\boldsymbol{b_1}$	35	58.07
$\boldsymbol{b_2}$	1	4.46

As a result, the system matrix $\boldsymbol{A}$ with optimized parameters (Table 2) have eigenvalues of -2.2567 + 2.2984i, -2.2567, - 2.2984, -0.0291, -0.5460. It should be noticed that the real part of the eigenvalues of the system matrix $\boldsymbol{A}$ used in the simulations are all negative, which shows that the system satisfies the condition of stability. Moreover, the stability of the model is discussed in APPENDIX C. The parameters obtained with this

optimization are used in the controller and tested in simulations, which are presented in the next section.

6.2.5. Simulation and Results

A case study is presented to show the performance and viability of the proposed method. The simulation model is constructed by using Matlab™ Simscape™ Multibody™ blocks. A simplified model of the MMM presented in Chapter 5 with the physical parameters presented in Table 6.2 is built in this simulation environment and its visual representation is presented in Figure 6.14.In Figure 6.4 the blue links represents the micro manipulator and the orange and green parts represents the macro manipulator. Initially, a dynamic analysis of the MMM is carried out and validated with the results of the model constructed with Matlab™ Simscape™ Multibody™ blocks. This validated model is used in computing the respective matrices (e.g., generalized inertia matrix) in the computed-torque method which is implemented as the control law for the primary task. Simulations are run with 2 kHz sampling rate and with ode4 (Runge-Kutta) solver. The sampling rate is chosen to match the sample rate used in the industrial application.

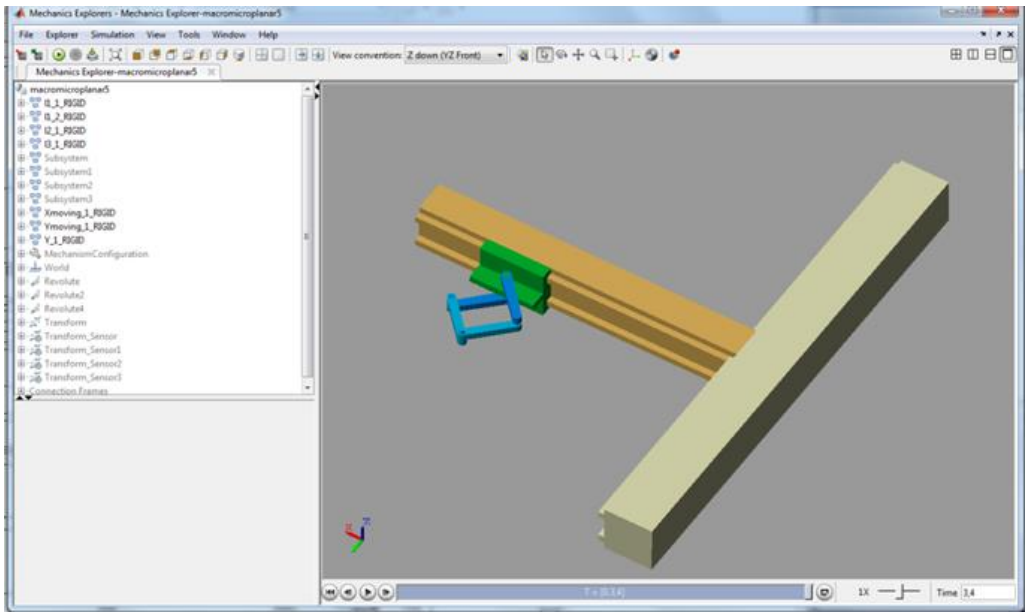

Figure 6.14. Visiualization of simulations done with Matlab™ Simscape™ Multibody™ model.

The contour, shown in Figure 6.15, for end-effector's trajectory is used for the planar laser cutting process as the benchmark test of the proposed controller. This contour is chosen for the case study because it is important to test the acceleration distribution capability of the proposed algorithm especially for sharp turns. For this contour, the trajectory is generated with 40 m/min velocity and 4150 m/s^3 jerk limits, where a maximum of 43.13 m/s^2 acceleration. These values are assigned with respect to the aimed capabilities of the MMM. The trajectory for the primary task is planned to have S-shaped velocity profiles, as explained in Chapter 5 for finite jerk limits, so the same algorithm is run.

With the above-mentioned limitations of the MMM, the task completion duration is calculated to be 7.22 s. The same trajectory with the conventional machine (only the macro manipulator) with 1 g acceleration limitation is calculated to be completed in 11.27 s. This result indicates that there is a 35.93% drop in the total task completion duration if the acceleration levels are increased for this case study. As the cutting path would have more small contours, the task completion duration decreases relative to the conventional machine's completion duration as reported in the previous Chapter.

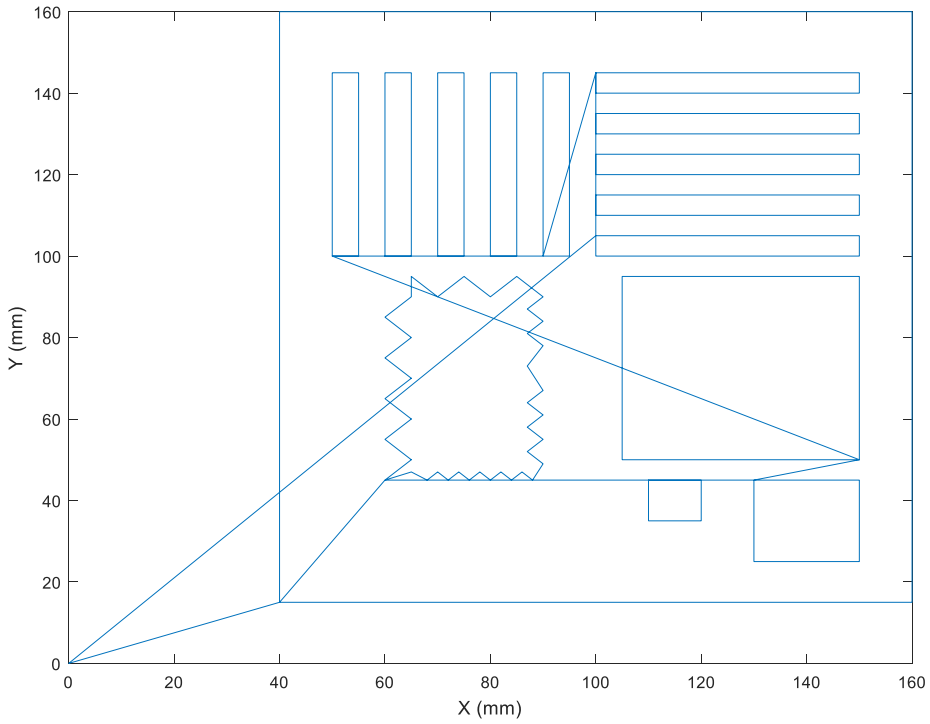

Figure 6.15. End-effector path used in simulations.

The controller is tested with the integrated secondary controller to investigate the impact of the proposed algorithm. Figures 6.16 and 6.17 show the accelerations realized along the global *y*- and *x*-axes, respectively, which are drawn for the macro manipulator's axes (q_1 and q_2) and end-effector's axes (x_e and y_e). It is observed from Figures 6.16 and 6.17 that the macro manipulator actuators' accelerations are kept within 1 g limitation (highlighted in figures with the green lines) along both axes. This result indicates that the first task of the secondary controller has been accomplished for limiting the acceleration of the macro manipulator. Hence, it is shown that the primary task is not affected in means position tracking.

The second task of the secondary controller was to keep the motion of the micro manipulator within its workspace boundaries. The result of the micro manipulator motion in terms of *u*-*v* coordinates of the end-effector with respect to the frame that is fixed to the micro manipulator is presented in Figure 6.18. This figure indicates that the workspace boundaries are not violated during the operation, and the second task of the secondary controller is also accomplished.

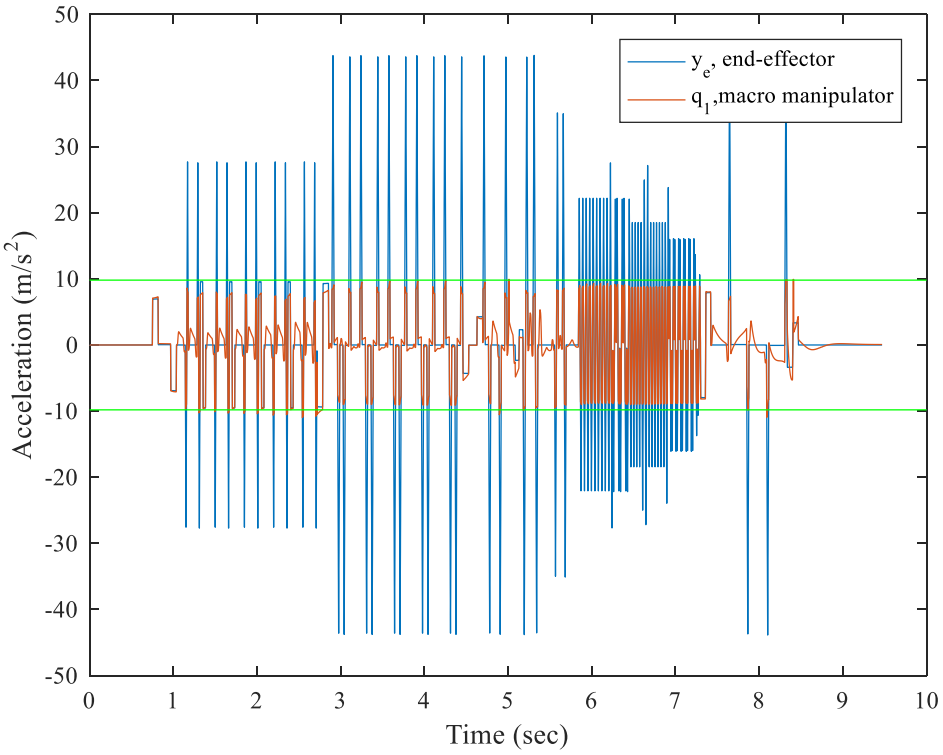

Figure 6.16. Macro mechanism's, q_1, joint acceleration and end-effector's acceleration along y-axis.

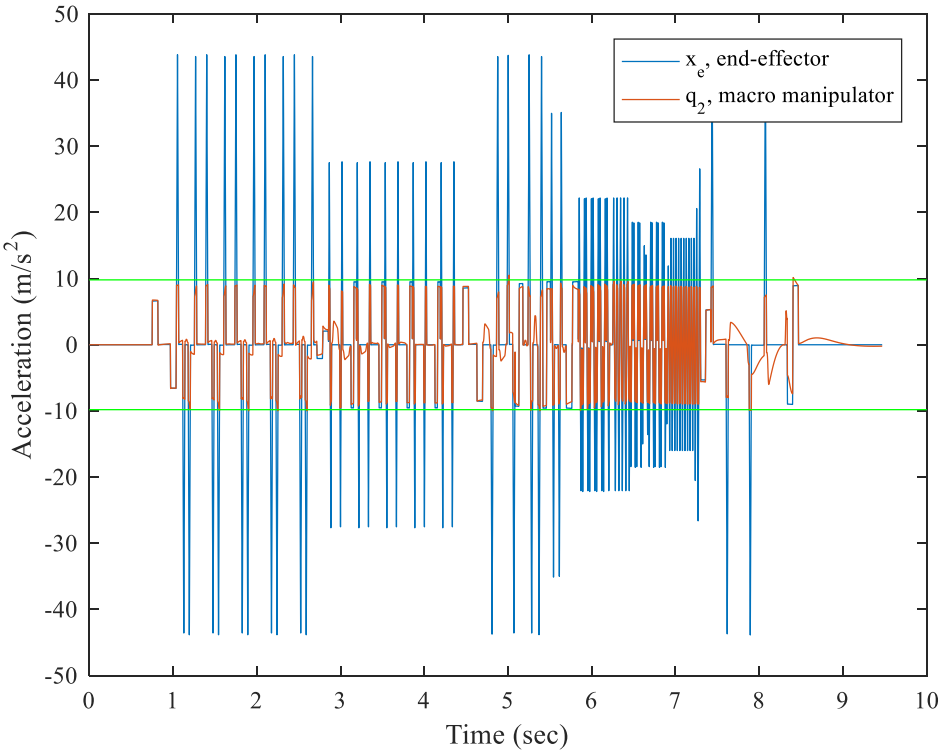

Figure 6.17. Macro mechanism's, q_2, joint acceleration and end-effector's acceleration along x-axis.

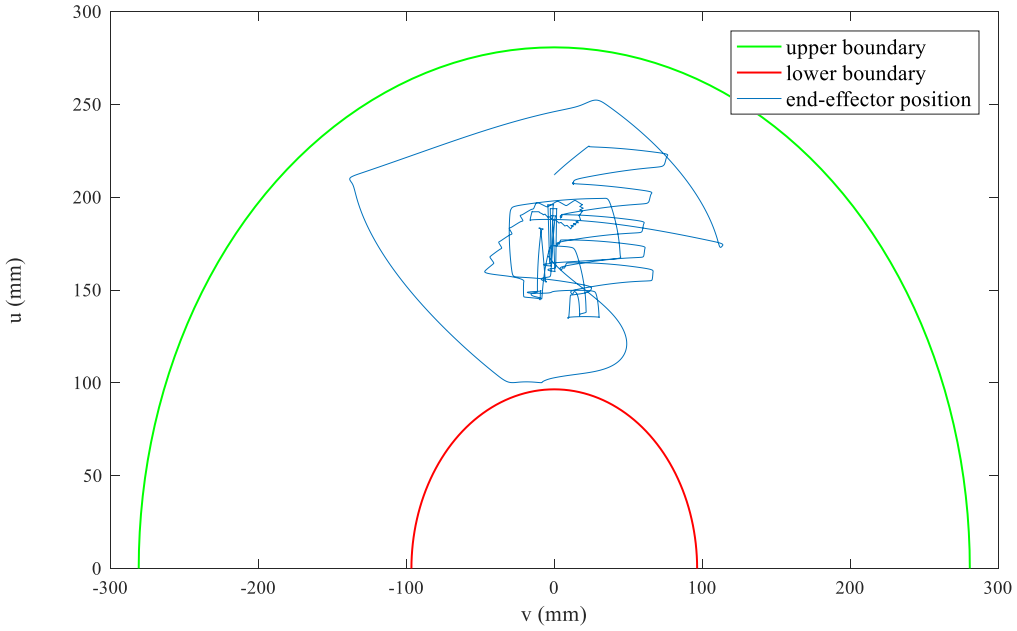

Figure 6.18. End-effector position with respect to micro manipulator's fixed axes.

The same trajectory is run for the conventional case (while only macro manipulator's joints are activated) where the motion limits in terms of acceleration and jerk are kept same. In reality, the trajectory generated for the combined motion capability of MMM is not feasible for the conventional machine since it would call for much larger actuation capacity to move a large amount of moving mass at the selected motion limits. However, in order to compare the effectiveness of MMM with the proposed algorithm with a conventional machine, the simulation tests are repeated with the conventional machine. As a result, the total actuator effort calculated as the drawn power by the total system with the MMM and conventional machine that has the same motion limits are shown in Figure 6.19. It should be noted that the friction models are not included in the simulation model of both machines. It is clear that the effort is considerably lower when the MMM is used for the same task instead of the conventional machine. The total energy consumed when the MMM is used is 2397.82 *J* while it is 8118.56 *J* for the conventional machine for this specific task. The end-effector positioning errors calculated for both the MMM and the conventional machine simulation tests are shown in Figure 6.20 and 6.21.

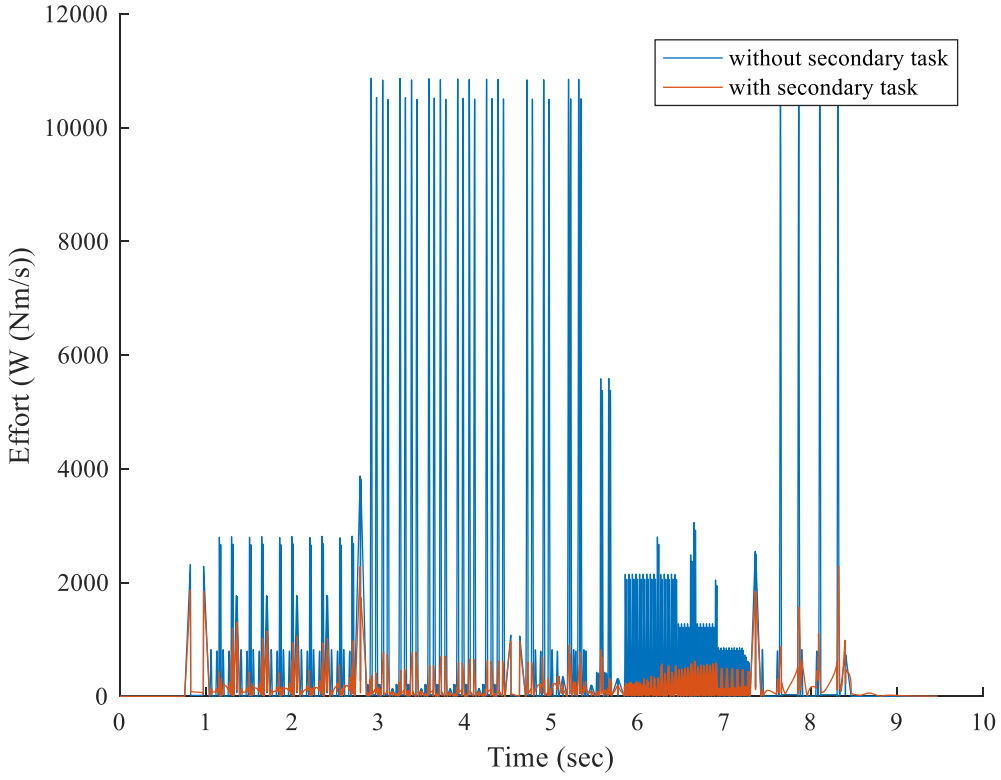

Figure 6.19. Total actuator effort for two simulation cases.

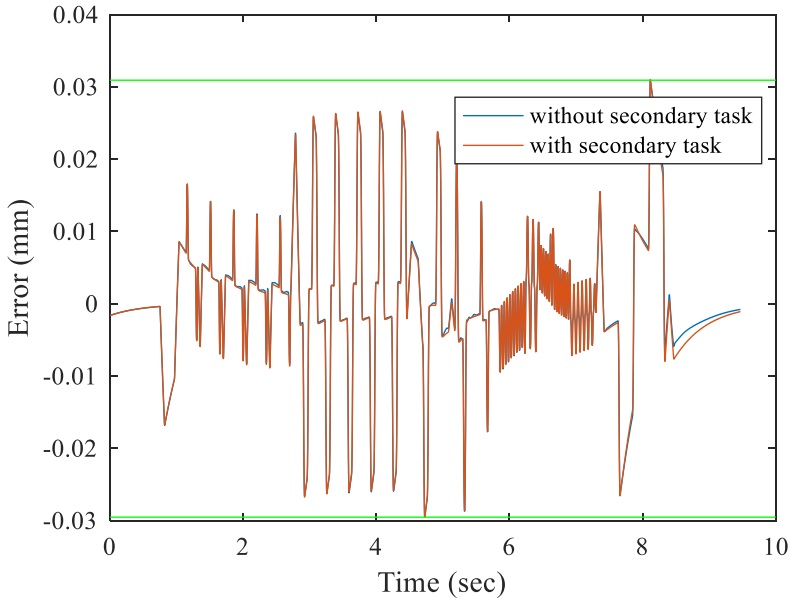

Figure 6.20. End-effector position error in y-direction

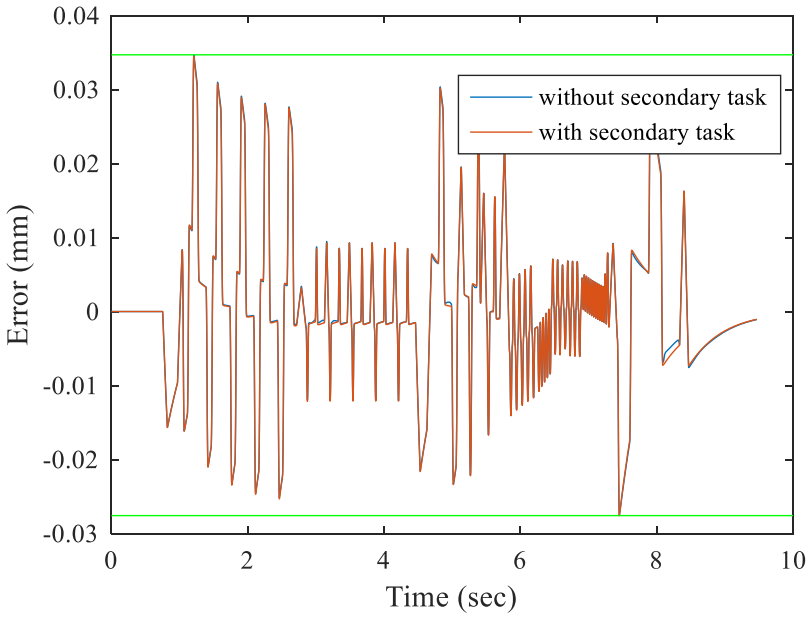

Figure 6.21. End-effector position error in x-direction.

6.2.6. Conclusions

The major contribution of the multi-priority controller is the implementation of a control algorithm utilizing redundancy resolution for the MMM. A multi-priority

controller making use of virtual dynamics, which is a double mass-spring-damper system, is introduced in null-space projection to achieve two desired secondary tasks. The primary task is set as end-effector trajectory tracking which is realized with computed torque control. Moreover, a secondary task is designed to distribute the acceleration demands of the end-effector to macro and micro manipulators, complying with their acceleration and workspace capabilities.

The algorithm is tested in simulations using a model based on an industrial setup presented. A trajectory is designed according to the selected motion limitations of the MMM so that the task completion duration is reduced by 35.93% with respect to the conventional machine operation. The test results indicate that the secondary tasks for keeping the macro manipulator's acceleration below 1 g and not violating the micro manipulator's workspace are accomplished. These results prove that the design algorithm can be used in MMM systems in which the acceleration and workspace limits are to be regulated.

When compared to the previously devised algorithm which is tested on an industrial setup, the proposed algorithm is not task-specific. The VDM utilized in the secondary controller makes the control of MMM versatile, since the parameters and even the model can be adjusted to obtain desired internal behavior of a redundant robot in MMM configuration. The control strategy along with the MMM concept introduced here can be utilized for various sub-task strategies in MMMs. The results achieved in this paper can be extended to the generation of anthropomorphic motions for MMMs that imitate human arm-wrist motions.

Another advantage of this novel algorithm with respect to applied methods in Chapter 5, is that it enables online control without the need to process the desired end-effector trajectory, which overcomes many problems in the previous study. Specifically, if a trajectory is paused during an operation, the trajectory must be re-calculated with the previously studied pre-processing algorithms. However, with the algorithm proposed, trajectory tracking can be re-initiated at any moment.

Finally, if the same trajectory is cut with only the macro mechanism, with same end-effector motion constraints, it is seen that actuator effort is increased relative to the results obtained with the MMM that uses the proposed algorithm. The effectiveness of the proposed method in terms of actuator effort is maximized when contours of the cutting path are relatively small and complex. The actuator effort is mainly reduced as a result of

saturating macro manipulator's accelerations by using the secondary controller. The main reason to focus on the macro manipulator's acceleration is that the macro manipulator has relatively larger inertia and mass and, therefore, higher influence relative to the micro manipulator in terms of energy consumption. Although this controller needs an accurate model of the manipulator, the formulation for kinematic redundancy can be adapted to kinematic control.

CHAPTER 7

CONCLUSIONS

In this dissertation, macro-micro manipulation is first defined as an area of robotics, which is a unique sub-set of kinematically redundant manipulators. The core aim of this dissertation is the development of new methodologies in order to make use of the combined use of macro and micro-scaled manipulators in MMM concept. To achieve this, the characteristics of both manipulator types are taken into consideration and the novel methodologies are developed to make the most of the MMM concept. In the scope of this dissertation, MMM concept and developed methodologies are used for an industrial planar laser cutting application to increase the acceleration capabilities of conventional systems, thereby to decrease the process duration. It is important to increase the acceleration capability of such machines since the laser cutting tool/end-effector velocity limitations are determined with the laser power and workpiece specifications (material and thickness). Regarding this, MMM concept, laser cutting technologies, and their combined usage are investigated in this dissertation. In conclusion, the summary of the industrial application's outcome, developed methodologies, and future works are presented in this Chapter.

For the Industrial application, to utilize the MMM concept, a relatively lightweight and more agile micro manipulator attached to the conventional macro manipulator is utilized to increase the acceleration capability with combined motions of MMM. The macro manipulator is set as a conventional XY table and the micro manipulator is designed as a modified six-bar parallel planar mechanism.

As a result of the SANTEZ project, a novel kinematically redundant planar laser cutting machine prototype, which reaches acceleration values of 3.5 g in task space while preserving its precision, have been designed and prototyped in the industry. It is deduced that considering the time the prototype is commissioned, it is the first highly dynamic redundant planar laser cutting machine in the Turkish Industry, and third of its kind in the world. It should be noted that the prototype commissioned is a high-end product for the industrial machinery market. Controller design, integration, and commissioning activities have been carried out through the dissertation. For the case study, the developed controller

algorithms are converted to embedded codes, and finally, by the integration of mechanical structure, electromechanical components, and the controller, the machine integration is completed and tested. Besides kinematics and dynamics of the micro parallel manipulator, calibration of micro manipulator, individual system's tests are realized and verifications are done. Another challenge in this case study is overcome with the integration of custom the algorithms/methodologies to an industrial setup.

As a contribution of this dissertation, a semi-online controller and three different motion planning/division algorithms are presented in Chapter 4. In the end, the most feasible method, a novel semi-online motion generation is adapted with MPFA and jerk-limited trajectory generation with G-code. Experimental verification of the proposed method is presented with data collected on industrial setup and an attentive discussion is made for future considerations in Chapter 5. It is shown with a cutting process on industrial setup, that the process duration can be reduced up to 83.64% in completion time when compared to conventional cutting with 1 g accelerations. Furthermore, an investigation can be made as a future study by comparing the total actuator effort of the conventional case and MMM case.

A multi-priority general framework controller is proposed inspiring form the industrial case study. The novelty of this method is the implementation of a control algorithm utilizing redundancy resolution for the MMM. In that manner, the multi-priority controller for macro-micro manipulators is introduced by utilizing virtual dynamics, which is introduced in null-space projection to achieve secondary tasks. The VDM utilized in the secondary controller of the multi-priority controller makes the control of MMM versatile, since the parameters and even the model can be adjusted to obtain desired internal behavior of a redundant robot in MMM configuration. The control strategy, along with the MMM concept introduced here, can be utilized for various sub-task strategies in MMMs. The controller is evaluated on a simulation model based on a previously constructed macro-micro manipulator for planar laser cutting. Task completion duration and total actuator effort are investigated and the results are compared with the conventional process scenario. It is shown with an example of a contour cutting scenario, that the total actuator effort is reduced to 70.46% when compared to a conventional cutting scenario with 1 g accelerations. It should be noted that dissipative forces are neglected in the simulation models. It is seen that this controller is advantageous when compared to algorithms adapted to the industrial case study since it

provides versatility and needs no necessary complex algorithms in the pre-process. However, the integration of such controllers into industrial setup needs attentive work. This work should cover the implementation of proper methods for modeling of the drive system and the mechanism. Actuator and gear systems' model can be tested with experimental tests using torque sensors, from which the drive system models can be adjusted. The current controller of the servo drivers inherits an embedded gain scheduling strategy using look-up tables, which can be tuned with the result of the experiments. Additionally, adaptive and learning techniques can be implemented for such a system. After the motor model is verified, the manipulator's model should also be tested. Especially for highly dynamic motion, the friction and stiffness correction/compensation methods should be investigated for model-based controllers.

In Section 6.1, a parallel over-constrained mechanism's simplified dynamic model and controller development are proposed in the scope of the TÜBİTAK project. This project is established for further investigation of over-constrained mechanisms and their adaptation to the industrial case. It is aimed to enhance the positioning accuracy of the micro manipulator by utilizing calibration, dynamic balancing, and controllers based on dynamic and stiffness models. In this dissertation, first, the micro part of the machine/manipulator is re-modeled using reduced order method with hidden robot analogy to be used in controller development. Exact model knowledge (EMK)/computed-torque and an adaptive controller are designed and applied with simulations to be used in the project. The adaptive controller is used to estimate the dynamic parameters of the model developed and compared with EMK control. The simulation results indicate that the adaptive controller's positioning errors are bounded for extreme cases, e.g. the maximum error is bounded below 16 μm for the case when the initial dynamic parameters in the model-based-controller are reduced 80%.

The industrial application presented here is an encouraging example of university and industry collaboration. Moreover, it proves its statements by presenting the enhancements done on a conventional system. The applied methodologies show that the multi-disciplinary branch of mechatronic engineering can provide novel improvements both in means of mechanical design and control systems. The proposed framework and methodology can find further applications in a variety of industrial and academic studies, e.g., space robotics, medical robots, long-reach manufacturing robots, and humanoid robots.

The micro manipulator developed in this dissertation can be utilized for systems that can make use of high-acceleration and high-precision motion, e.g., an adaption can be made for additive manufacturing technology. Further studies carried out by Iztech Modeling & Protoyping Research Group on this unique over-constrained manipulator type is valuable for both mechanical and control engineering in means of academic research contribution.

The multi-priority controller developed in this dissertation can be adapted to the industrial case with an attentive work on model-based torque control of manipulators. Furthermore, the controller can be used on a kinematically redundant anthropomorphic robot arm where the control parameters could be adjusted for a variety of tasks, e.g., fine motion tasks and motion tasks that would require force handling. The controller can be adapted for the hybrid position/force controller. Further research can be made to observe the human arm and wrist-hand motion to arrange the parameters on multi-priority control. Bio-inspired manipulation techniques can broaden the scope of the MMM concept.

REFERENCES

Abiko, S., and Yoshida, K. (2005). An adaptive control of a space manipulator for vibration suppression. In *2005 IEEE/RSJ International Conference on Intelligent Robots and Systems*, 2167-2172.

Antonelli, G., and Chiaverini, S. (1998). Task-priority redundancy resolution for underwater vehicle-manipulator systems. In *Proceedings. 1998 IEEE International Conference on Robotics and Automation*, 1,768-773.

Arifin, A. S., Ang, M. H., Lai, C. Y., and Lim, C. W. (2013, July). General framework of the force and compliant motion control for macro mini manipulator. In *2013 IEEE/ASME International Conference on Advanced Intelligent Mechatronics*. 949-954.

Ata, A.A., and Myo, T.R. (2005). Optimal point-to-point trajectory tracking of redundant manipulators using generalized pattern search. *International Journal of Advanced Robotic Systems*, 2(3), 24.

Barbazza, L., Zanotto, D., Rosati, G., and Agrawal, S. K. (2017). Design and optimal control of an underactuated cable-driven micro–macro robot. *IEEE Robotics and Automation Letters*, *2*(2), 896-903.

Bassan, H. S., Patel, R. V., and Moallem, M. (2009). A novel manipulator for percutaneous needle insertion: Design and experimentation. *IEEE/ASME transactions on mechatronics*, 14(6), 746-761.

Battheu, C. (2011). Manipulator of Low Inertia for Laser Cutting Machines for Flat Sheet Metals, Patent no: US20110017714.

Battheu, C. (2012). Combined Machine for Punching and Laser Cutting of Flat Sheet Metal, Patent no: US20120097652.

Bellows, G., Kohls, J. (1982). Drilling without drills. *American Machinist*, 173- 188.

Bourges, J. L., Hubschman, J. P., Wilson, J., Prince, S., Tsao, T. C., and Schwartz, S. (2011). Assessment of a hexapod surgical system for robotic micro-macro manipulations in ocular surgery. *Ophthalmic research*, 46(1), 25-30.

Bowling, A., Khatib, O. (1997). Design of macro/mini manipulators for optimal dynamic performance. In IEEE *Proceedings of International Conference on Robotics and Automation*, 1, 449-454.

Cardinale, M., Carpanzano, E., Carracoi, M., Chirico, M., Lacasella, A., Masotti, S., Mininno, E. (2007). Method for Managing Systems, Provided with Redundant Actuators, Patent no: US20070040527

Chen, J.L., Liu, J.S., Lee, W.C., and Liang, T.C. (2002). On-line multi-criteria based collision-free posture generation of redundant manipulator in constrained workspace. Robotica, 20, 625-636.

Chen, H., Li, J., Xing, G., and Sun, H. (2010). Trajectory tracking control of a macro-micro welding robot based on the vision navigation. In *2010 IEEE International Conference on Robotics and Biomimetics*, 667-672.

Chen, K., Yao, Y. L., Modi, V. (2001). Gas Dynamic Effects on Laser Cut Quality. *Journal of Manufacturing Processes*, 3(1), 38- 49.

Cheng, X. P., and Patel, R. V. (2003). Neural network based tracking control of a flexible macro–micro manipulator system. *Neural Networks*, 16(2), 271-286.

Chettibi, T., Lehtihet H. E., Haddad M., and Hanchi S. (2004) Minimum cost trajectory planning for industrial robots. *European Journal of Mechanics-A/Solids.* 23 (4), 703-715.

Cho, C., Kang, S., Kim, M., and Song, J. B. (2005). Macro-micro manipulation with visual tracking and its application to wheel assembly. *International Journal of Control, Automation, and Systems*, 3(3), 461-468.

Chryssolouris, G. (1991). Laser Machining—Theory and Practice. *Mechanical Engineering Series, Springer-Verlag,* New York Inc.

Conkur, E. Sahin, and Rob Buckingham. (1997). Clarifying the definition of redundancy as used in robotics. Robotica, 15(5), 583-586.

Craig, J. J. (2009). Introduction to robotics: mechanics and control, 3/E. *Pearson Education India*.

De Stefano, M., Artigas, J., Giordano, A., Lampariello, R., Albu-Schaeffer, A. (2015). On-ground experimental verification of a torque controlled free-floating robot. *13th Symposium on Advanced Space Technologies in Robotics and Automation 2015 (ASTRA)*.

Dede, M.İ.C., Gezgin, E., Kiper, G., Mastar, E., Sığırtmaç, T. and Uzunoğlu, E., (2014). Design and analysis of a parallel mechanism for kinematically redundant hybrid planar laser cutting machine. *16th International Conference on Machine Design and Production*. 810-822, 2014.

Dede, M.İ.C., Kiper, G., and Uzunoğlu, E. (2016). A macro-micro mechanism design for laser cutting process. *The 17th International Conference on Machine Design and Production, Bursa, Turkey.*

Deng, Y., Jin, X., and Zhang, Z. (2015). A macro–micro compensation method for straightness motion error and positioning error of an improved linear stage. *The International Journal of Advanced Manufacturing Technology*, 80(9-12), 1799-1806.

Dietrich A., Ott C. and Albu-Schäffer A. (2015). An overview of null space projections for redundant, torque-controlled robots. *The International Journal of Robotics Research*, 34(11), 1385-1400.

Dolgui, A., Pashkevich, A. (2009). Manipulator motion planning for high-speed robotic laser cutting. *International Journal of Production Research*, 47(20), 5691-5715,

Duan, X., Qiu, Y., Du, J., Zhao, Z., and Duan, Q. (2011, May). Real-time motion planning for the macro-micro parallel manipulator system. *In 2011 IEEE International Conference on Robotics and Automation*, 4214-4219. IEEE.

Duan, X., Qiu, Y., Mi, J., and Zhao, Z. (2011). Motion prediction and supervisory control of the macro–micro parallel manipulator system. *Robotica*, *29*(7), 1005-1015.

Dubey, A. K., Yadava, V. (2008) Laser beam machining—A review. *International Journal of Machine Tools & Manufacture*, 48, 609–628.

Egeland, O. and Sagli, J. R. (1990, December). Kinematics and control of a space manipulator using the macro-micro manipulator concept. In *29th IEEE Conference on Decision and Control*, 3096-3101.

Einstein, A. (1917). Zur Quantentheorie der Strahlung. *Physikalische Zeitschrift*, 18, 121–128.

Field, G. and Stepanenko, Y. (1996). April. Iterative dynamic programming: an approach to minimum energy trajectory planning for robotic manipulators. *In Proceedings of IEEE International Conference on Robotics and Automation*, 3, 2755-2760.

Fleisig, R.V. and Spence, A.D. (2001). A constant feed and reduced angular acceleration interpolation algorithm for multi-axis machining. *Computer-Aided Design*, 33(1), 1-15.

Frevel., A. , Steffensen. B., Vassie, L.(1995). Safe laser application requires more than laser safety. *Optics & Laser Technology*, 27(1), 1-4.

From, P. J., Gravdahl, J. T., Lillehagen, T., and Abbeel, P. (2011). Motion planning and control of robotic manipulators on seaborne platforms. *Control engineering practice*, *19*(8), 809-819.

Fukazu, Y., Hara, N., Kanamiya, Y., and Sato, D. (2009, February). Reactionless resolved acceleration control with vibration suppression capability for JEMRMS/SFA. In *2008 IEEE International Conference on Robotics and Biomimetics*, 1359-1364.

Gattiglio, M., Chirico, M. (2011). Laser Punching Machine, Patent no: US8076610.

Gattiglio, M., Sartorio, F., Chirico, M. (2008). Laser Machine Tool, Patent no: US20080197118.

Ghany, K. A., Newishy , M. (2005). Cutting of 1.2 mm thick austenitic stainless steel sheet using pulsed and CW Nd:YAG laser. *Journal of Materials Processing Technology* 168, 438–447.

Gross, A.J., Hermann T.R.W. (2007). History of lasers. *World J Urol.* 2007, 25(3), 217-220.

Grote, K. H., Antonsson, E. K. (2009). Springer Handbook of Mechanical Engineering, Grüzburg, Springer.

Hassan, D.S.M., Naveed, Abdulrahman M.(2017) Laser Beam Micro-milling of Micro-channels in Aerospace Alloys. *Advanced Structured Materials, Springer, ISBN 978-981-10-3602-6.*

Hilton, P. A. (2007). The early days of laser cutting. *11th Nordic Conference in Laser Processing of Materials, Lappeenranta, Finland.*

Hsu, P., Hauser, J., and Sastry, S. (1988). Dynamic control of redundant manipulators. P*roceedings of the 1988 IEEE Internat. Conf. Robot. Automat., IEEE Computer Society Press,* Washington, 183-187.

Huang, J., Hara, M., and Yabuta, T. (2010). Controlling a finger-arm robot to emulate the motion of the human upper limb by regulating finger manipulability. In *Motion Control*. IntechOpen.

Huang, J., Yamada, D., Hori, T., Hara, M., and Yabuta, T. (2009, May). Integration of impedance control and manipulability regulation for a finger-arm robot. In *2009 IEEE International Conference on Robotics and Automation* (pp. 4006-4012).

Huang, S., Bergström, N., Yamakawa, Y., Senoo, T., and Ishikawa, M. (2016). Applying high-speed vision sensing to an industrial robot for high-performance position regulation under uncertainties. *Sensors*, *16*(8), 1195.

Huang, R. K., Chann , B., Kaiman, M. Overman ,R., Glenn, J.D, Tayebati, P. (2012). Direct diode lasers with comparable beam quality to fiber, CO2, and solid state lasers. *Proc. SPIE 8241, High-Power Diode Laser Technology and Applications*, 8241.

Kellens, K. , Rodrigues, G. C., Dewulf, W.,. Duflou, J. R (2014). Energy and Resource Efficiency of Laser Cutting Processes. *Physics Procedia*, 56, 854-864.

Khatib, O. (1988). Augmented object and reduced effective inertia in robot systems. *1988 American Control Conference*, 2140-2147.

Khatib, O. (1989). Reduced effective inertia in macro-/mini-manipulator systems. *Japan-USA Symposium on Flexible Automation*, 329-334.

Kim, S. M., Yi, B. J., Chung, J. H., Cheong, J., and Kim, W. (2017). Development of a new neurosurgical 5-DOF parallel robot for stereotactic DBS operations. *International Journal of Precision Engineering and Manufacturing*, *18*(3), 333-343.

Kiper G., Dede M. İ. C., Uzunoğlu E., Mastar E. (2015a). Use of Hidden Robot Concept for Calibration of an Over-Constrained Mechanism. *The 14th IFToMM World Congress*, Taipei, Taiwan, 25-30.

Kyriakopoulos, K.J. and Saridis, G.N. (1988). Minimum jerk path generation. In Proceedings. *1988 IEEE International Conference on Robotics and Automation*, 364-369.

Labrecque, P. D., Haché, J. M., Abdallah, M., and Gosselin, C. (2016). Low-impedance physical human-robot interaction using an active–passive dynamics decoupling. *IEEE Robotics and Automation Letters*, *1*(2), 938-945.

Lai, Y., Wang, H., and Chen, W. (2015). Kinematics and time optimal trajectory planning of a 10-DOF redundant manipulator. In *2015 IEEE International Conference on Cyber Technology in Automation, Control, and Intelligent Systems (CYBER)*, 560-565.

Lees, S. and Lee, J. M. (1990, May). Multiple task point control of a redundant manipulator. In *Proceedings., IEEE International Conference on Robotics and Automation*, 988-993.

Leibinger, P., Rauser, T., Zeygerman, L. (2004). Laser Cutting Machine with Multiple Drives, Patent no: US20040178181.

Lentjes, B. (2012). Metal Cutting with Multi kW Diode Laser, *Laser Technik Journal, WILEY-VCH*, Weinheim, Germany.

Lew, J. Y. (1997). Contact control of flexible micro/macro-manipulators. In *Proceedings of International Conference on Robotics and Automation*. 4, 2850-2855.

Lew, J. Y., Moon, S. M. (1999). Acceleration feedback control of compliant base manipulators. In *Proceedings of the 1999 American Control Conference (Cat. No. 99CH36251)*. 3, 1955-1959.

Lin, C., Chang, P. and Luh, J. (1983). Formulation and optimization of cubic polynomial joint trajectories for industrial robots. *IEEE Transactions on automatic control* 28(12), 1066-1074.

Luh, J. and Gu, Y. (1985). March. Industrial robots with seven joints. *In Proceedings. 1985 IEEE International Conference on Robotics and Automation*, 2, 1010-1015. IEEE.

Lum, M. J., Rosen, J., Sinanan, M. N., and Hannaford, B. (2006). Optimization of a spherical mechanism for a minimally invasive surgical robot: theoretical and experimental approaches. *IEEE Transactions on Biomedical Engineering*, *53*(7), 1440-1445.

Ma, Z., Hong, G. S., Ang, M. H., Poo, A. N. (2015). Mid-ranging control of a macro/mini manipulator. In *2015 IEEE International Conference on Advanced Intelligent Mechatronics (AIM)*, 755-760.

Ma, Z., Hong, G. S., Ang, M. H., Poo, A. N. (2016). Design and control of an end-effector module for industrial finishing applications. *In 2016 IEEE International Conference on Advanced Intelligent Mechatronics*. 339-344.

Maaroof O., Gezgin E., Dede M.İ.C. (2012) General subtask controller for redundant robot manipulators. In: 12. IEEE International Conference on Control, Automation, Jeju Island, Korea, 1352-1357.

Macfarlane, S. and Croft, E.A. (2003). Jerk-bounded manipulator trajectory planning: design for real-time applications. *IEEE Transactions on Robotics and Automation*, 19(1), 42-52.

Mannani, A., and Talebi, H. A. (2007). A fuzzy Lyapunov-based control strategy for a macro–micro manipulator: Experimental results. *IEEE transactions on control systems technology*, *15*(2), 375-383.

Martin, D.P., Baillieul, J. and Hollerbach, J.M. (1989). Resolution of kinematic redundancy using optimization techniques. *IEEE Transactions on Robotics and Automation*, 5(4), 529-533.

Matthew, S., Craig, B. (2010). Fundamentals of Laser-Material Interaction and Application to Multiscale Surface Modification. *Springer Series in Materials Science*, 135, 91-120.

Meijer, J. (2004). Laser beam machining (LBM), state of the art and new opportunities. *Journal of Materials Processing Technology*, 149, 2–17.

Mohammad, A. E. K., Hong, J., and Wang, D. (2018). Design of a force-controlled end-effector with low-inertia effect for robotic polishing using macro-mini robot approach. *Robotics and Computer-Integrated Manufacturing*, *49*, 54-65.

Nagai, K., Nakagawa, Y., Iwasa, S., and Ohno, K. (1997). Development of a redundant macro-micro manipulator and contour tasks utilizing its compliant motion. *Proceedings of the 1997 IEEE/RSJ International Conference on Intelligent Robot and Systems. Innovative Robotics for Real-World Applications. IROS'97*, 1, 279-284.

Nakamura Y, Hanafusa H and Yoshikawa T (1987) Task-Priority Based Redundancy Control of Robot Manipulators. The International Journal of Robotics Research 6(2), 3–15.

Narwell, N. I., Weker, D. R., and Wang, Y. (1994). A Force controllable macro-micro manipulator and its application to medical robotics. *JPL Computer Motion Inc.*, 94, 30441.

Nenchev, D. N., Yoshida, K., Vichitkulsawat, P., and Uchiyama, M. (1999). Reaction null-space control of flexible structure mounted manipulator systems. *IEEE Transactions on Robotics and Automation*, 15(6), 1011-1023.

Osumi, H., Arai, T., Fukuoka, T., Moriyama, K., and Torii, H. (1995). Cooperative control of two industrial robots with force control devices. In *Proceedings 1995 IEEE/RSJ International Conference on Intelligent Robots and Systems. Human Robot Interaction and Cooperative Robots*, 3, 550-555

Pål J., Jan T. Gravdahl, Tommy Lillehagen, and Pieter Abbeel (2011). Motion planning and control of robotic manipulators on seaborne platforms. *Control engineering practice*, 19(8), 809-819.

Parsa, K., Angeles, J., and Misra, A. K. (2005). Control of macro-micro manipulators revisited. *Journal of dynamic systems, measurement, and control*, 127(4), 688-699.

Piazzi, A. and Visioli, A. (1998). Global minimum-time trajectory planning of mechanical manipulators using interval analysis. *International journal of Control*, 71(4), 631-652.

Piazzi, A. and Visioli, A. (2000). Global minimum-jerk trajectory planning of robot manipulators. *IEEE transactions on industrial electronics*, 47(1), 140-149.

Platt, R., Abdallah, M., and Wampler, C. (2011). Multiple-priority impedance control. *2011 IEEE International Conference on Robotics and Automation*, 6033-6038.

Potkonjak, V., Popovic, M., Lazarevic, M., and Sinanovic, J. (1998). Redundancy problem in writing: From human to anthropomorphic robot arm. *IEEE Transactions on Systems, Man, and Cybernetics, Part B (Cybernetics)*, 28(6), 790-805.

Powell, J., Kaplan, J. (2012). A technical and commercial comparison of fiber laser and CO^2 laser cutting. *In Proc. 31th International Congress on Applications of Lasers and Electro-Optics*, Anaheim, CA, USA, 277-281.

Preco SL, accessed on August 03, 2019. http://www.precoinc.com/systems/sl.html.

Preda, N., Manurung, A., Lambercy, O., Gassert, R., and Bonfè, M. (2015). Motion planning for a multi-arm surgical robot using both sampling-based algorithms and motion primitives. In *2015 IEEE/RSJ International Conference on Intelligent Robots and Systems (IROS)*, 1422-1427.

Prima Platino, accessed on August 03, 2019. http://www.primapower.com/platino/.

Qijun, C., and Halang, W. (2002, November). Development of 4 DOF planar macro-micro manipulators system. In *IEEE 2002 28th Annual Conference of the Industrial Electronics Society. IECON 02*. 3, 2231-2236.

Quan, B. T., Huang, J., Harada, M., and Yabuta, T. (2006). Control of a macro-micro robot system using manipulability of the micro robot. *JSME International Journal Series C Mechanical Systems, Machine Elements and Manufacturing*, 49(3), 897-904.

Rodrigues, G. C., Vanhove, H., Duflou, J.R. (2014). Direct diode lasers for industrial laser cutting: a performance comparison with conventional fiber and CO^2 technologies. *8th International Conference on Photonic Technologies LANE*.

Rodriguez, O. R. (2008). Characterization and Modeling of a High Power Thin Disk Laser, *Msc Thesis, University of Central Florida*.

Sadeghian, H., Villani, L., Keshmiri, M., Siciliano, B. (2013). Dynamic multi-priority control in redundant robotic systems. *Robotica*, 31(7), 1155-1167.

Sakamoto, K. (1994). Trajectory generation for redundant robot manipulator by variational approach. *Advanced Motion Control-San Francisco*, 378-385.

Sartorio, F. (2004). Machine Tool and Manipulator Devise Adapted to be Mounted on Such Machine, Patent no: US20040025761.

Sartorio, F., Balbi, M. (2006). Counterbalance Moving Device for a Machine Tool, Patent no: EP1724054.

Schindlbeck, C., Janz, A., Pape, C., Reithmeier, E. (2017). Increasing milling precision for macro-micro-manipulators with disturbance rejection control via visual feedback. *IEEE/RSJ International Conference on Intelligent Robots and Systems (IROS)*, 4686-4693.

Schneider, U., So, O., Drust, M., Robertsson, A., Hägele, M., and Johansson, R. (2014). Integrated approach to robotic machining with macro/micro-actuation. *Robotics and Computer-Integrated Manufacturing*, 30(6), 636-647.

Seraji H. (1992). Task-based configuration control of redundant manipulators. Journal of Robotic Systems, 9(3), 411-451.

Sharon, A. and Hardt, D. (1984). Enhancement of robot accuracy using endpoint feedback and a macro-micro manipulator system. In *1984 American Control Conference, IEEE.*1836-1845

Sharon, A., Hogan, N., Hardt, D. E. (1988). High bandwidth force regulation and inertia reduction using a macro/micro manipulator system. In *Proceedings. 1988 IEEE International Conference on Robotics and Automation*, 126-132.

Sharon, A., Hogan, N., Hardt, D. E. (1993). The macro/micro manipulator: An improved architecture for robot control. *Robotics and computer-integrated manufacturing*, 10(3), 209-222.

Shim, J. H. and Cho, H. S. (1999). A new macro/micro robotic probing system for the in-circuit test of PCBs. *Mechatronics*, *9*(6), 589-613.

Siciliano, B. and Khatib, O. eds., (2016). Springer handbook of robotics. *Springer*.

Simon, D. and Isik, C. (1993). A trigonometric trajectory generator for robotic arms. International Journal of Control, 57(3), 505-517.

Sörnmo, O., Olofsson, B., Schneider, U., Robertsson, A., and Johansson, R. (2012, July). Increasing the milling accuracy for industrial robots using a piezo-actuated high-dynamic micro manipulator. *2012 IEEE/ASME international conference on advanced intelligent mechatronics (AIM)*, 104-110.

Steen, W. M., Mazumder, J. (2010). Laser Cutting, Drilling and Piercing. *Laser material processing, 4th Edition*, 131-198.

Suarez, A., Giordano, A. M., Kondak, K., Heredia, G., and Ollero, A. (2018). Flexible link long reach manipulator with lightweight dual arm: Soft-collision detection, reaction, and obstacle localization. In *2018 IEEE International Conference on Soft Robotics (RoboSoft)*, 406-411.

Sun, S., Brandt, M. (2013). Laser Beam Machining. *Nontraditional Machining Processes*, 35-96.

Sundar, J.K.S., Joshi, S.V. (2009). Laser cutting of materials, Centre for Laser Processing of Materials. *International Advance Research Centre for Powder Metallurgy and New Materials, Hyderabad.*

Taghirad, H. D. and Nahon, M. (2008). Kinematic analysis of a macro–micro redundantly actuated parallel manipulator. *Advanced Robotics*, *22*(6), 657-687.

Tatlıcıoğlu E, Braganza D, Burg TC and Dawson DM (2009) Adaptive control of redundant robot manipulators with subtask objectives. *Robotica*, 27(6), 873–881.

Tatlıcıoğlu, E., McIntyre, M. L., Dawson, D. M., and Walker, L. D. (2008). Adaptive non-linear tracking control of kinematically redundant robot manipulators. *International Journal of Robotics and Automation*, 23(2), 98-105.

Tol, U. A., Clerc, J. P., and Wiens, G. J. (2002). Micro/macro approach for dexterity enhancement of PKM's. In *Workshop on Fundamentals Issues and Future Research Directions for Parallel Mechanisms and Manipulators*, 34-39.

Uzunoğlu, E., Dede, M.İ.C. and Kiper, G. (2015). Trajectory planning for a redundant planar laser-cutting machine with macro-micro manipulation. *The 14th IFToMM World Congress, Taipei, Taiwan*.

Uzunoglu, E., Dede, M.I.C. and Kiper, G. (2016). Trajectory planning for a planar macro-micro manipulator of a laser-cutting machine. *Industrial Robot: An International Journal*, 43(5), 513-523.

Uzunoğlu, E., Dede, M.İ.C., Kiper, G., Mastar, E. and Sığırtmaç, T. (2014). Trajectory planning of redundant planar mechanisms for reducing task completion duration. *In Advances on Theory and Practice of Robots and Manipulators*, 215-223.

Wang, F.C. and Yang, D.C.H., (1993). Nearly arc-length parameterized quintic-spline interpolation for precision machining. Computer-Aided Design, 25(5), pp.281-288.

Wang, L., Xi, F., and Zhang, D. (2006). A parallel robotic attachment and its remote manipulation. *Robotics and Computer*-Integrated *Manufacturing*, *22*(5-6), 515-525.

Wu, S. T., and Marquez, M. R. G. (2003). A non-self-intersection Douglas-Peucker algorithm. *In 16th Brazilian Symposium on Computer Graphics and Image Processing (SIBGRAPI 2003)*. 60-66.

Xu, W. L., Yang, T. W., and Tso, S. K. (2000). Dynamic control of a flexible macro–micro manipulator based on rigid dynamics with flexible state sensing. *Mechanism and Machine Theory*, 35(1), 41-53.

Yang, Y. L., Wei, Y. D., Lou, J. Q., Fu, L., and Zhao, X. W. (2017). Nonlinear dynamic analysis and optimal trajectory planning of a high-speed macro-micro manipulator. *Journal of Sound and Vibration*, 405, 112-132.

Yang, Y. L., Wei, Y. D., Lou, J. Q., Fu, L., Fang, S., and Chen, T. H. (2018). Dynamic modeling and adaptive vibration suppression of a high-speed macro-micro manipulator. *Journal of Sound and Vibration*, 422, 318-342.

Yao, S., Li, H., Zeng, L., and Zhang, X. (2018). Vision-based adaptive control of a 3-RRR parallel positioning system. *Science China Technological Sciences*, 1-12.

Yim, W., and Singh, S. N. (1997). Nonlinear inverse and predictive end point trajectory control of flexible macro-micro manipulators. *Journal of dynamic systems, measurement, and control*, 119(3), 412-420.

Yoshida, K., Nenchev, D. N., and Uchiyama, M. (1999). Vibration suppression and zero reaction maneuvers of flexible space structure mounted manipulators. *Smart materials and structures*, 8(6), 847.

Yoshikawa, T., Harada, K., Matsumoto, A. (1996). Hybrid position/force control of flexible-macro/rigid-micro manipulator systems. *IEEE Transactions on Robotics and Automation*, 12(4), 633-640.

Yousef, B., Patel, R., and Moallem, M. (2006). A macro-robot manipulator for medical applications. In *2006 IEEE International Conference on Systems, Man and Cybernetics* (Vol. 1, pp. 530-535). IEEE.

Yun, Y., and Li, Y. (2012). Modeling and control analysis of a 3-PUPU dual compliant parallel manipulator for micro positioning and active vibration isolation. *Journal of Dynamic Systems, Measurement, and Control*, *134*(2).

Zhang, Y., Sun, Z., and Yang, T. (2006). Optimal motion generation of a flexible macro-micro manipulator system using genetic algorithm and neural network. *2006 IEEE Conference on Robotics, Automation and Mechatronics*, 1-6.

Zheng, Y. F., and Luh, Y. S. (1993). On the inertia duality of parallel-series connections of two robots in operational space. *IEEE transactions on robotics and automation*, 9(6), 846-854.

APPENDIX A

LIST OF STANDARDS

• VDI/DGQ 3441 Statistical Testing of the Operational and Positional Accuracy of Machine Tools

• DIN 2310-5 Thermal cutting; laser cutting of metallic materials; principles of process, quality and dimensional tolerances

• EN 12417 Machine tools. Safety. Machining centres

• EN 60825 Safety of laser products. Equipment classification and requirements

• EN 11553 Safety of machinery. Laser processing machines.

• TS EN ISO 12100-1 Safety of machinery part 1

• TS EN ISO 12100-2 Safety of machinery part 2

• TS EN 294 Safety of machinery. Safety distances to prevent danger zones being reached by the upper limbs.

• ISO 14121-1 Safety of machinery. Risk assessment. Practical guidance and examples of methods

• EN 60204 – 1 Safety of machinery. Electrical equipment of machines. General requirements

• TS EN 61000 – 4 – 2 / 4 / 5 / 5 / 11 Electromagnetic compatibility.

APPENDIX B

MEASUREMENT REPORTS

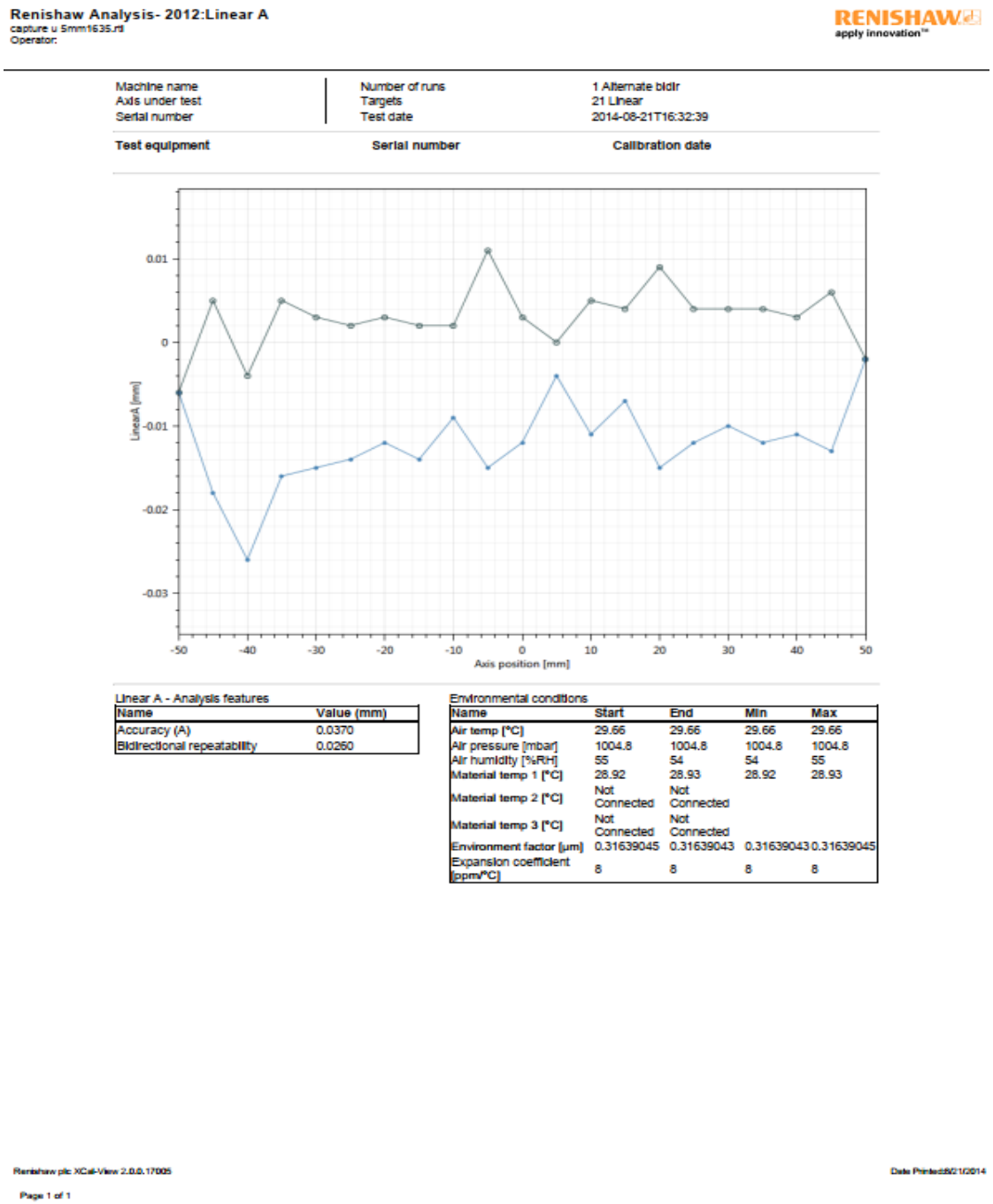

Renishaw Analysis- 2012:Linear A
capture u 5mm1635.rtl
Operator:

RENISHAW
apply innovation™

Machine name		Number of runs	1 Alternate bidir
Axis under test		Targets	21 Linear
Serial number		Test date	2014-08-21T16:32:39

Test equipment	Serial number	Calibration date

Linear A - Analysis features

Name	Value (mm)
Accuracy (A)	0.0370
Bidirectional repeatability	0.0260

Environmental conditions

Name	Start	End	Min	Max
Air temp [°C]	29.66	29.66	29.66	29.66
Air pressure [mbar]	1004.8	1004.8	1004.8	1004.8
Air humidity [%RH]	55	54	54	55
Material temp 1 [°C]	28.92	28.93	28.92	28.93
Material temp 2 [°C]	Not Connected	Not Connected		
Material temp 3 [°C]	Not Connected	Not Connected		
Environment factor [µm]	0.31639045	0.31639043	0.31639043	0.31639045
Expansion coefficient [ppm/°C]	8	8	8	8

Renishaw plc XCal-View 2.0.0.17005
Date Printed:8/21/2014
Page 1 of 1

Figure B.1.Micro manipulators positioning accuracy measurement report.

Renishaw Analysis- 2012:Linear A
x hata 2d COMP.rtl
Operator:

RENISHAW
apply innovation™

Machine name	Number of runs	1 Alternate bidir
Axis under test	Targets	121 Linear
Serial number	Test date	2014-08-20T14:28:10

Test equipment	Serial number	Calibration date

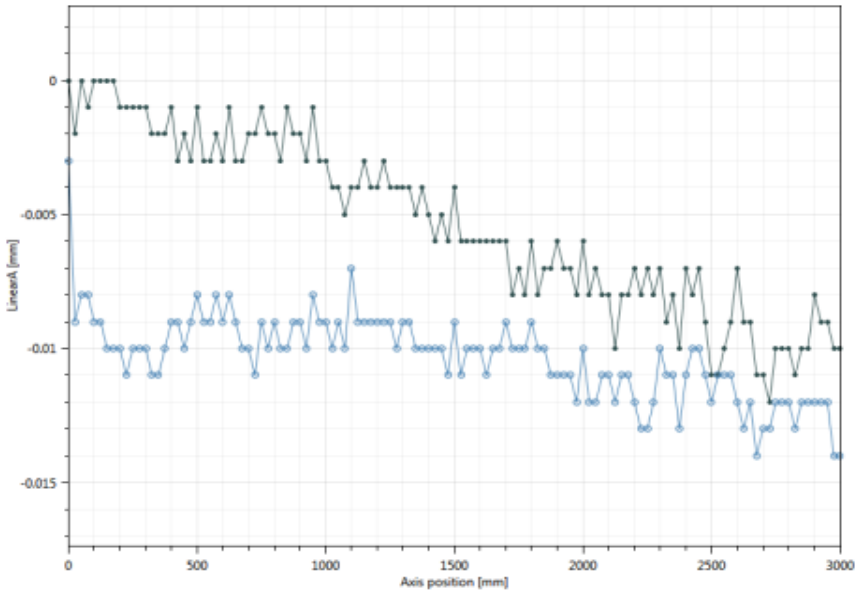

Linear A - Analysis features

Name	Value (mm)
Accuracy (A)	0.0140
Bidirectional repeatability	0.0100

Environmental conditions

Name	Start	End	Min	Max
Air temp [°C]	28.51	28.71	28.51	28.71
Air pressure [mbar]	1005.4	1005.2	1005.2	1005.4
Air humidity [%RH]	60	59	59	60
Material temp 1 [°C]	27.55	27.66	27.55	27.66
Material temp 2 [°C]	Not Connected	Not Connected		
Material temp 3 [°C]	Not Connected	Not Connected		
Environment factor [µm]	0.31639357	0.31639337	0.31639337	0.31639357
Expansion coefficient [ppm/°C]	8	8	8	8

Renishaw plc XCal-View 2.0.0.17005 Date Printed:8/20/2014

Page 1 of 1

Figure B.2. Macro manipulators positioning accuracy measurement report.

APPENDIX C

STABILITY FORMULATION FOR VDM

To investigate the stability of VDM, the isolated system's closed-loop characteristic polynomial can be shown with the following equation, which is governed by the state matrix given in Section 6.2.4.

$$s^4 + \frac{(b_1m_2+b_2m_1+b_2m_2)}{m_1m_2}s^3 + \frac{(b_1b_2+m_2k_1+m_1k_2+k_2m_2)}{m_1m_2}s^2 + \frac{(b_1k_2+b_2k_1)}{m_1m_2}s + \frac{k_2k_1}{m_1m_2} \quad \text{(D.1)}$$

Using the Routh-Hurwitz criterion, the elements of the first column of the Routh array are given in ***r***.

$$\boldsymbol{r} = \begin{bmatrix} r_1 \\ r_2 \\ r_3 \\ r_4 \\ r_5 \end{bmatrix} \quad \text{(D.2)}$$

According to Routh-Hurwitz criterion to have all its poles in the open left half-plane, providing that all first-column elements of the Routh array have the same sign. Regarding that, the following conditions must be valid for stability.

$$r_1 = 1 > 0$$

$$r_2 = (b_1m_2 + b_2m_1 + b_2m_2)/m_1m_2 > 0$$

$$r_3 = (b_1{b_2}^2m_1 + b_1{b_2}^2m_2 + b_2{b_1}^2m_2 + b_1k_1{m_2}^2 + b_2k_1{m_2}^2 + b_2k_2{m_1}^2 + b_2k_2{m_2}^2 + 2b_2k_2m_1m_2)/m_1m_2(b_1m_2 + b_2m_1 + b_2m_2) > 0 \quad \text{(D.3)}$$

$$r_4 = (b_1{}^3 b_2 k_2 m_2 + b_1{}^2 b_2{}^2 k_1 m_2 + b_1{}^2 b_2{}^2 k_2 m_1 + b_1{}^2 b_2{}^2 k_2 m_2 + b_1{}^2 k_2{}^2 m_2{}^2$$
$$+ b_1 b_2{}^3 k_1 m_1 + b_1 b_2{}^3 k_1 m_2 + b_1 b_2 k_1{}^2 m_2{}^2 - 2 b_1 b_2 k_1 k_2 m_1 m_2$$
$$+ b_1 b_2 k_2{}^2 m_1{}^2 + 2 b_1 b_2 k_2{}^2 m_1 m_2 + b_1 b_2 k_2{}^2 m_2{}^2$$
$$+ b_2{}^2 k_1{}^2 m_2{}^2)/(m_1 m_2 (b_1 b_2{}^2 m_1 + b_1 b_2{}^2 m_2 + b_1{}^2 b_2 m_2 + b_1 k_1 m_2{}^2$$
$$+ b_1 k_2 m_2{}^2 + b_2 k_1 m_2{}^2 + b_2 k_2 m_1{}^2 + b_2 k_2 m_2{}^2 + 2 b_2 k_2 m_1 m_2) > 0$$

$$r_5 = k_1 k_2 / m_1 m_2 > 0$$

When all dynamic matric parameters in Equation (18) are chosen positive, and the following condition is satisfied, the VDM system is stable according to Routh-Hurwitz stability criteria.

$$(b_1{}^3 b_2 k_2 m_2 + b_1{}^2 b_2{}^2 k_1 m_2 + b_1{}^2 b_2{}^2 k_2 m_1 + b_1{}^2 b_2{}^2 k_2 m_2 + b_1{}^2 k_2{}^2 m_2{}^2 + b_1 b_2{}^3 +$$
$$b_1 b_2{}^3 k_1 m_2 + b_1 b_2 k_1{}^2 m_2{}^2 + b_1 b_2 k_2{}^2 m_1{}^2 + 2 b_1 b_2 k_2{}^2 m_1 m_2 + b_1 b_2 k_2{}^2 m_2{}^2 +$$
$$b_2{}^2 k_1{}^2 m_2{}^2 > 2 b_1 b_2 k_1 k_2 m_1 m_2 \qquad \text{(D.4)}$$

VITA

Emre Uzunoğlu

emreuzuno@gmail.com

Experience: (1) Project Assistant- "Kinematically Redundant Planar Laser Cutting Machine Design" SANTEZ Project on State-of-Art Laser Cutting Machine with the collaboration of industrial partner. (2012-2014) **(2)** Co-founder of Start-up Company: NLFD Tech Co. @ Technopark Izmir (2015-2017) **(3)** Project Assistant- "Methodologies for Increasing the Positioning Accuracy of High-Acceleration Parallel Robots Used in Industrial Applications" Funded by Tubitak 1001 The Support Program for Scientific and Technological Research Projects. (2017-2019)

Awards/Grants: (1) 100/2000 CoHE (Council of Higher Education, TURKEY) Doctoral Scholarship **(2)** International Federation for the Promotion of Mechanism and Machine Science (IFToMM) Young Delegate Program Award @Romansy 2014 XX CISM-IFToMM Symposium at Moscow.

Publications: Thesis: E. Uzunoğlu, "Position/Force Control of Systems Subjected to Communication Delays and Interruptions in Bilateral Teleoperation," M.Sc. Thesis, 2013. **Articles: (1)** E. Uzunoğlu, M. İ. C. Dede, G. Kiper, "Trajectory planning for a planar macro-micro manipulator of a laser-cutting machine", Industrial Robot: An International Journal, Vol 43/5, 2016. (Doi:10.1108/IR-02-2016-0057).**(2)** E. Uzunoğlu and M. İ. C. Dede, "Extending model-mediation method to multi-degree-of-freedom teleoperation systems experiencing time delays in communication," Robotica, Volume 35, Issue 5, pp. 1121-1136, 2017. (DOI: 10.1017/S0263574715001010). **(3)** O. N. Sahin, E. Uzunoglu, E. Tatlicioglu, and M. I. C. Dede, "Design and development of an educational desktop robot R3D." Computer Applications in Engineering Education Vol 25/2 (2017): 222-229. **(4)** E. Uzunoğlu, E. Tatlıcıoğlu, M. İ. C. Dede, " A Multi-Priority Controller for Industrial Macro-Micro Manipulation" (Under Review). **Peer-reviewed Conference Papers (First Author): (1)** E. Uzunoğlu, M. İ. C. Dede, G. Kiper "Trajectory Planning for a Redundant Planar Laser-Cutting Machine with Macro-Micro Manipulation," The 14th IFToMM World Congress, Taipei, Taiwan, October 25-30, 2015 (DOI: 10.6567/IFToMM.14TH.WC.OS13.094). **(2)** E. Uzunoğlu, M. İ. C. Dede, G. Kiper, E. Mastar, T. Sığırtmaç "Trajectory Planning of Redundant Planar Mechanisms for Reducing Task Completion Duration," Advances on Theory and Practice of Robots and Manipulators Mechanisms and Machine Science, Marco Ceccarelli and Victor A. Glazunov (Eds.), Volume 22, pp 215-223 Springer, Dordrecht, The Netherlands, 2014 (ISBN: 978-3-319-07057-5)**. (3)** E. Uzunoğlu ve M. İ. C. Dede "İletişim Hatalarına Maruz Kalan İki Yönlü Teleoperasyon Sisteminin Geliştirilmiş Kuvvet Takibi Performanslı Model-Aracılı Denetimi (Model Mediation Control of Bilateral Teleoperation System under Communication Delays with Enhanced Force Tracking Performance)," TOK 2013 Bildiri Kitabı, Malatya, Türkiye, pp. 1017-1022, 26-28 Eylül, 2013.